Cooperative binding of cucurbit[n]urils and β-cyclodextrin to heteroditopic imidazolium-based guests.

Petra Branná,[a] Jarmila Černochová,[a, b] Michal Rouchal,[a] Petr Kulhánek,[c] Martin Babinský,[c] Radek Marek,[c, d] Marek Nečas,[c, d] Ivo Kuřitka,[b] and Robert Vícha*[a]

[a]Department of Chemistry, [b] Polymer Centre, Faculty of Technology, Tomas Bata University in Zlín, Vavrečkova 275, 76001 Zlín, Czech Republic

[c] CEITEC – Central European Institute of Technology, [d] Department of Chemistry, Faculty of Science, Masaryk University, Kamenice 5, 62500 Brno, Czech Republic

SUPPORTING INFORMATION

Table of Contents
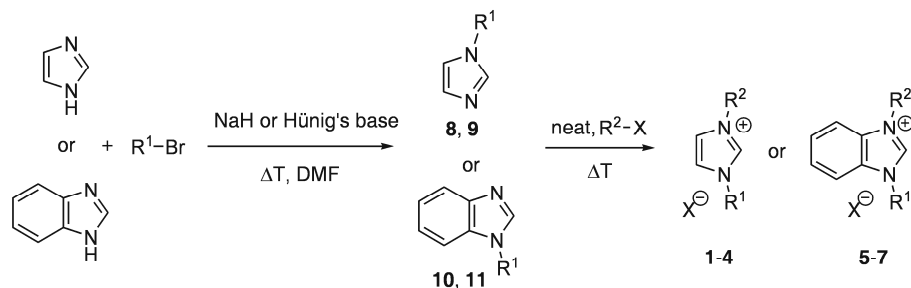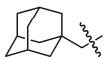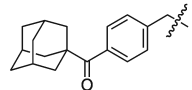
Synthetic procedures

General methods.

Guests **1**–**7** were prepared according to a previously published method.[1a] Preparation of the compounds **8** and **10** has been described previously.[1b] Hosts CB6, CB7, and β-CD were purchased from commercial sources. β-CD was dried prior to use under reduced pressure at 50°C to constant weight. The concentrations of the CB7 solutions were determined by ITC titrations with L-Phe as the standard. NMR spectra were recorded on a 700 MHz instrument equipped with a room-temperature (^{1}H, ^{13}C, ^{15}N) inverse triple resonance probe. 1D proton spectra were recorded at 303 K using a 7.0 kHz spectral width and a 3.3 kHz transmitter offset. Data were collected in 8–32 scans using 1.5 s recycle delay and 16k complex points were recorded per scan. The FIDs were apodized by a square cosine window function, zero filled to 32k complex points, and Fourier transformed to yield the resulting spectra. The 2D ROESY spectra were recorded using a spectral width of 7.0 kHz and a transmitter offset of 3.3 kHz in both dimensions and employing 150–400 ms continuous wave spinlock during the mixing period. A total of 2k complex points were collected in the t2 dimension and a total of 512 t1 increments were recorded using 16–32 scans per increment and 1.5 s recycle delay. The raw data were apodized by a squared cosine window function, zero filled to 4096 t2 and 2048 t1 points and Fourier transformed to yield the resulting 2D spectra. The residual HDO signal in both the 1D and 2D ROESY experiments was suppressed by employing pre-saturation during the recycle delay. Performing ^{1}H NMR titration experiments, no time-depending changes in signal intensities were observed. The association constants and thermodynamic parameters for the complexation of guests 1–7 with CB7, CB6, and/or β-CD were determined by isothermal titration calorimetry. A solution of the host in water or in 2.5 mM NaCl was placed in the sample cell, to which a solution of the guest was added in a series of 20–30 injections (10 μl). The concentrations of the CB6, CB7 and β-CD solutions were determined via ITC titrations using 1,6-hexanediamine·2HCl and 1-adamantaneamine·HCl, respectively. For the ternary systems, a solution of an equimolar mixture of guest and host in the sample cell was titrated with solution of the second host. The heat evolved was recorded at 303 K. The net heat effect was obtained by subtracting the heat of guest dilution from the overall observed heat effect. The association constants exceeding 10^7 M^{-1} were determined by the multistep competition method as described by Rekharsky *et al.*[2] 1,6-Hexanediamine·2HCl with $K_a(H_2O)=2.05\times10^9$ M^{-1} and $K_a(2.5$ mM NaCl$)=2.97\times10^8$ M^{-1}, dopamine·HCl with $K_a(H_2O)=4.58\times10^5$ M^{-1} and L-phenylalanine with $K_a(H_2O)=9.86\times10^5$ M^{-1} and $K_a(2.5$ mM NaCl$)=3.01\times10^5$ M^{-1} were used as the competitors. The complexation enthalpies for the multistep titration experiments were calculated as a sum of enthalpies for each complexation step. The values of K obtained from competitive titrations were verified using different concentrations of competitors. The typical ITC thermograms are shown in Figure 3 and Figures S48–70 in the Supporting Information.

[1] (a) Branná, P.; Rouchal, M.; Prucková, Z.; Dastychová, L.; Lenobel, R.; Pospíšil, T.; Maláč, K.; Vícha, R. *Chem. Eur. J.* **2015**, *21*, 11712–11718; (b) Černochová, J.; Branná, P.; Rouchal, M.; Kulhánek, P.; Kuřitka, I.; Vícha, R. *Chem. Eur. J.* **2012**, *18*, 13633–13637.

[2] Rekharsky, M. V.; Mori, T.; Yang, C.; Ko, H. K.; Selvapalam, N.; Kim, H.; Sobransingh, D.; Kaifer, A. E.; Liu, S.; Isaacs, L.; Chen, W.; Moghaddam, S.; Gilson, M. K.; Kim, K.; Inoue, Y. *Proc. Natl. Acad. Sci. U.S.A.* **2007**, *104*, 20737–20742.

Scheme S1

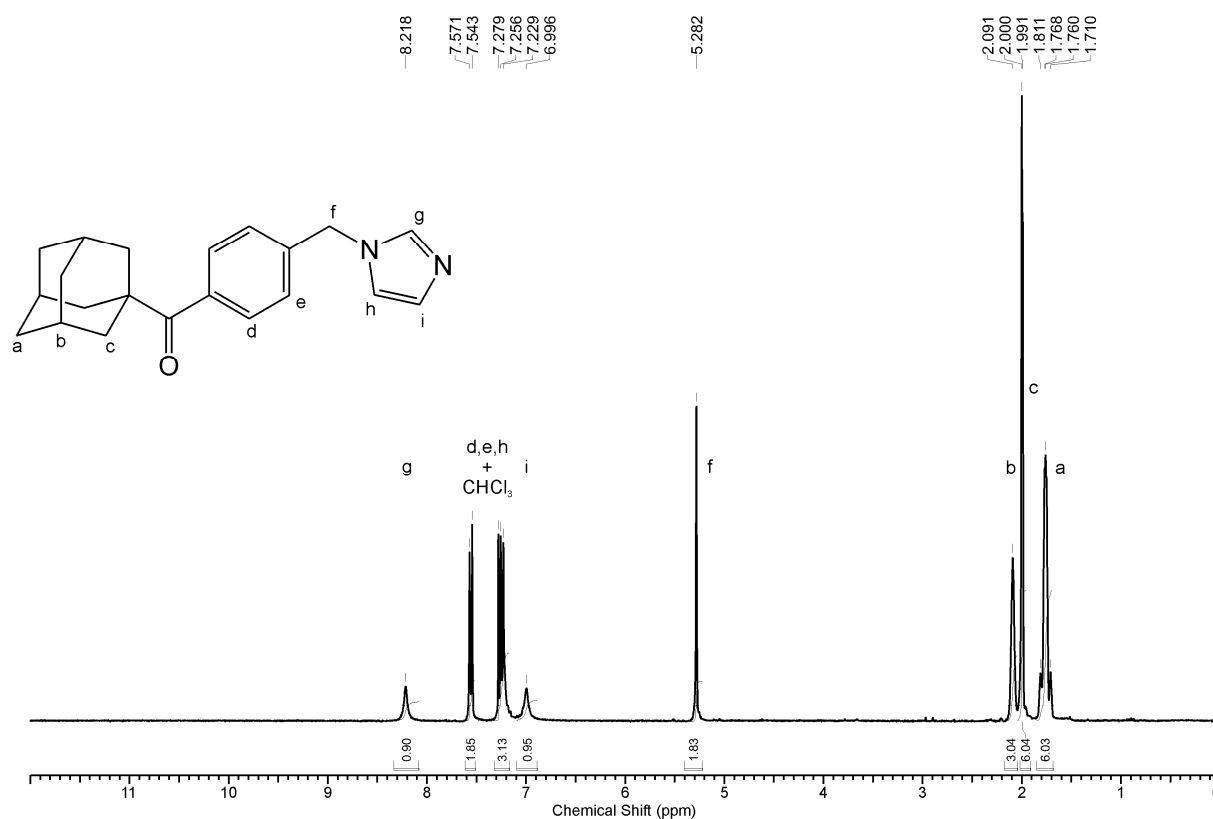| compound	R¹		compound	R¹	R²	X
8	[adamantyl structure] = A		**1⁺ X⁻**	A	Me	I
			2⁺ X⁻	A	Bu	Br
9	[adamantyl-phenyl ketone structure] = B		**3⁺ X⁻**	B	Me	I
			4⁺ X⁻	B	Bu	Br
10	A		**5⁺ X⁻**	A	Me	I
			6⁺ X⁻	A	Bu	Br, I, MsO
11	B		**7⁺ X⁻**	B	Bu	MsO

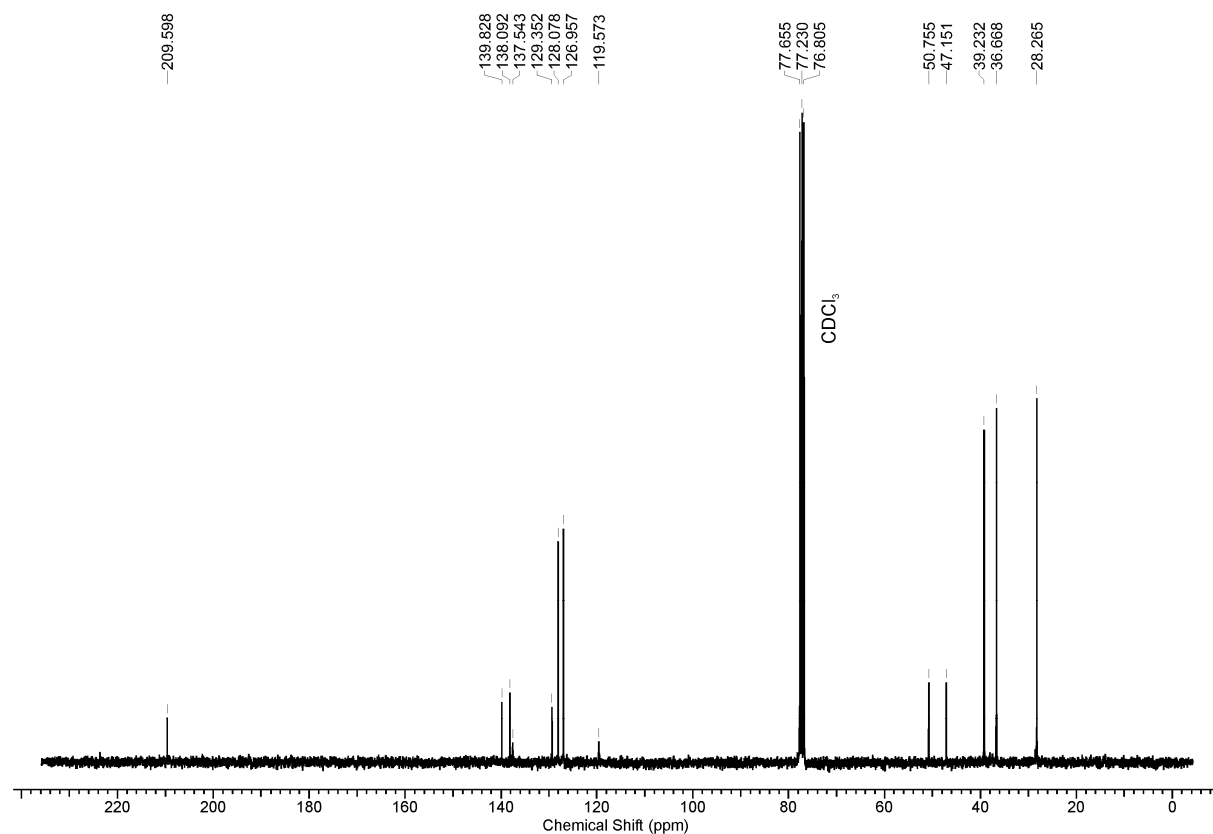Figure S1: The ^{1}H NMR (CDCl$_3$, 300 MHz) spectrum of compound **9**.

Figure S2: The ^{13}C NMR (CDCl$_3$, 75 MHz) spectrum of compound **9**.

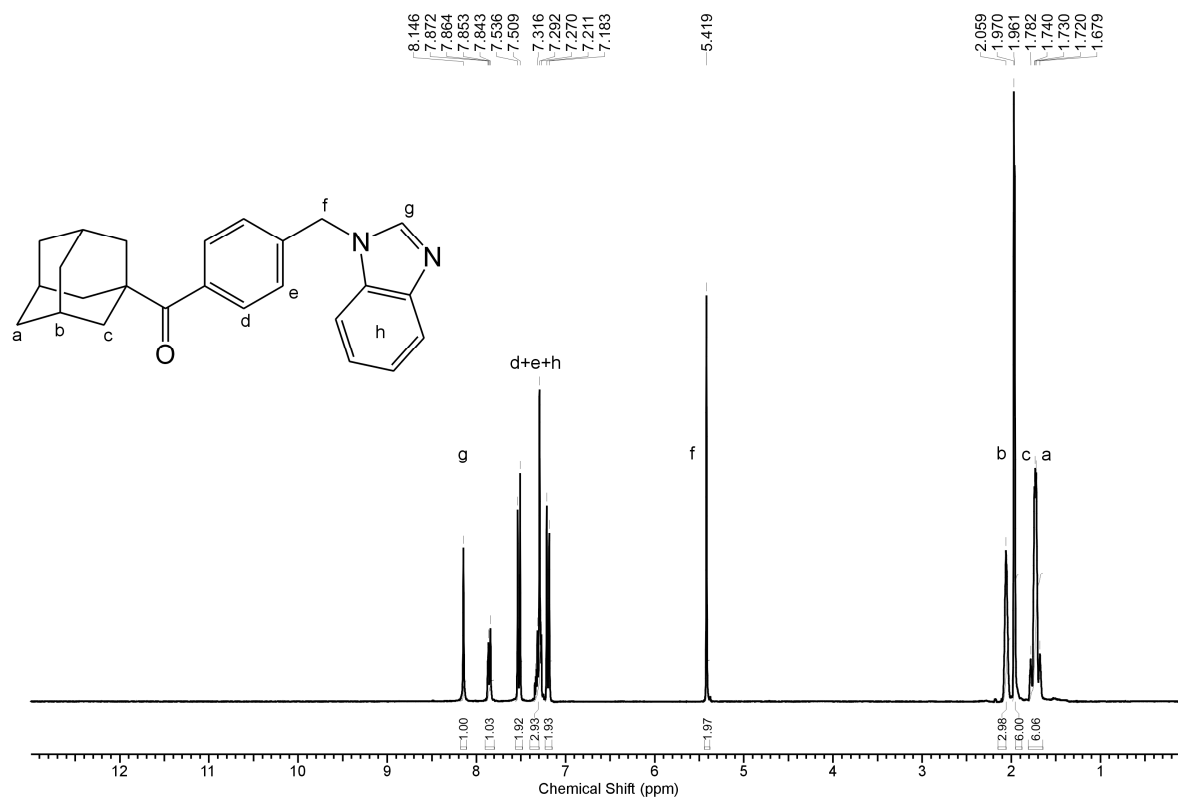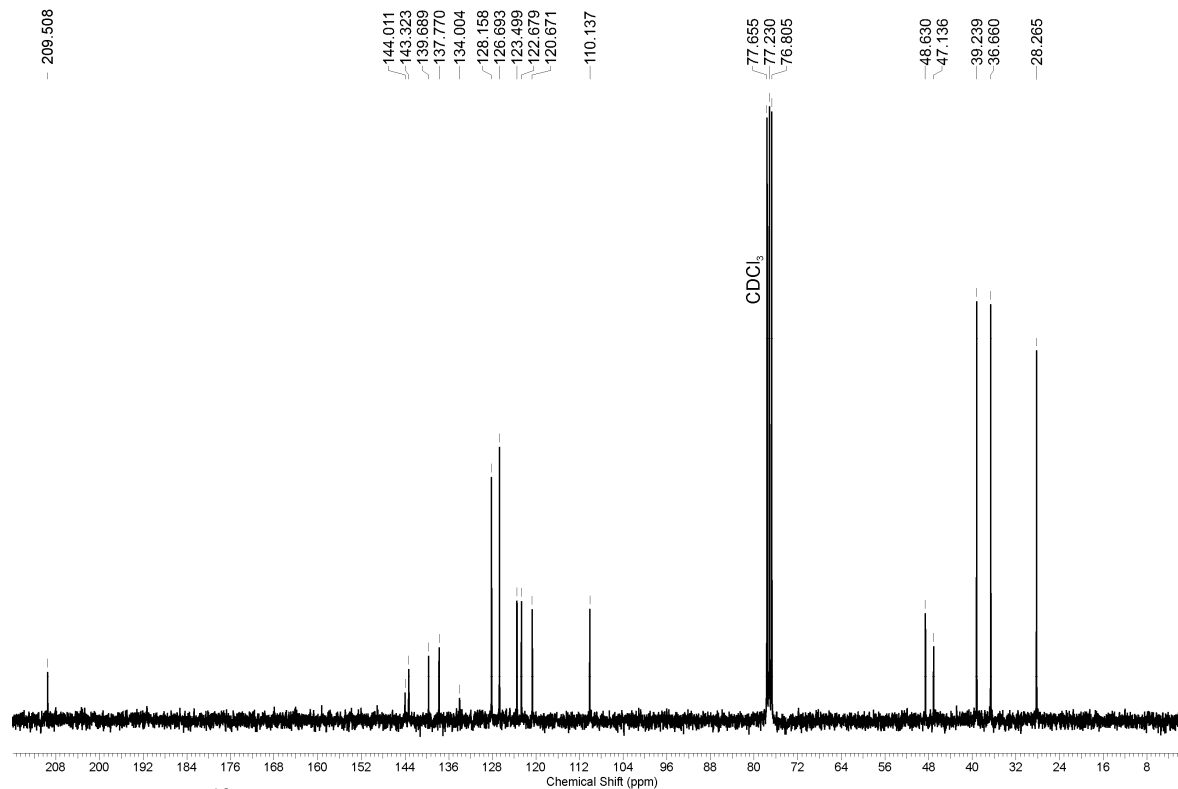Figure S3: The ^{1}H NMR (CDCl$_3$, 300 MHz) spectrum of compound **11**.

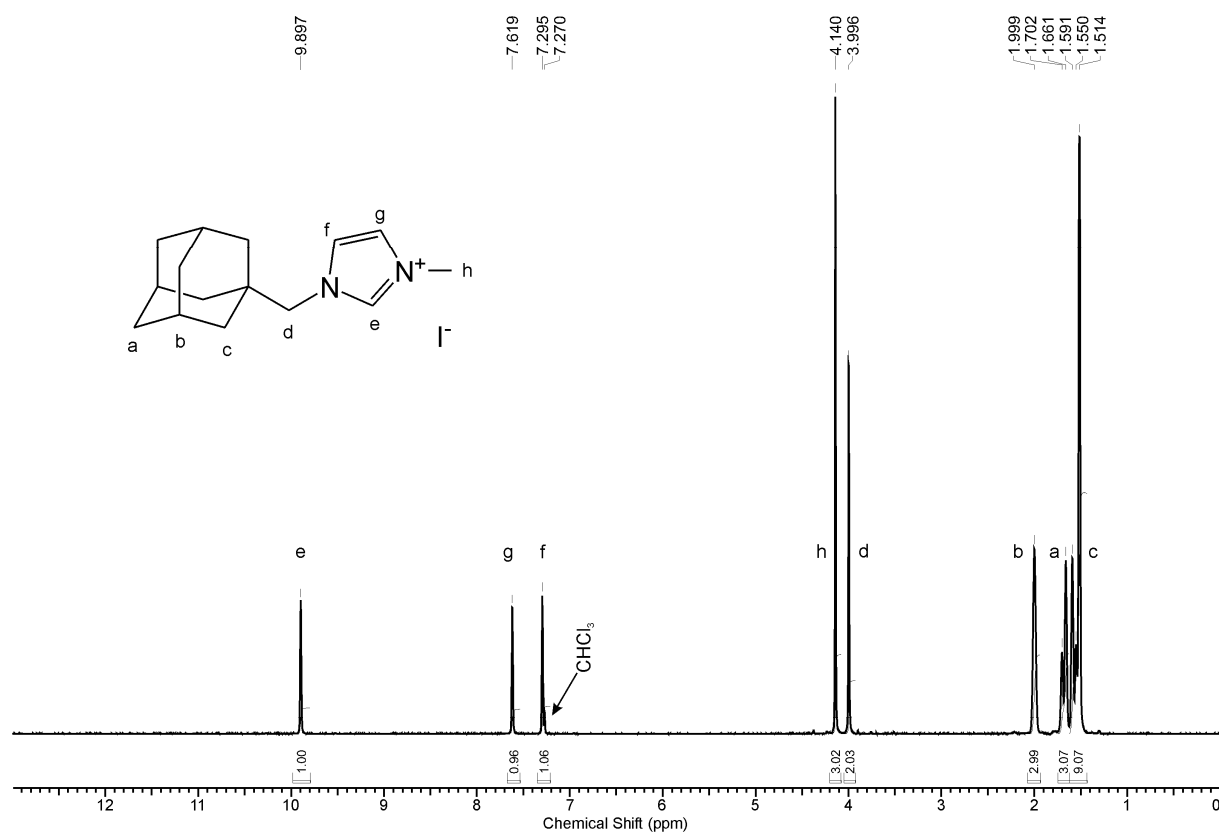Figure S4: The ^{13}C NMR (CDCl$_3$, 75 MHz) spectrum of compound **11**.

9.897

7.619
7.295
7.270

4.140
3.996

1.999
1.702
1.661
1.591
1.550
1.514

f   g

N+—h

e

d

a   b   c

I⁻

e   g   f   h d   b a c

CHCl₃

1.00   0.96 1.06   3.02 2.03   2.99 3.07 9.07

| 12 | 11 | 10 | 9 | 8 | 7 | 6 | 5 | 4 | 3 | 2 | 1 | 0 |

Chemical Shift (ppm)

Figure S5: The ^{1}H NMR (CDCl$_3$, 300 MHz) spectrum of salt **1**$^+$I$^-$.

137.477

123.924
123.382

77.655
77.230
76.805

61.641

39.840
37.261
36.382
34.067

27.943

CDCl₃

| 190 | 180 | 170 | 160 | 150 | 140 | 130 | 120 | 110 | 100 | 90 | 80 | 70 | 60 | 50 | 40 | 30 | 20 | 10 |

Chemical Shift (ppm)
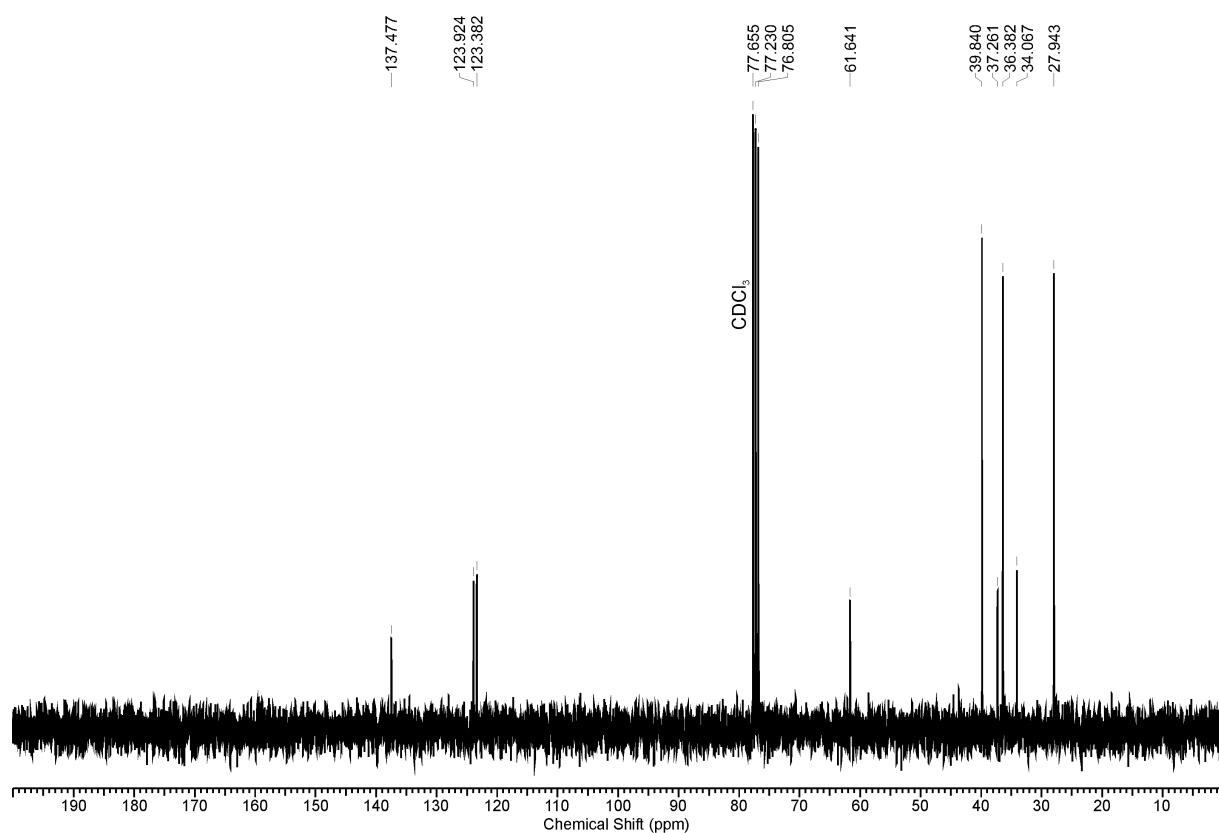
Figure S6: The ^{13}C NMR (CDCl$_3$, 75 MHz) spectrum of salt **1**$^+$I$^-$.

231.1

[M]+

100　200　300　400　500　600　700　800　900　1000　1100　1200　1300　*m/z*
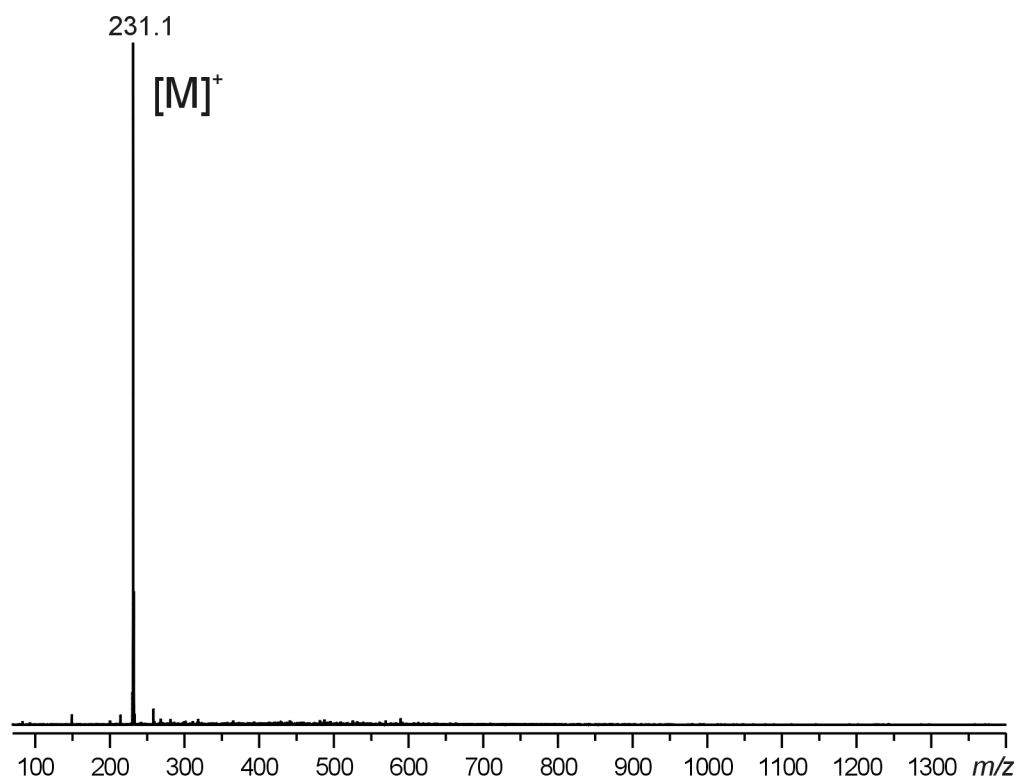
Figure S7: ESI-MS of salt **1**+I−
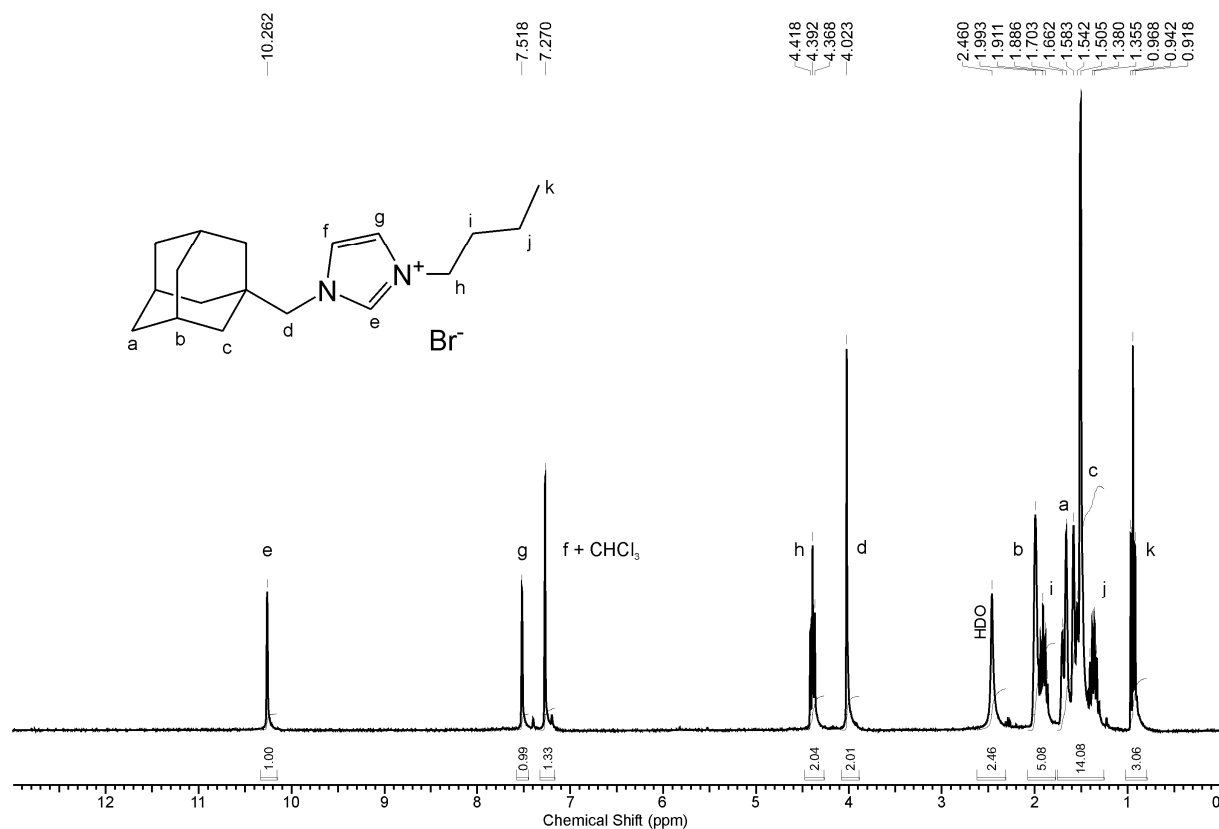
Figure S8: The ^{1}H NMR (CDCl$_3$, 300 MHz) spectrum of salt **2$^+$Br$^−$**.
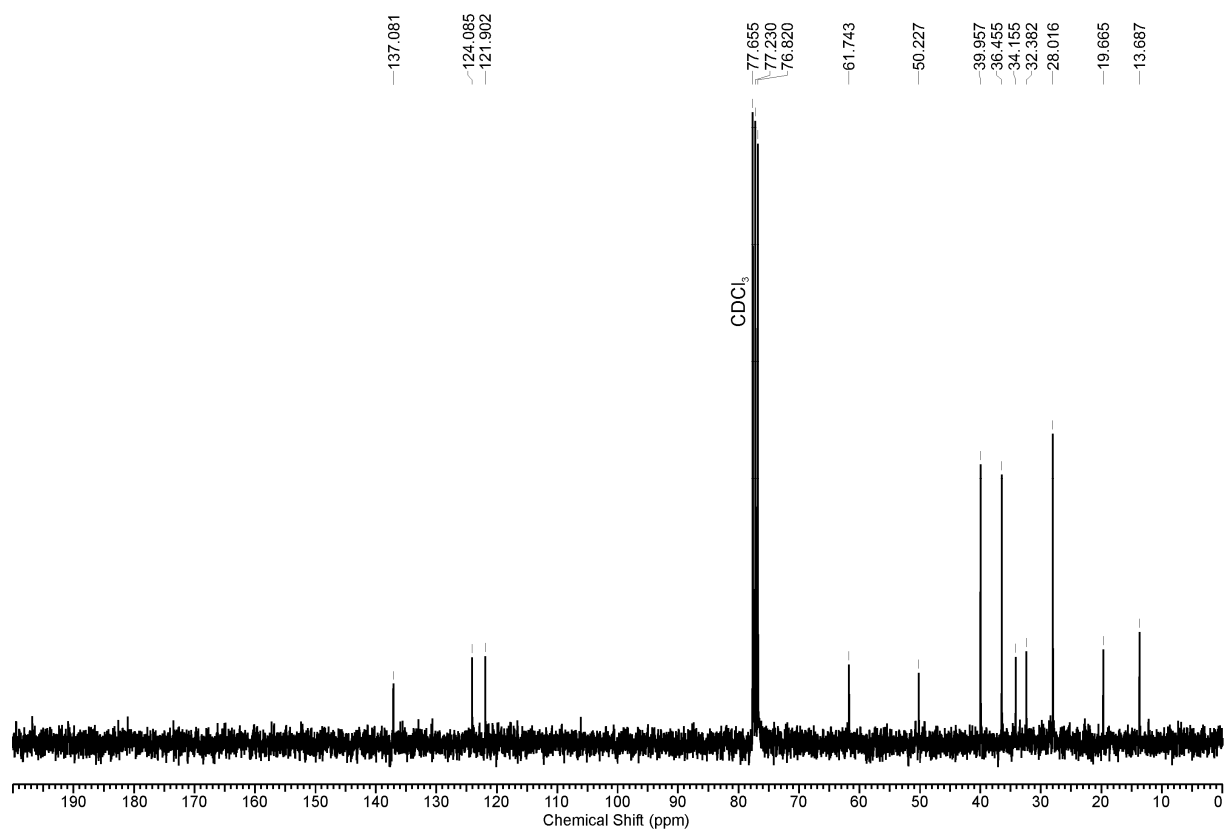
Figure S9: The ^{13}C NMR (CDCl$_3$, 75 MHz) spectrum of salt **2$^+$Br$^−$**.

273.3

[M]$^+$

[2•M$^+$-Br$^-$]$^+$

625.3/627.3

100 200 300 400 500 600 700 800 900 1000 1100 1200 1300 *m/z*
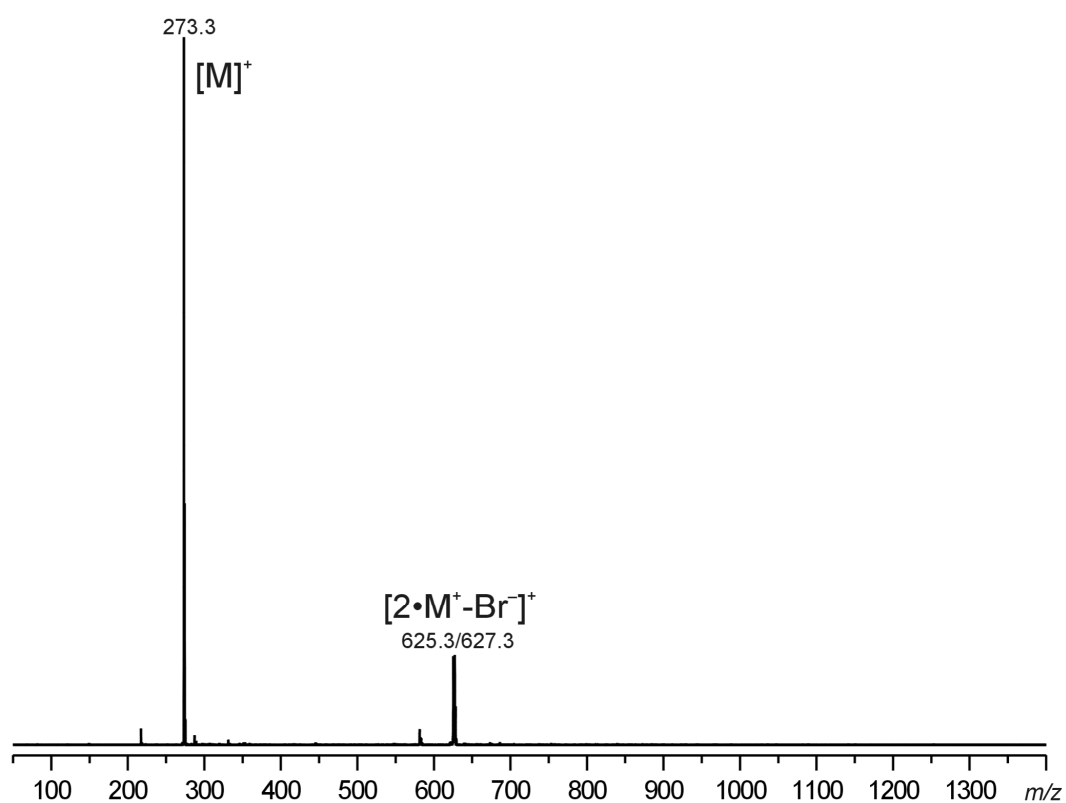
Figure S10: ESI-MS of salt **2**$^+$Br$^-$
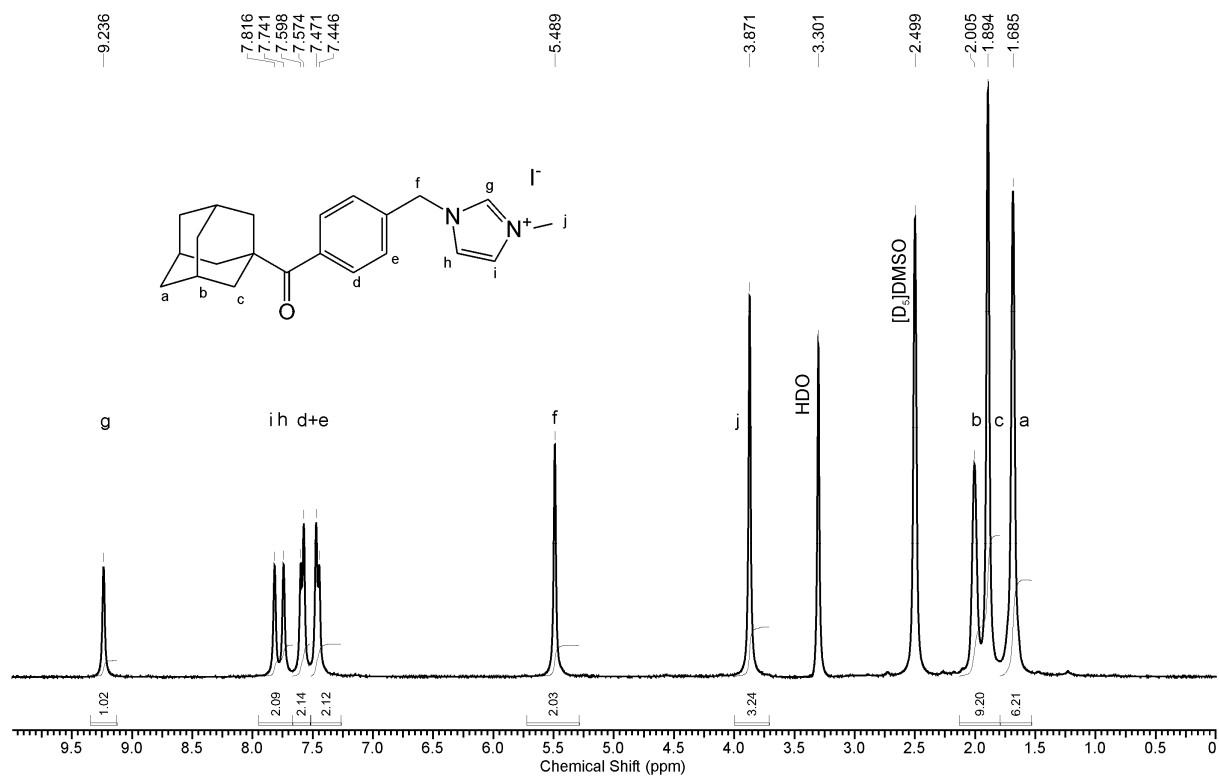
Figure S11: The ^{1}H NMR ([D$_6$]DMSO, 300 MHz) spectrum of salt **3$^+$I$^-$**.
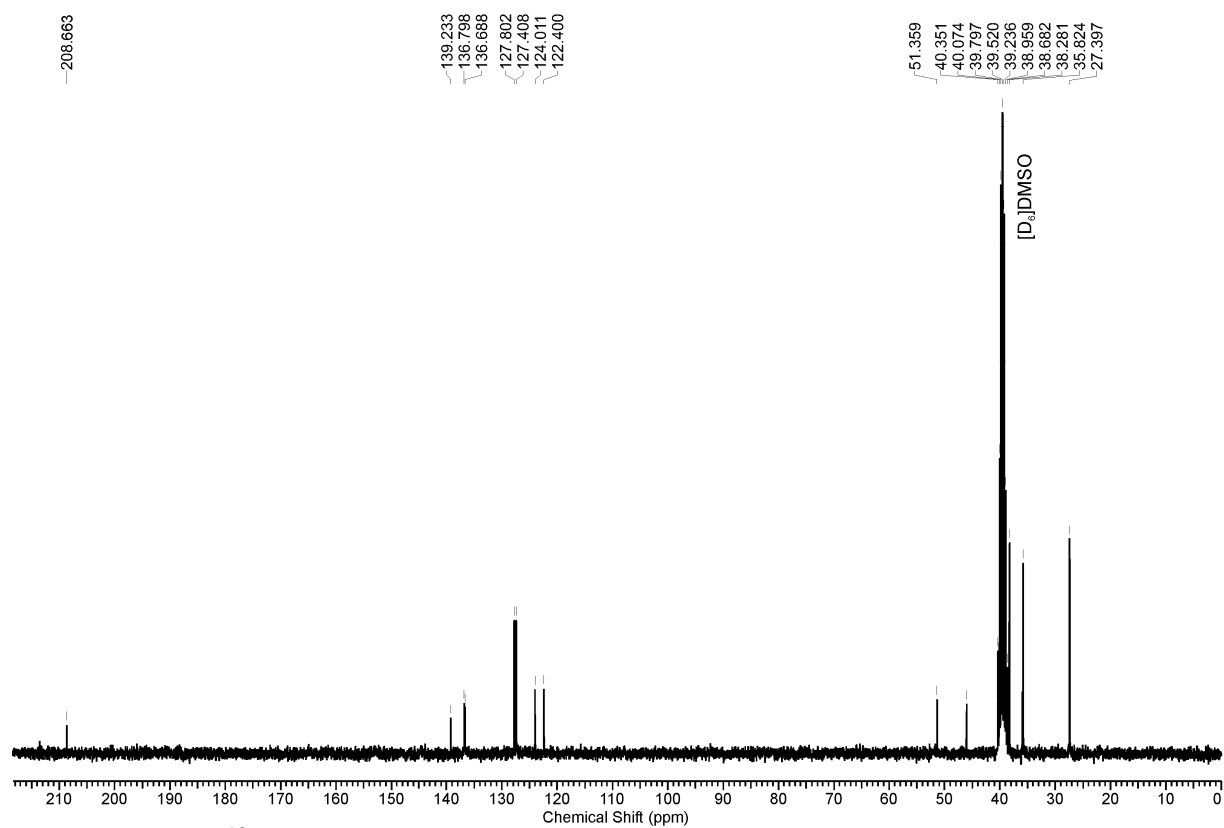
Figure S12: The ^{13}C NMR ([D$_6$]DMSO, 75 MHz) spectrum of salt **3$^+$I$^-$**.

335.3

[M]$^+$

100 200 300 400 500 600 700 800 900 1000 1100 1200 1300 *m/z*
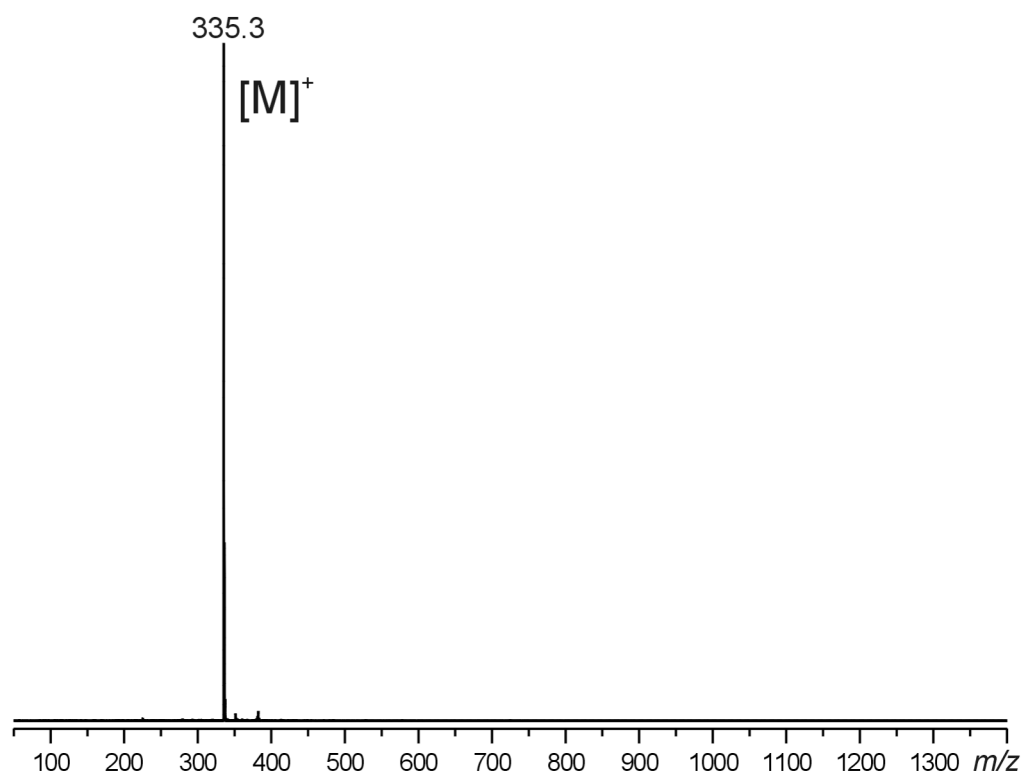
Figure S13: ESI-MS of salt **3**$^+$I$^-$
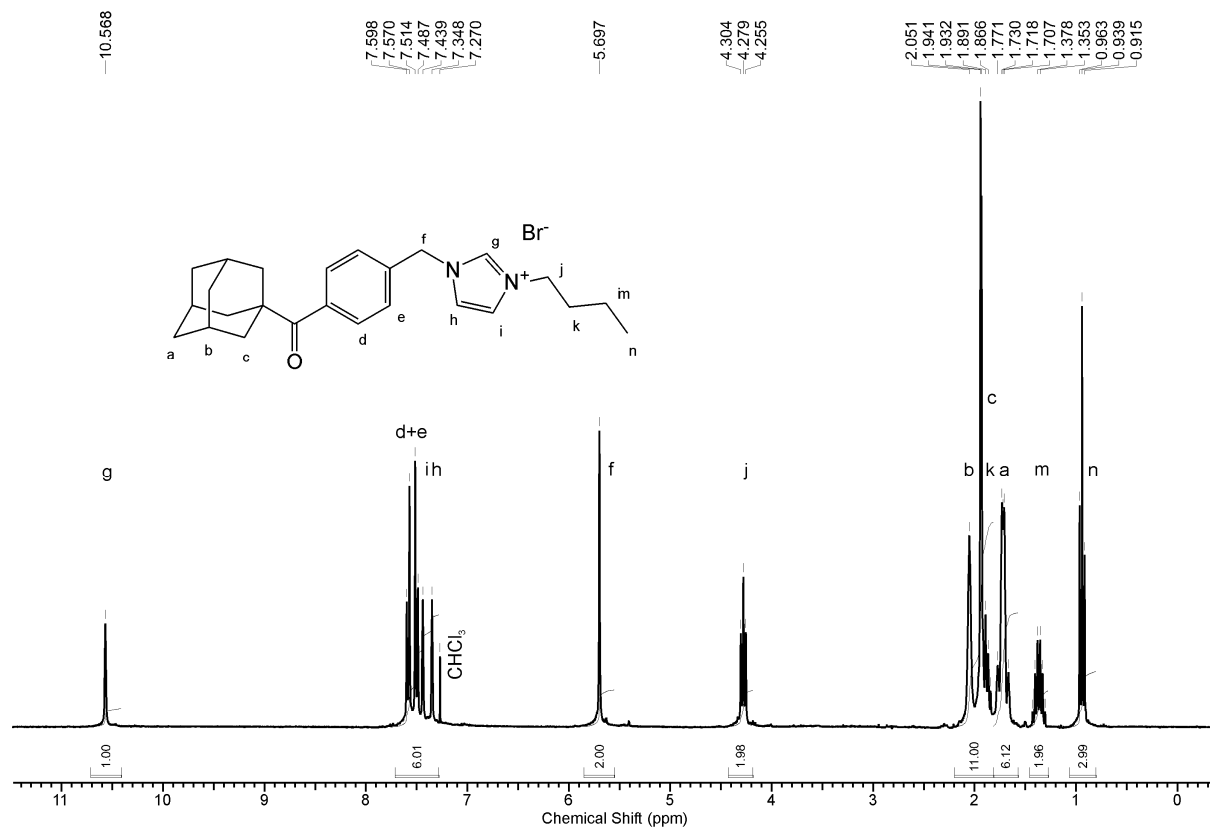
Figure S14: The ^{1}H NMR ([D$_6$]DMSO, 300 MHz) spectrum of salt **4$^+$Br$^-$**.
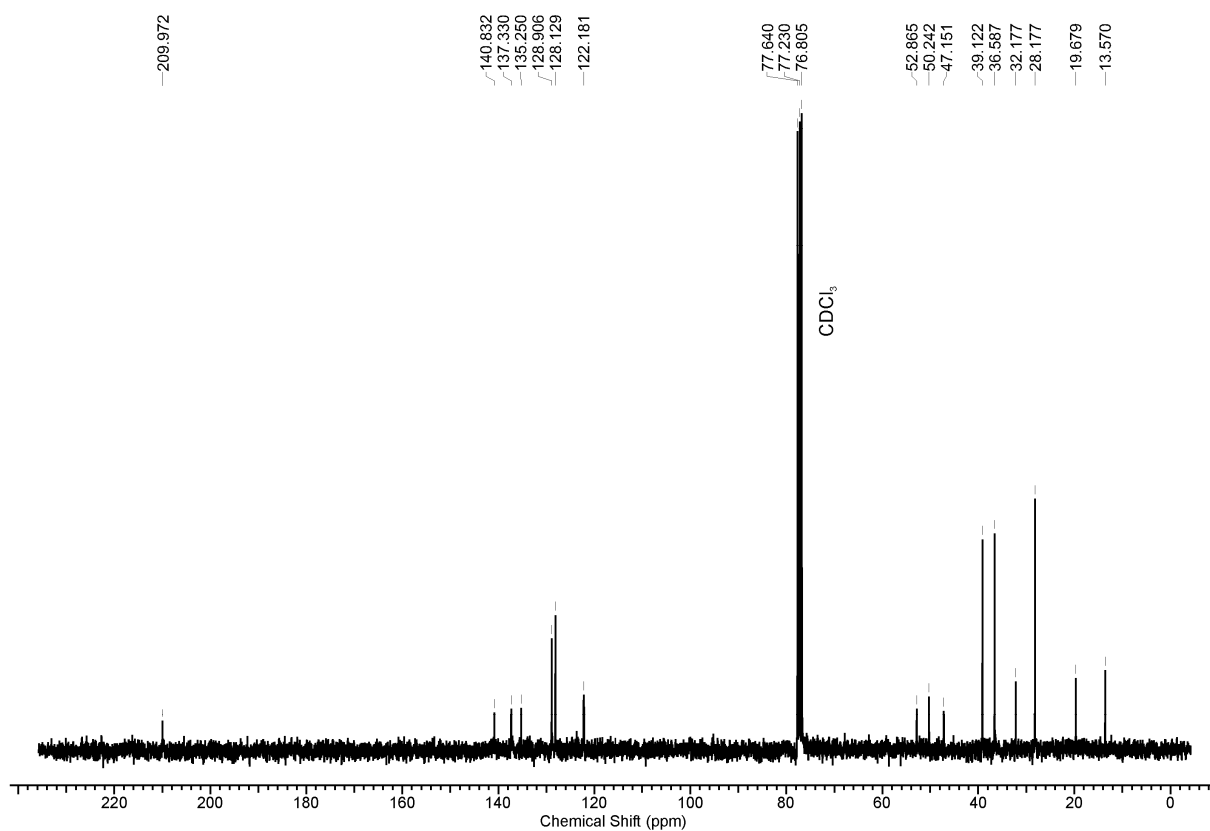
Figure S15 The ^{13}C NMR ([D$_6$]DMSO, 75 MHz) spectrum of salt **4$^+$Br$^-$**.
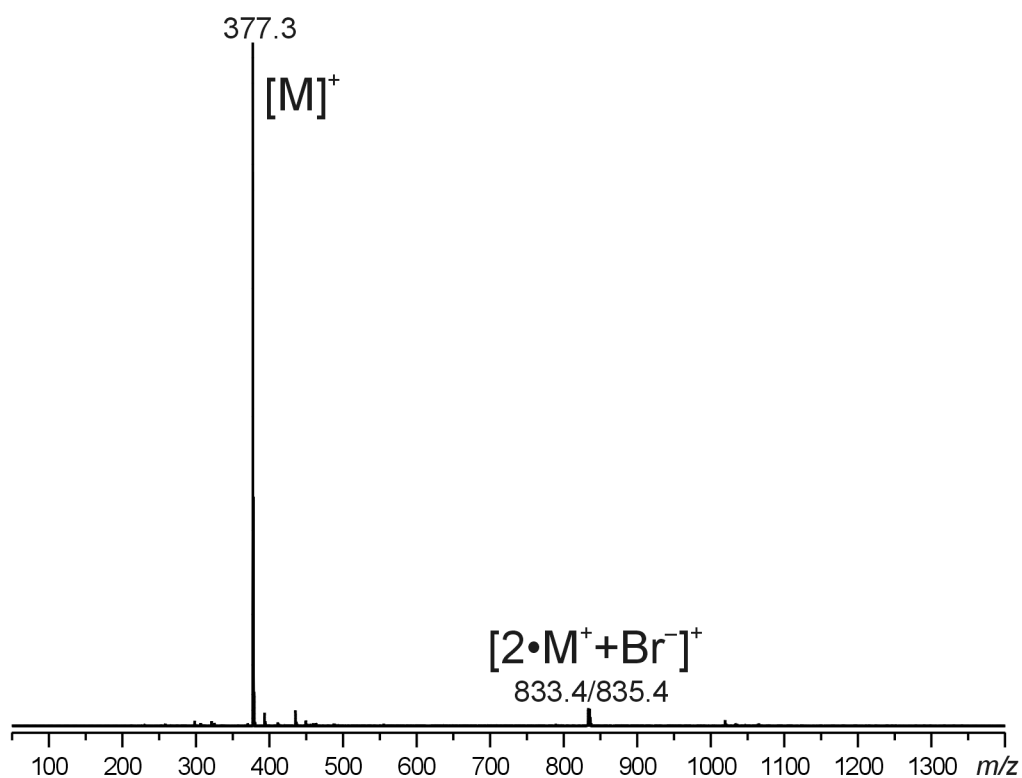
Figure S16: ESI-MS of salt **4**$^+$Br$^-$
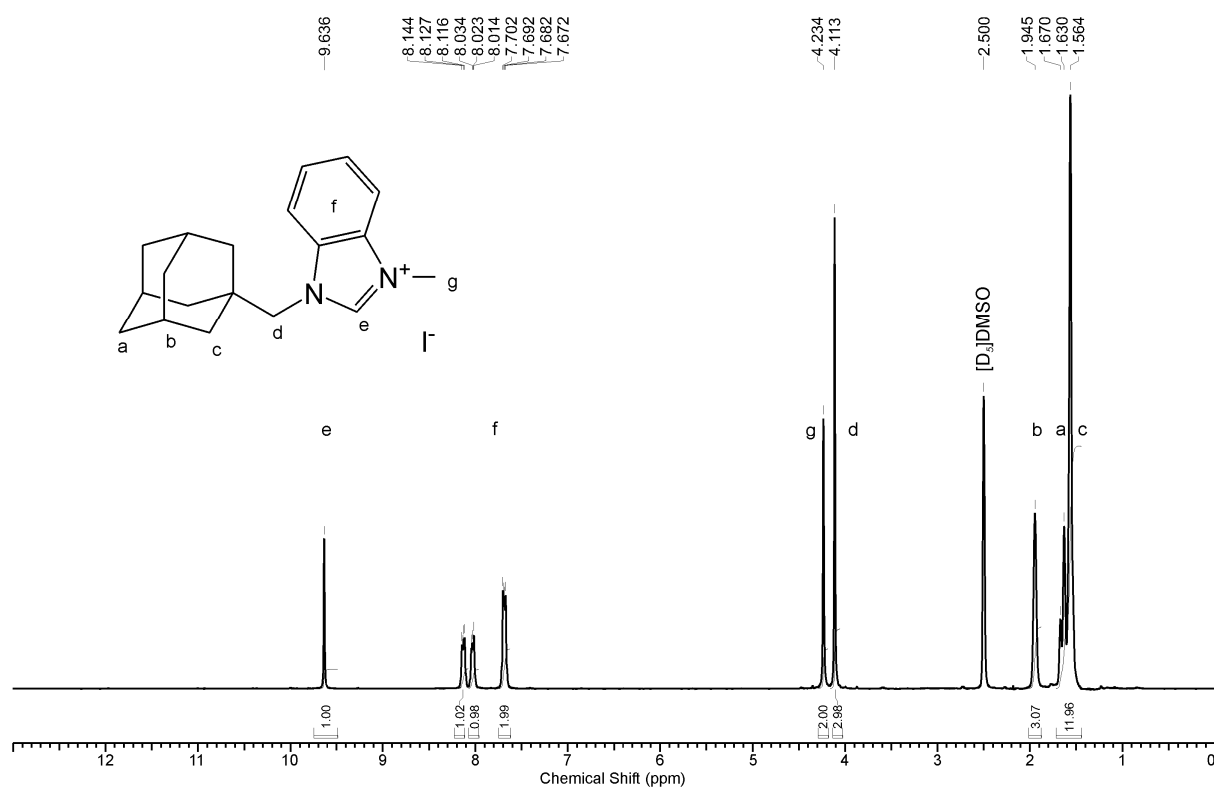
Figure S17: The ^{1}H NMR ([D$_6$]DMSO, 300 MHz) spectrum of salt **5**$^+$I$^-$.
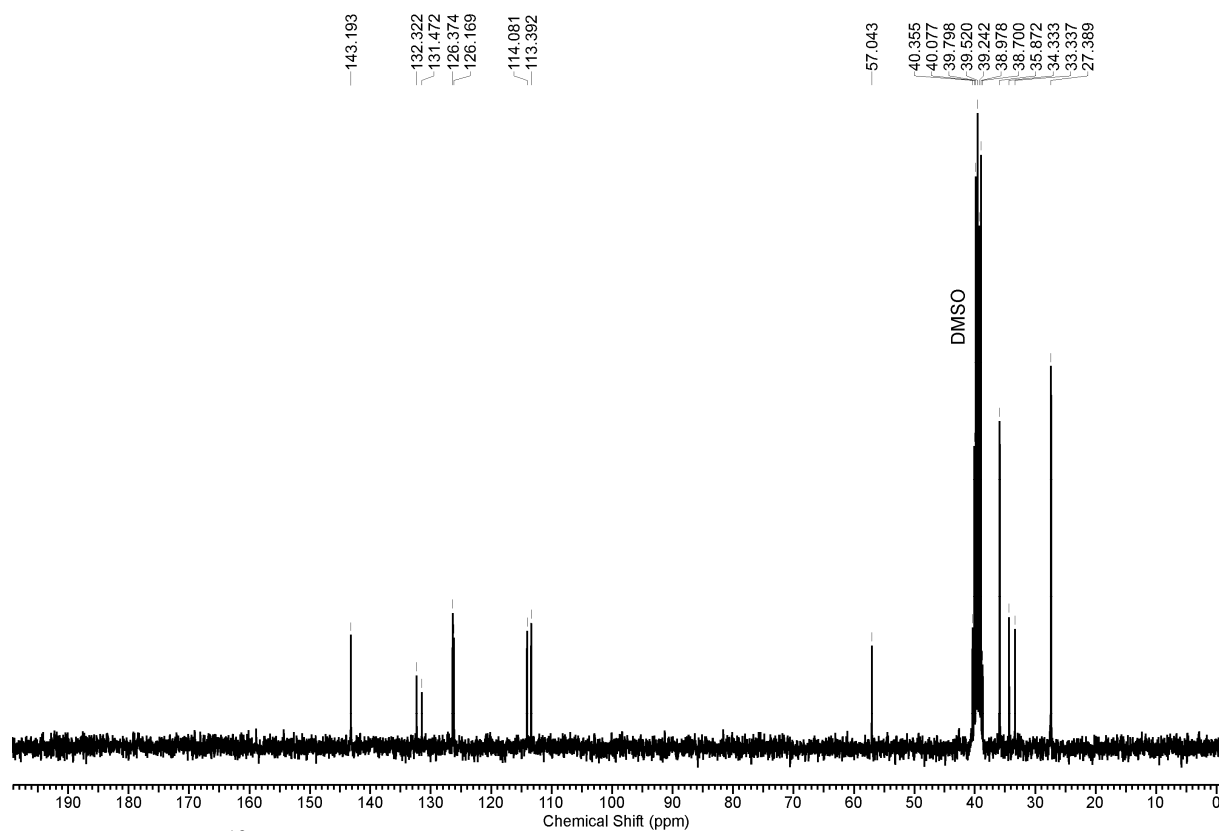
Figure S18: The ^{13}C NMR ([D$_6$]DMSO, 75 MHz) spectrum of salt **5**$^+$I$^-$.

281.2

[M]⁺

100 200 300 400 500 600 700 800 900 1000 1100 1200 1300 *m/z*
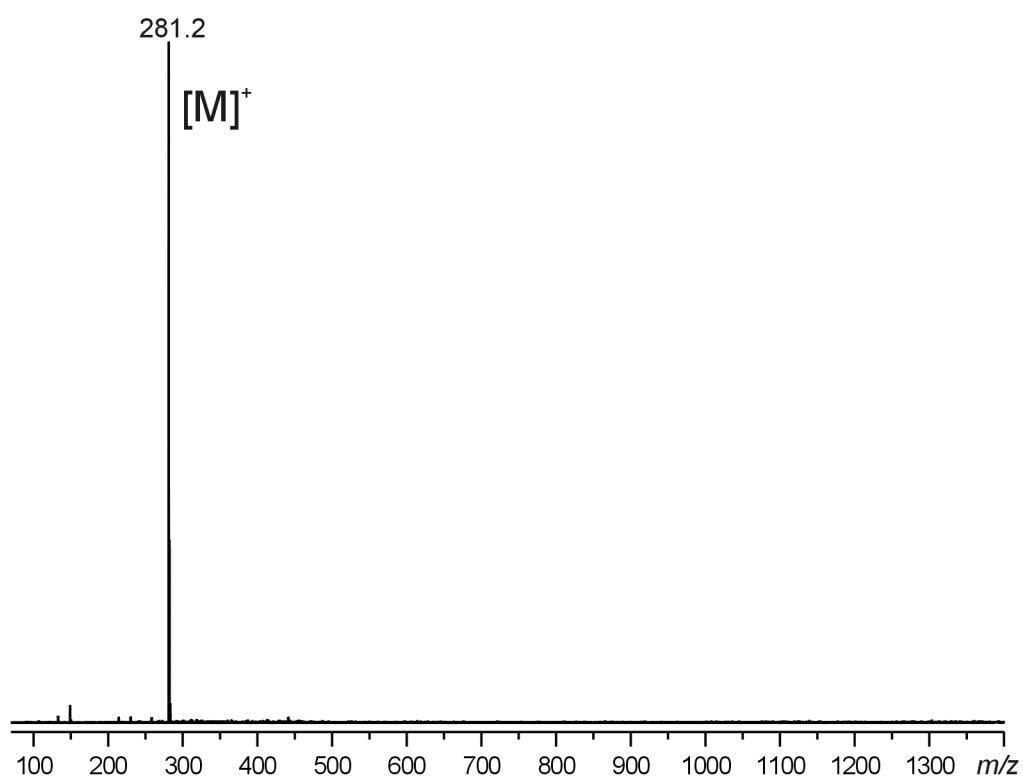
Figure S19: ESI-MS of salt **5**⁺I⁻
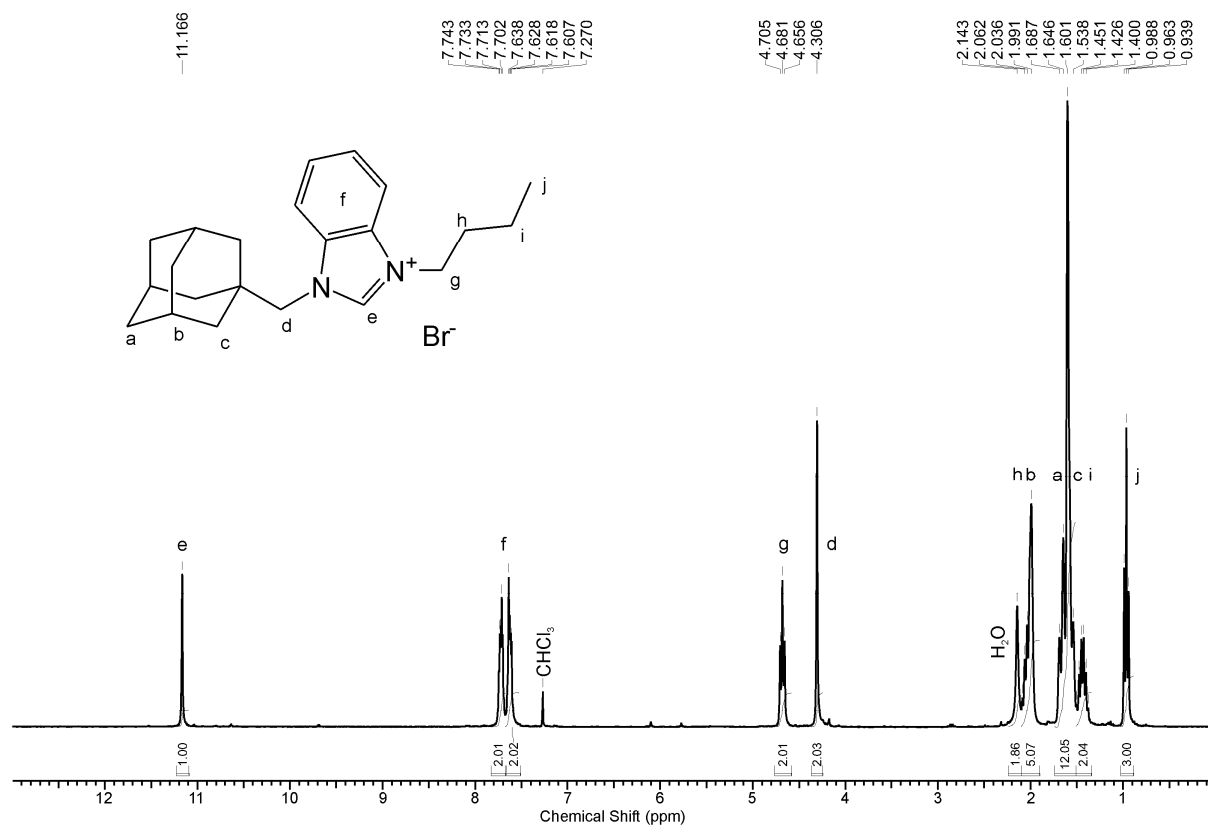
Figure S20: The ^{1}H NMR (CDCl$_3$, 300 MHz) spectrum of salt **6$^+$Br$^-$**.
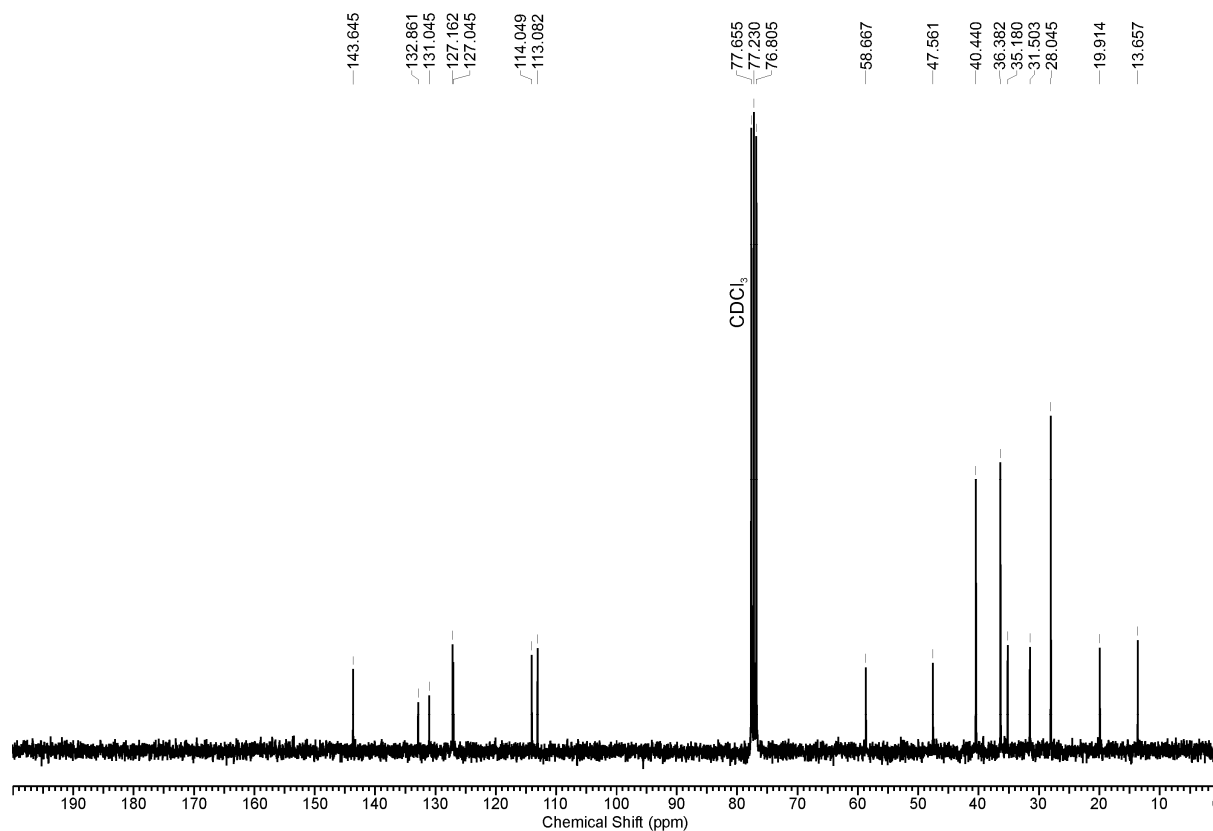
Figure S21: The ^{13}C NMR (CDCl$_3$, 75 MHz) spectrum of salt **6$^+$Br$^-$**.
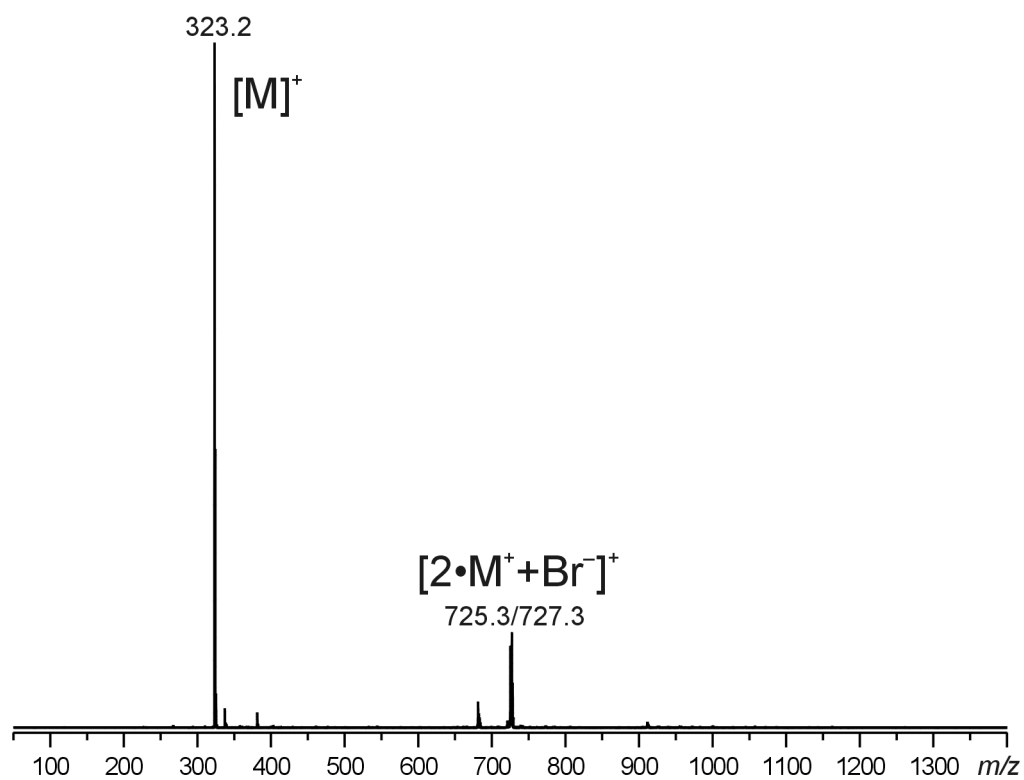
Figure S22: ESI-MS of salt **6**⁺Br⁻
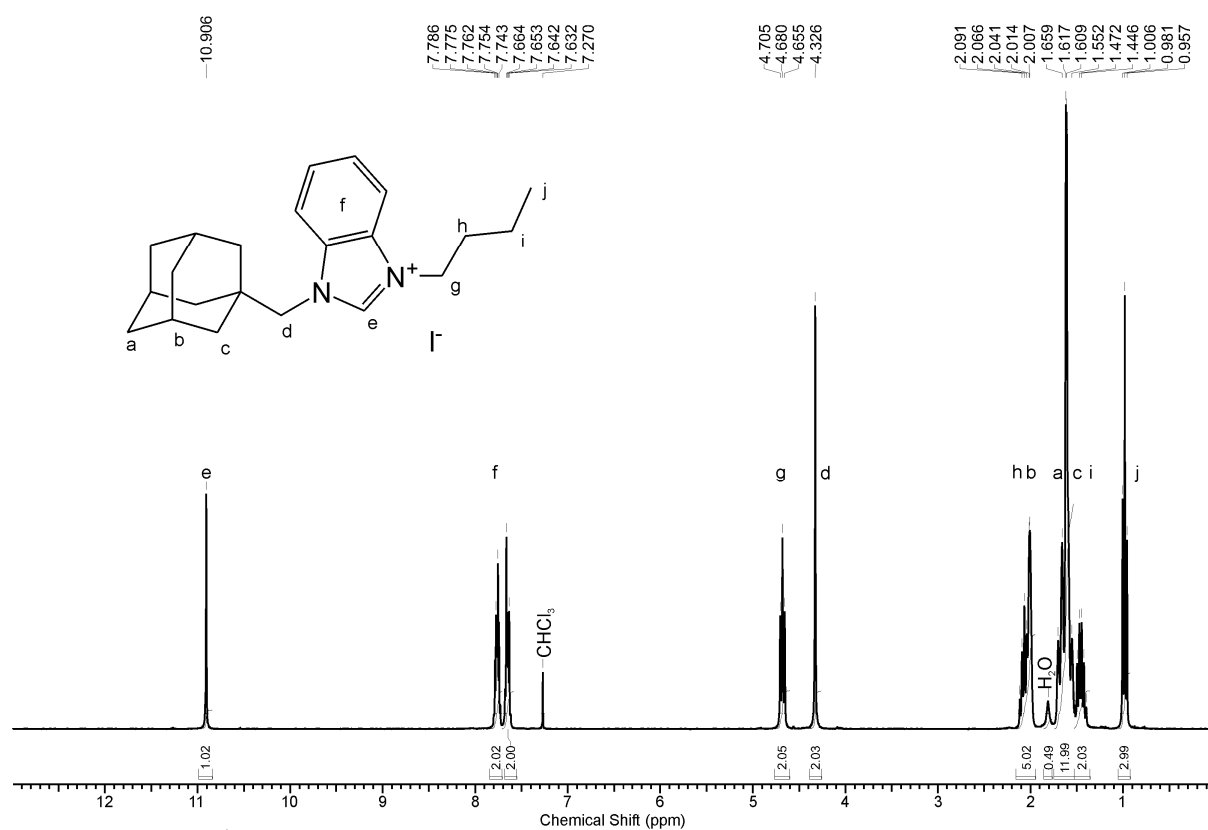
Figure S23: The ^{1}H NMR (CDCl$_3$, 300 MHz) spectrum of salt **6**$^+$I$^-$.
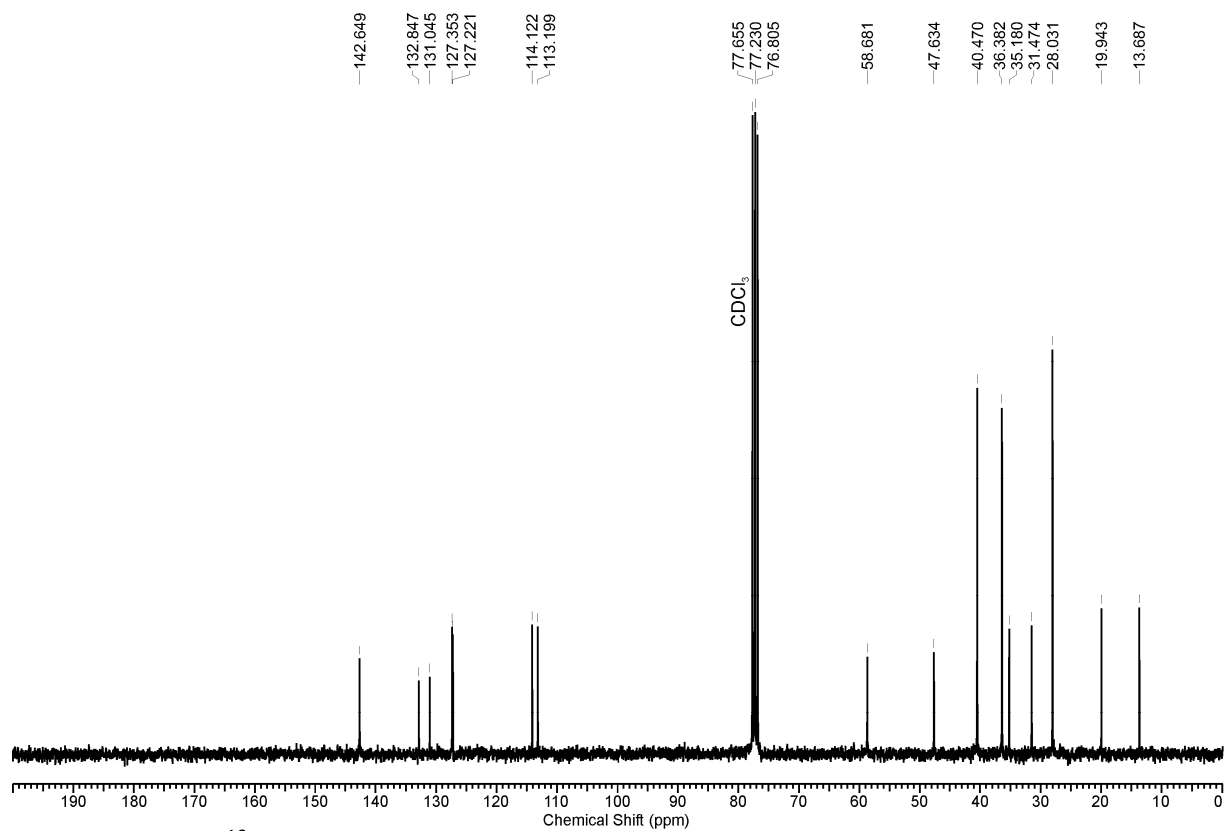
Figure S24: The ^{13}C NMR (CDCl$_3$, 75 MHz) spectrum of salt **6**$^+$I$^-$.
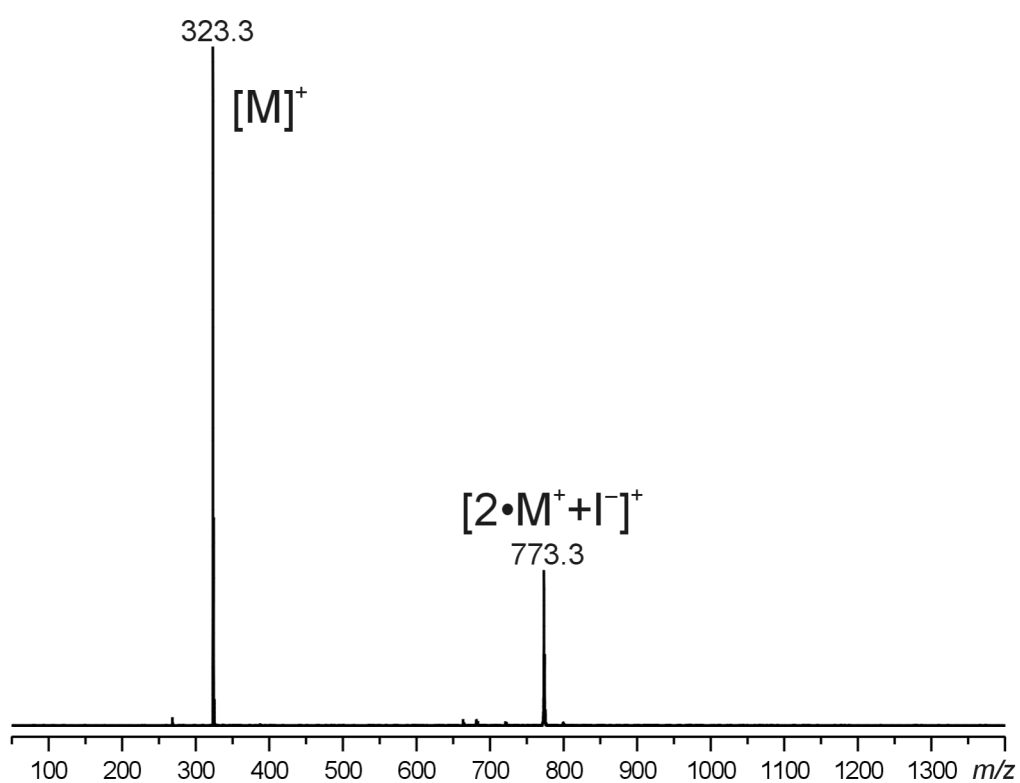
Figure S25: ESI-MS of salt **6**⁺I⁻
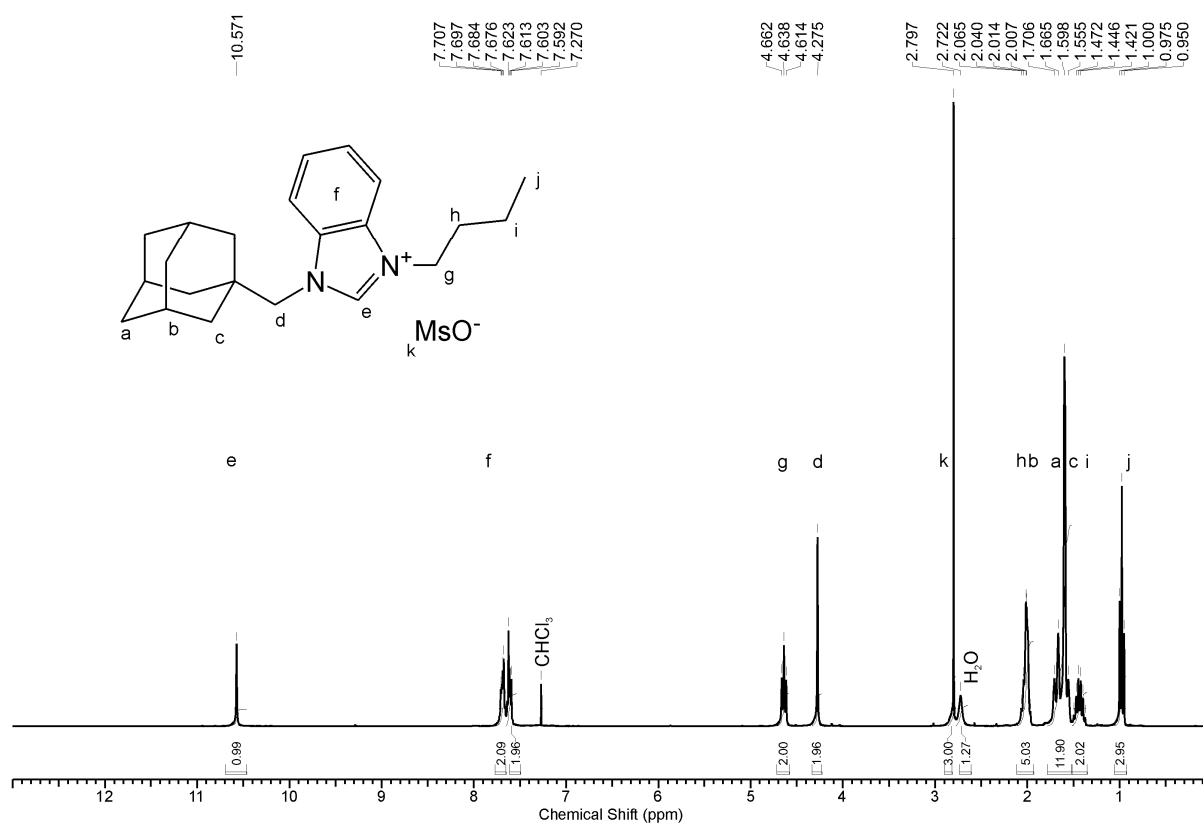
Figure S26: The ^{1}H NMR (CDCl$_3$, 300 MHz) spectrum of salt $\mathbf{6}^+$MsO$^-$.
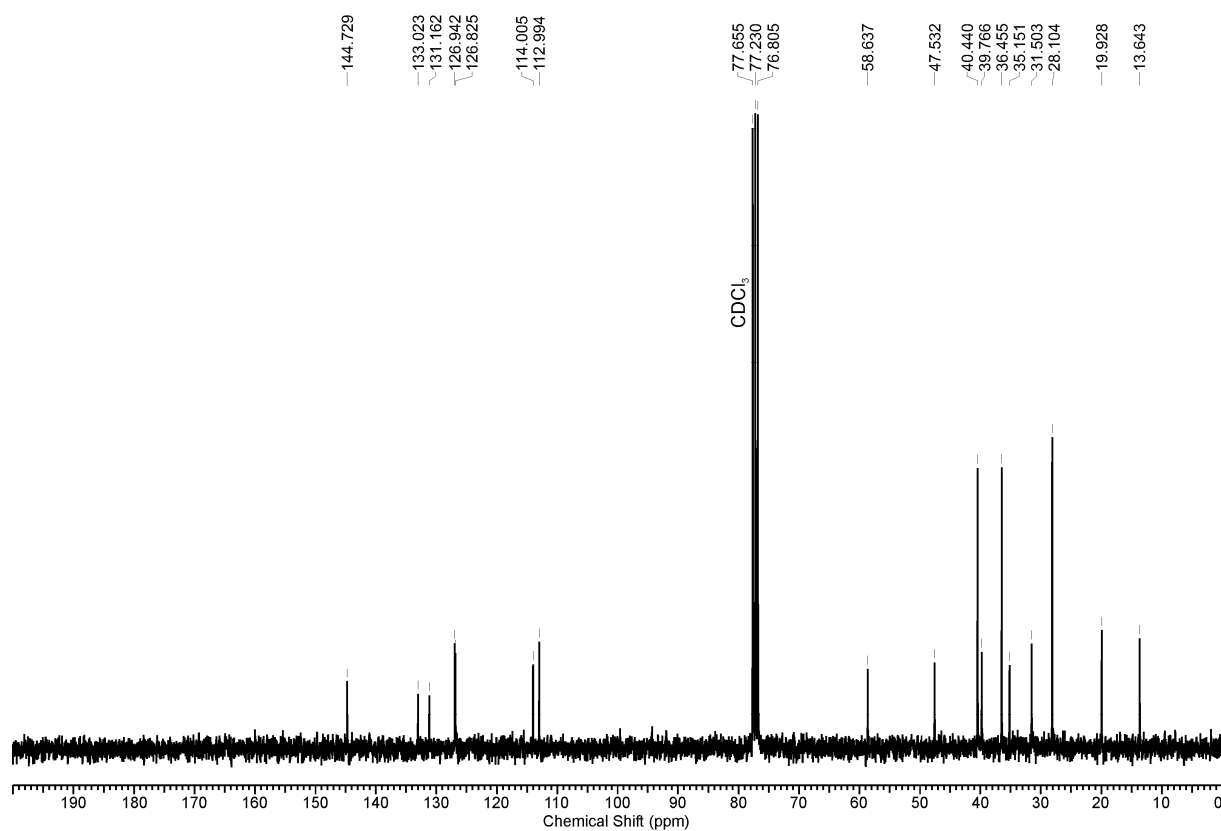
Figure S27: The ^{13}C NMR (CDCl$_3$, 75 MHz) spectrum of salt $\mathbf{6}^+$MsO$^-$.
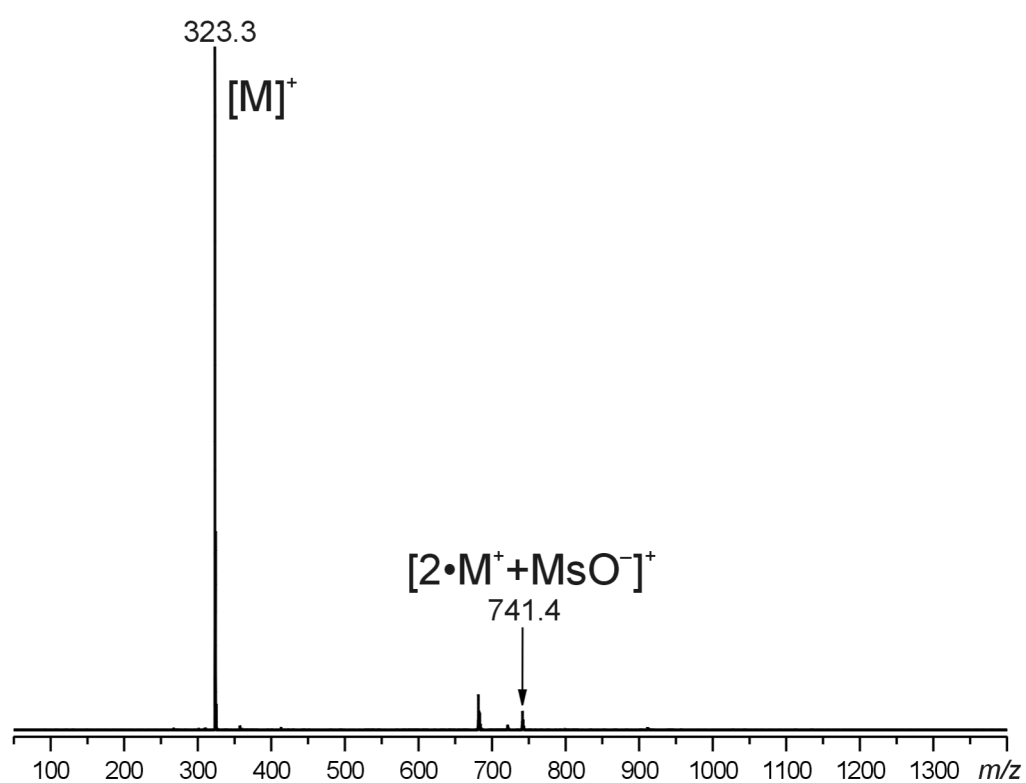
Figure S28: ESI-MS of salt **6**$^+$MsO$^-$
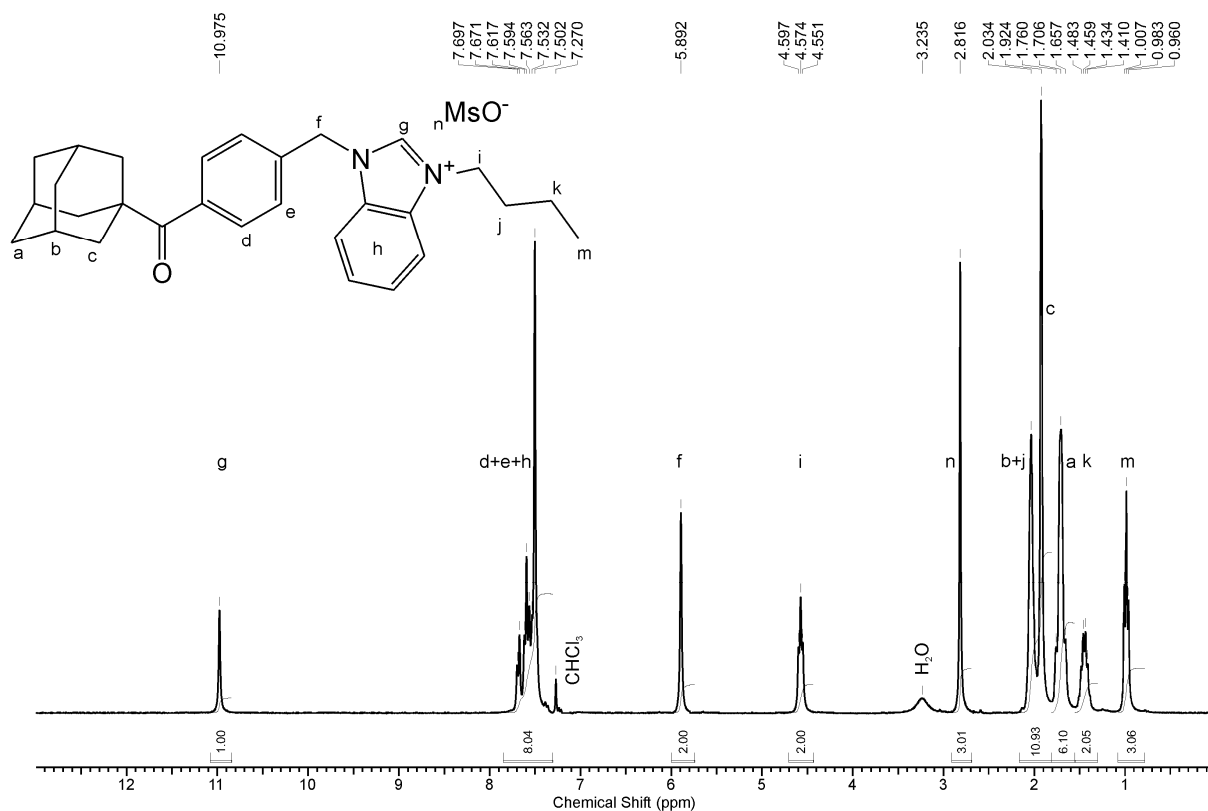
Figure S29: The ^{1}H NMR ([D$_6$]DMSO, 300 MHz) spectrum of salt $\mathbf{7^+}$MsO$^-$.
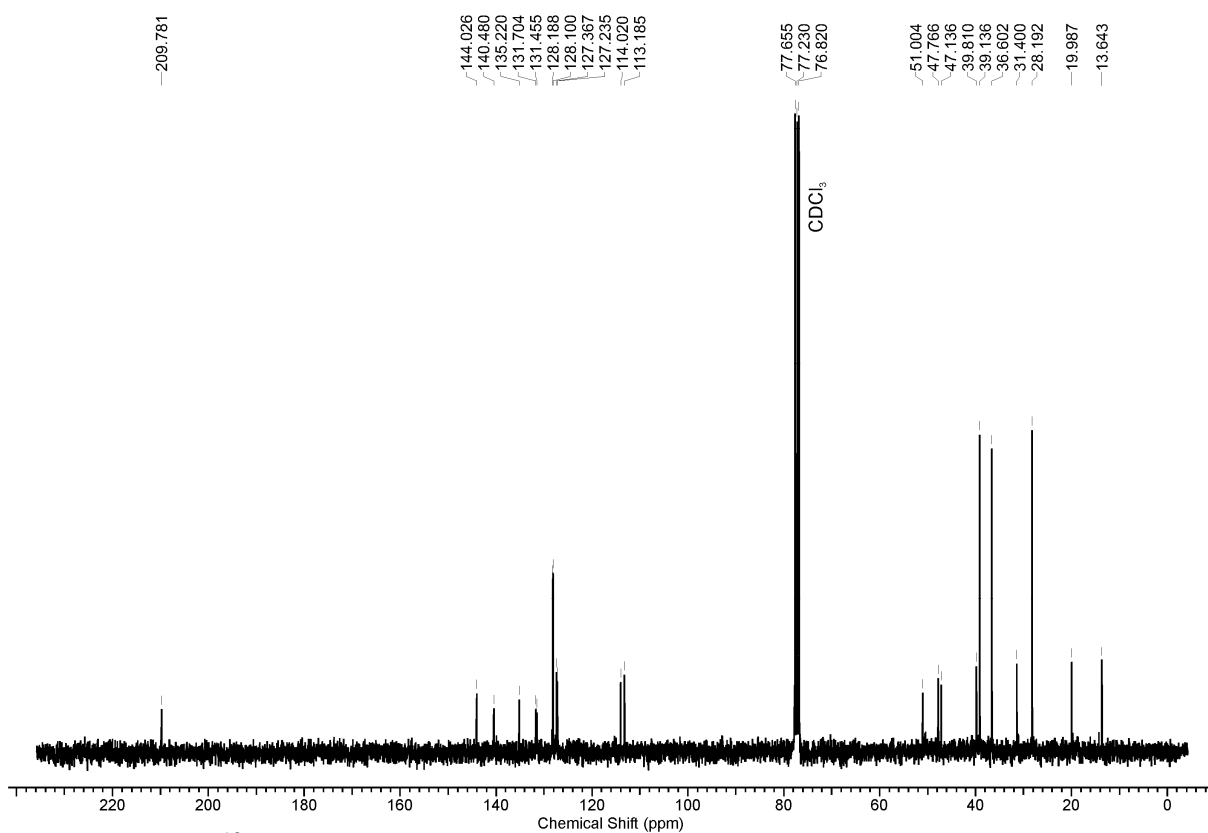
Figure S30: The ^{13}C NMR ([D$_6$]DMSO, 75 MHz) spectrum of salt $\mathbf{7^+}$MsO$^-$.

Branná, Černochová, Rouchal, Kulhánek, Babinský, Marek, Nečas, Kuřitka and Vícha

S.I.

Page S22
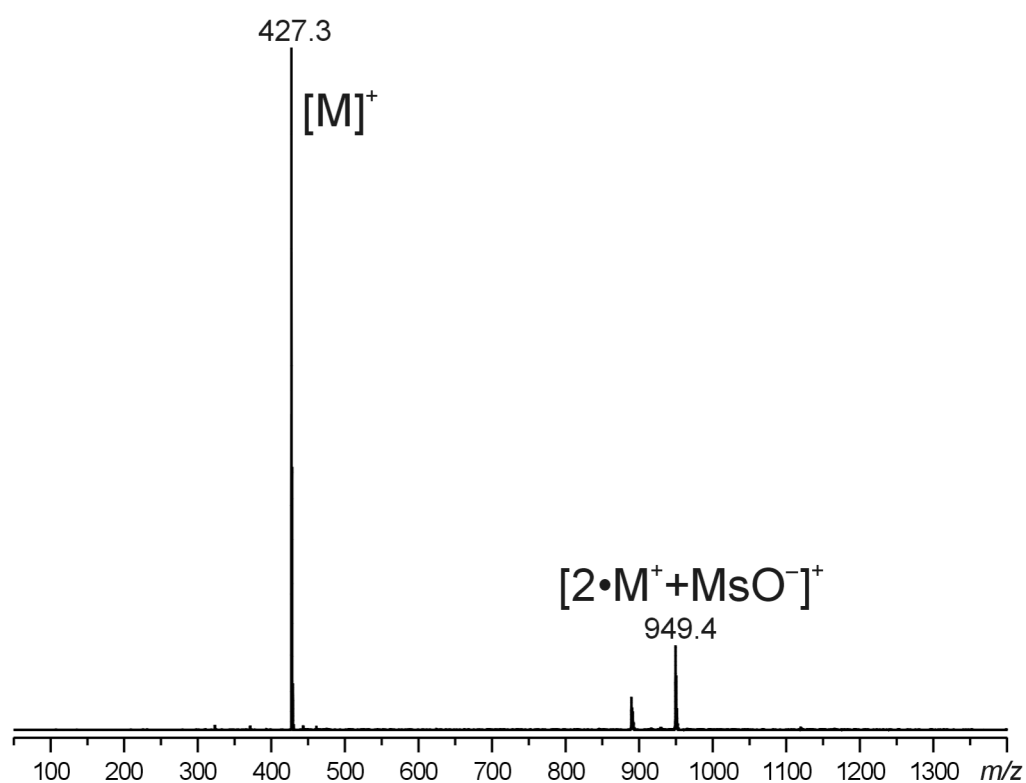
Figure S31: ESI-MS of salt **7**[+]MsO[−]

Table S1. X-ray diffraction analysis of salts 6^+I^- and 6^+MsO^-

Compound		$6^+I^-\cdot H_2O$	$6^+MsO^-\cdot H_2O$
CCDC reference no.		1009676	1009677
Empirical formula		$C_{22}H_{33}IN_2O$	$C_{23}H_{36}N_2O_4S$
Formula weight		468.40	436.60
Color, shape		colorless, block	colorless, block
Crystal size		0.40×0.40×0.30	0.40×0.40×0.30
Measured temperature (K)		120(2)	120(2)
Crystal system		monoclinic	monoclinic
Space group		$P2_1/c$	$C2/c$
Unit cell dimensions (Å, °)	a	11.5996(2)	27.482(2)
	b	17.8298(3)	10.0377(5)
	c	10.5067(2)	20.0803(15)
	$\alpha = \gamma$	90.00	90.00
	β	90.025(2)	124.255(11)
Volume ($Å^3$)		2172.98(7)	4578.4(6)
Z		4	8
D_x (g·cm^{-3})		1.432	1.267
Absorption coefficient μ (mm^{-1})		1.486	0.173
Absorption corrections		0.745–1.000	0.934–0.950
$F(000)$		960	1888
θ range for data collection (°)		3.43–25.00	3.00–25.00
Completeness to θ (%)		0.998	0.998
h, k, l		$-13 \le h \le 13$	$-32 \le h \le 18$
		$-20 \le k \le 21$	$-11 \le k \le 9$
		$-11 \le l \le 12$	$-20 \le l \le 23$
Reflections collected		26268	9046
Reflections unique		3822[R(int)=0.0211]	4026[R(int)=0.0160]
Unique reflections with $I \ge \sigma(I)$		3670	2744
Number of parameters		253	281
Goodness-of-fit on F^2		1.039	0.972
Final R indices [$I \ge \sigma(I)$]		R_1=0.0171, wR_2=0.0445	R_1=0.0373, wR_2=0.0921
R indices (all data)		R_1=0.0181, wR_2=0.0447	R_1=0.0584, wR_2=0.0956
Residual highest peak and deepest hole (eÅ^{-3})		0.642 and −0.281	0.365 and −0.459
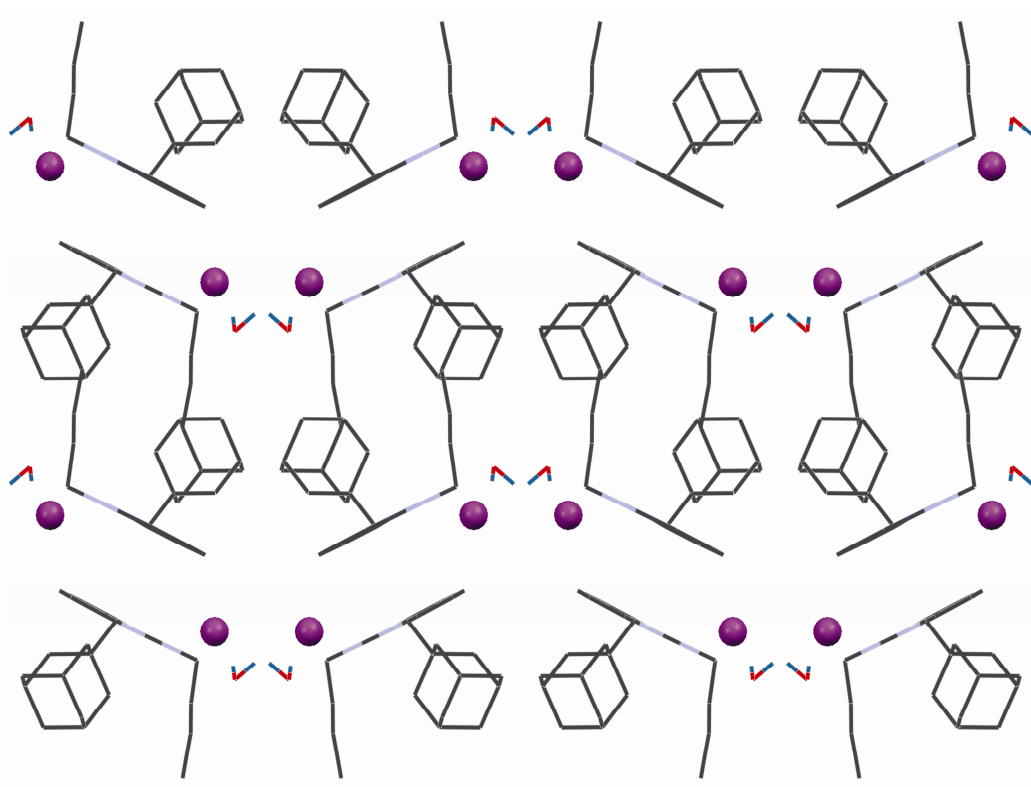
Figure S32: Crystal packing of the compound **6**$^+$I$^-$·H$_2$O viewed down the *c*-axis. Iodine atoms at the more populated positions [0.9457(8)] are displayed as a spheres at arbitrary radii. H-atoms have been omitted for clarity (with the exception to those constituting the water molecules).
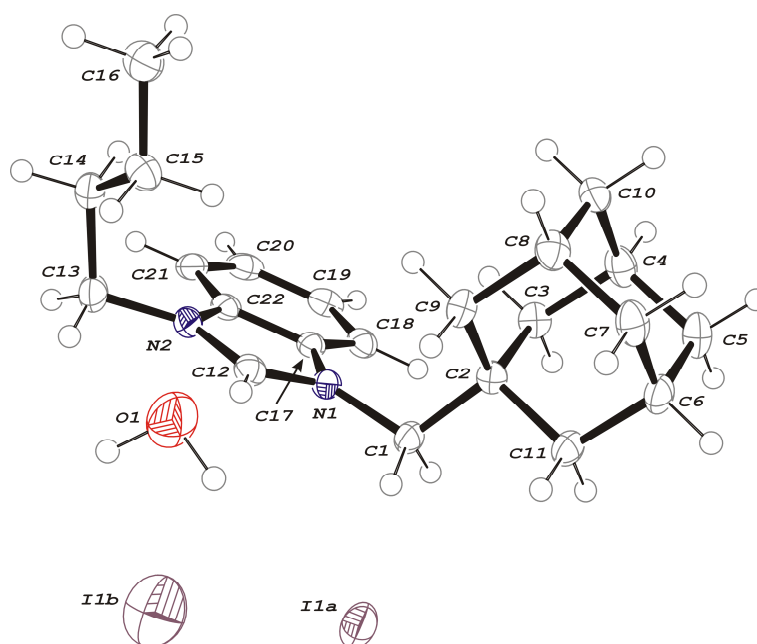
Figure S33: The asymmetric unit of the crystal of **6**$^+$I$^-$·H$_2$O. Anisotropic thermal ellipsoids have been drawn at the 50% probability level.
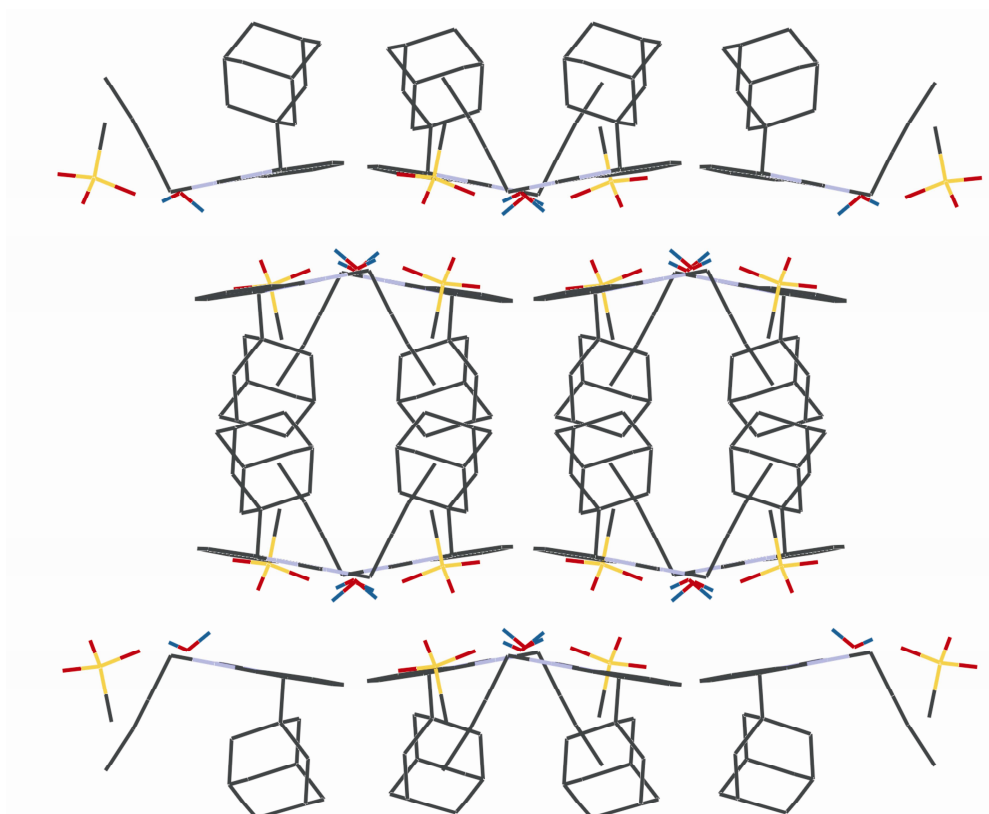
Figure S34: Crystal packing of the compound **6**$^+$MsO$^-$·H_2O viewed down the *c*-axis. H-atoms have been omitted for clarity (with the exception to those constituting the water molecules).
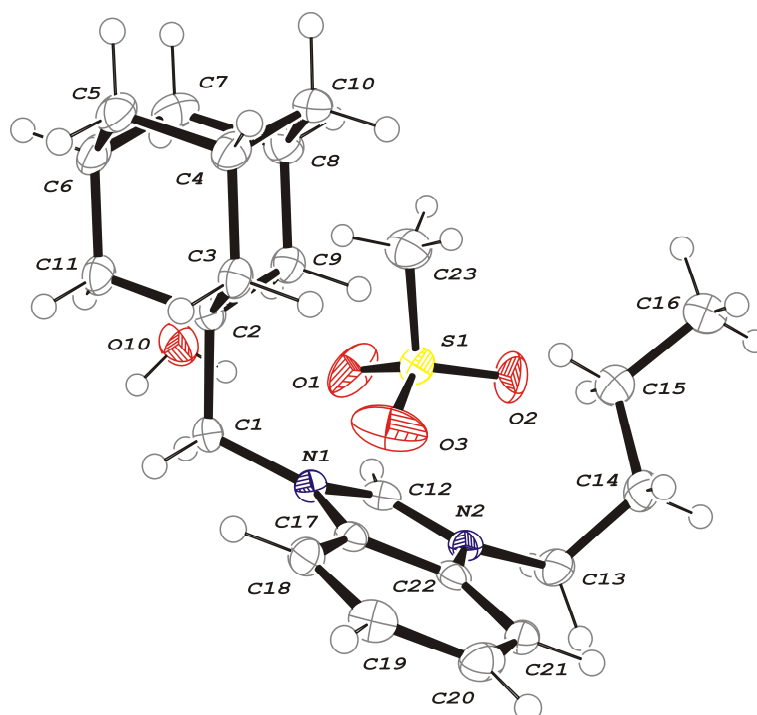
Figure S35: The asymmetric unit of the crystal of **6**$^+$MsO$^-$·H_2O. Anisotropic thermal ellipsoids have been drawn at the 50% probability level.
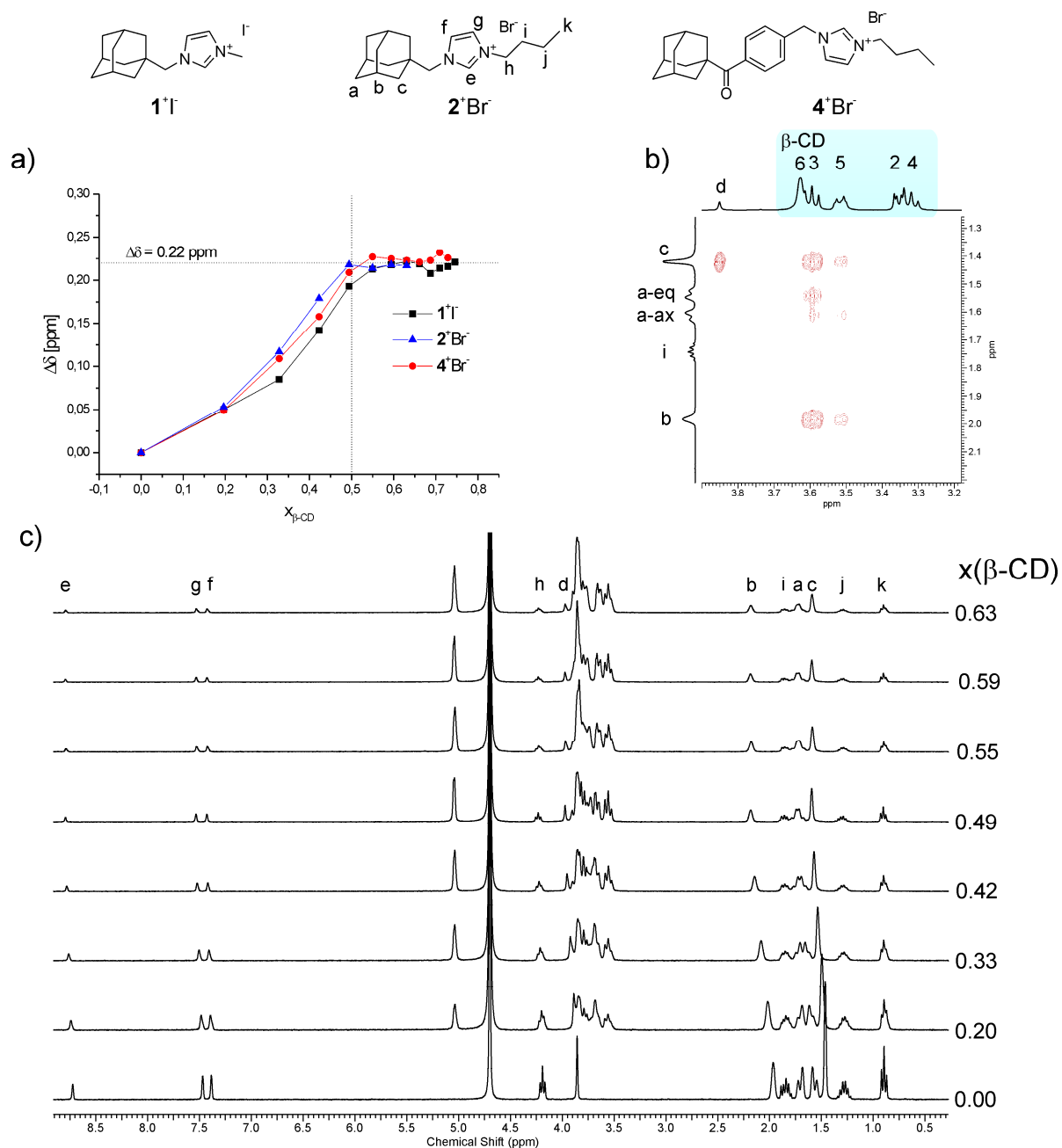
Figure S36: Typical results of ^{1}H NMR titration of imidazolium guests with β-CD in D_2O at 30°C. a) Plot of complexation induced shift of H^b against host molar ratio. b) Partial ROESY spectrum (500 MHz) of equimolar mixture of 2^+Br^- and β-CD. c) A stacking plot of ^{1}H NMR spectra (300 MHz) of mixtures of 2^+Br^- with β-CD, molar ratio x(β-CD) is given next to corresponding line.
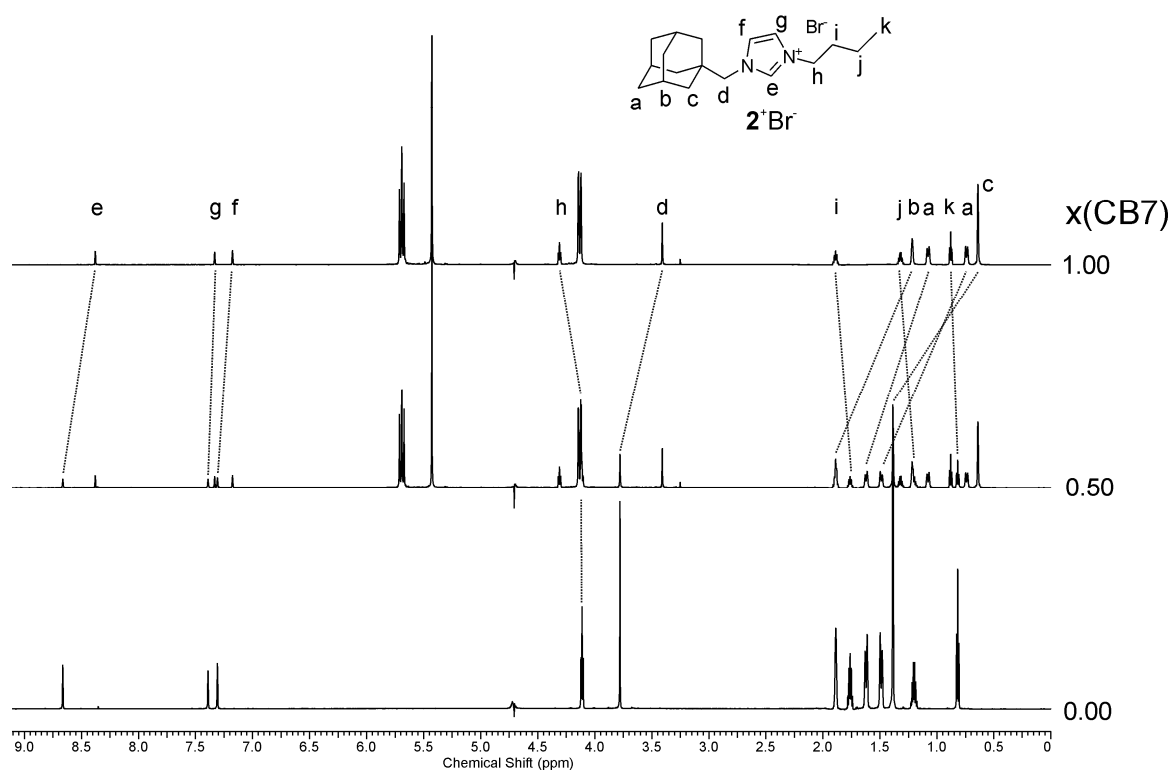
Figure S37: Stacking plot of ^{1}H NMR spectra (700 MHz) of mixtures of **2$^+$Br$^-$** with CB7 in D$_2$O at 30°C, molar ratio x(CB7) is given next to corresponding line. Signals assignment is based on 2D ROESY spectrum of mixture where x(CB7)=0.5.
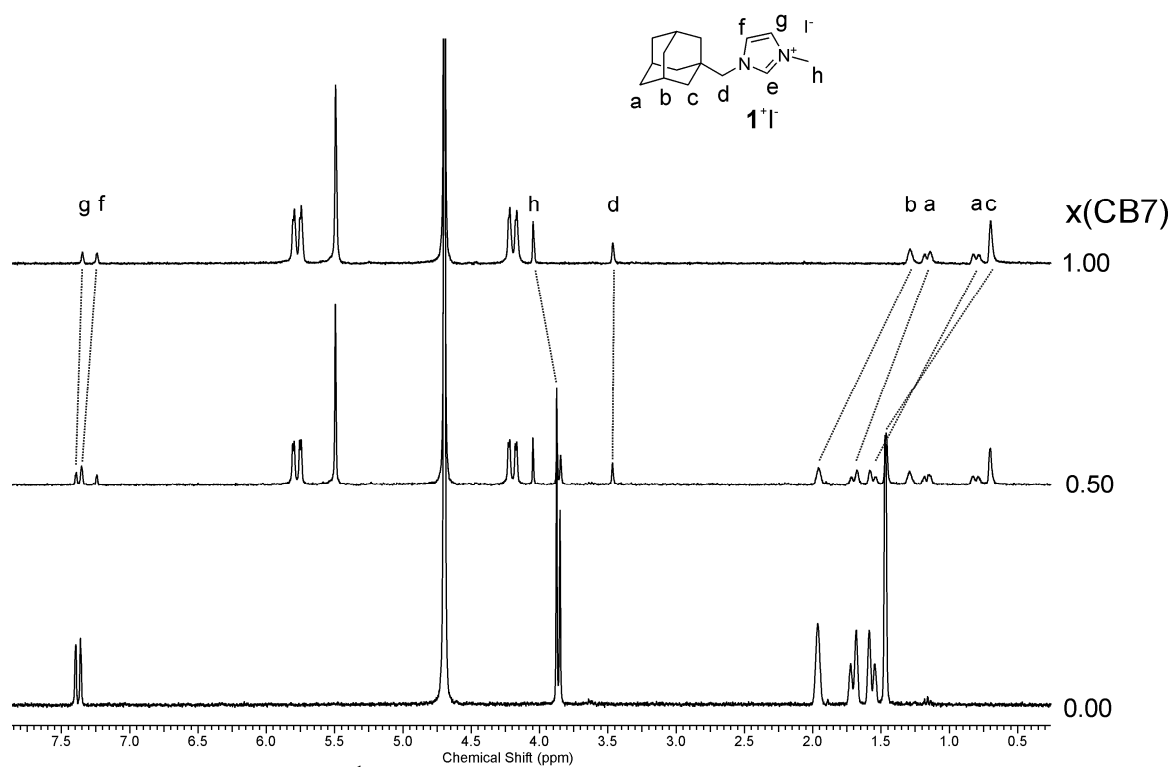
Figure S38: Stacking plot of ^{1}H NMR spectra (300 MHz) of mixtures of **1$^+$I$^-$** with CB7 in D$_2$O at 30°C, molar ratio x(CB7) is given next to corresponding line. Signals assignment is based on 2D ROESY spectrum of mixture where x(CB7)=0.5.

Branná, Černochová, Rouchal, Kulhánek, Babinský, Marek, Nečas, Kuřitka and Vícha

S.I.
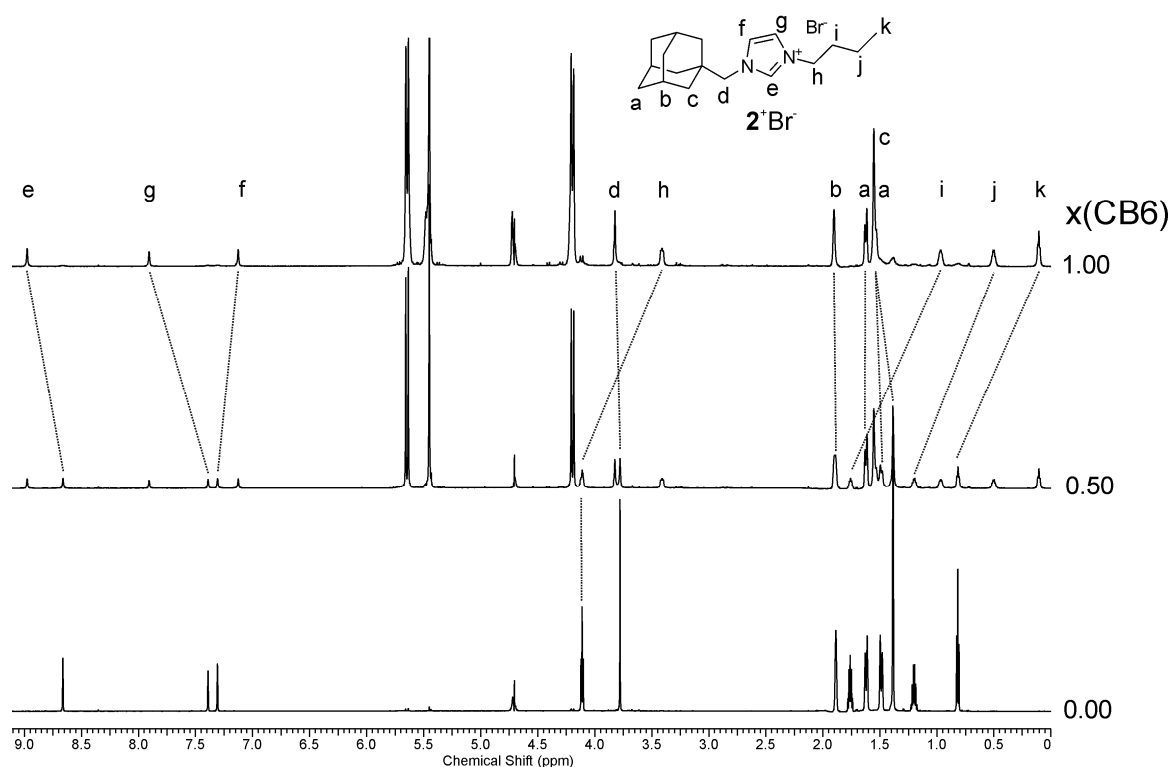
Figure S39: Stacking plot of ^{1}H NMR spectra (700 MHz) of mixtures of **2$^+$Br$^-$** with CB6 in 50 mM NaCl in D$_2$O at 30°C, molar ratio x(CB6) is given next to corresponding line. Signals assignment is based on 2D ROESY spectrum of mixture where x(CB6)=0.5.
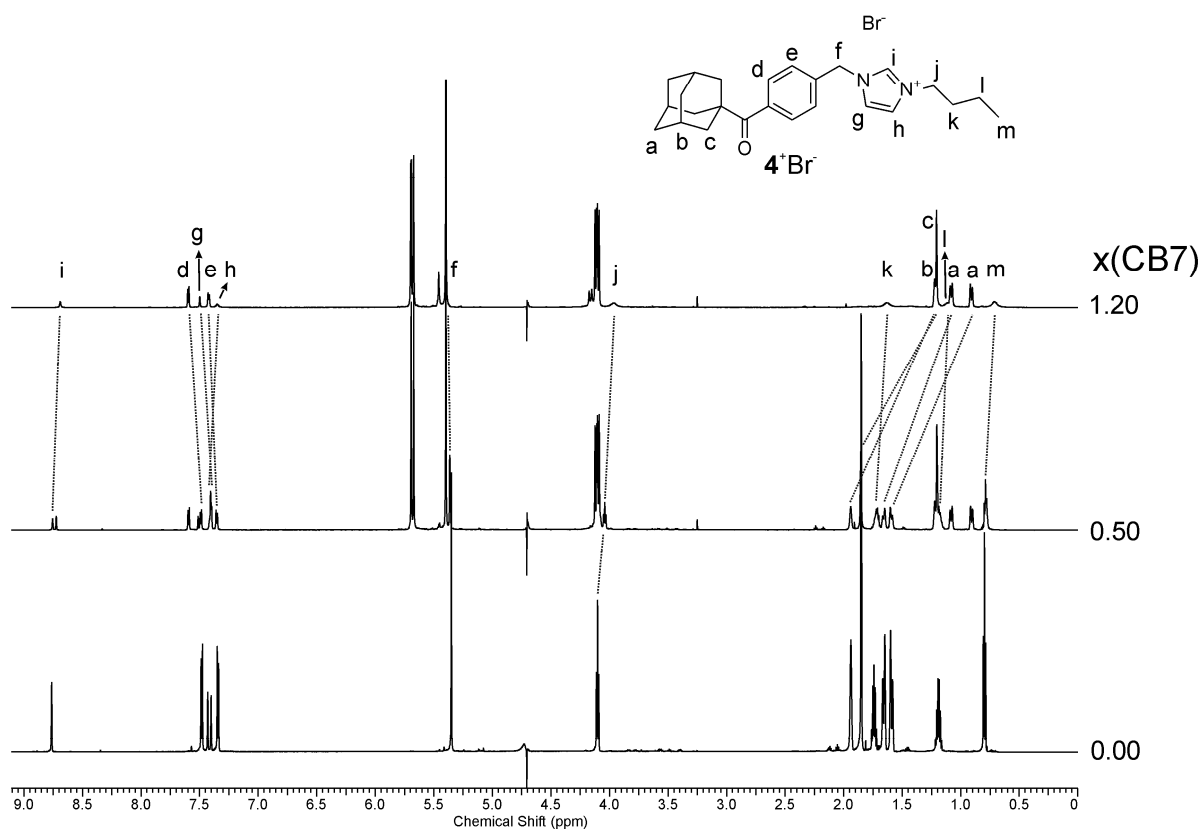
Figure S40: Stacking plot of ^{1}H NMR spectra (700 MHz) of mixtures of **4$^+$Br$^-$** with CB7 in D$_2$O at 30°C, molar ratio x(CB7) is given next to corresponding line. Signals assignment is based on 2D ROESY spectrum of mixture where x(CB7)=0.5.
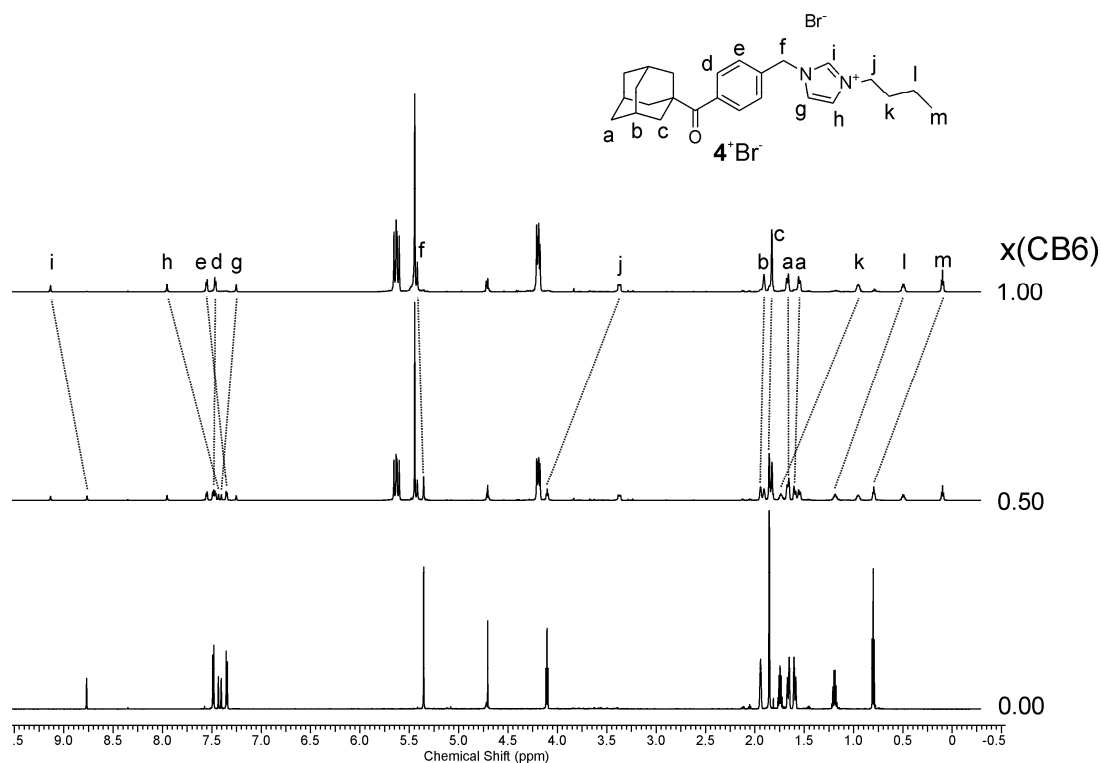
Figure S41: Stacking plot of ^{1}H NMR spectra (700 MHz) of mixtures of **4**$^+$Br$^-$ with CB6 in 50mM NaCl in D$_2$O at 30°C, molar ratio x(CB6) is given next to corresponding line. Signals assignment is based on 2D ROESY spectrum of mixture where x(CB6)=0.5.
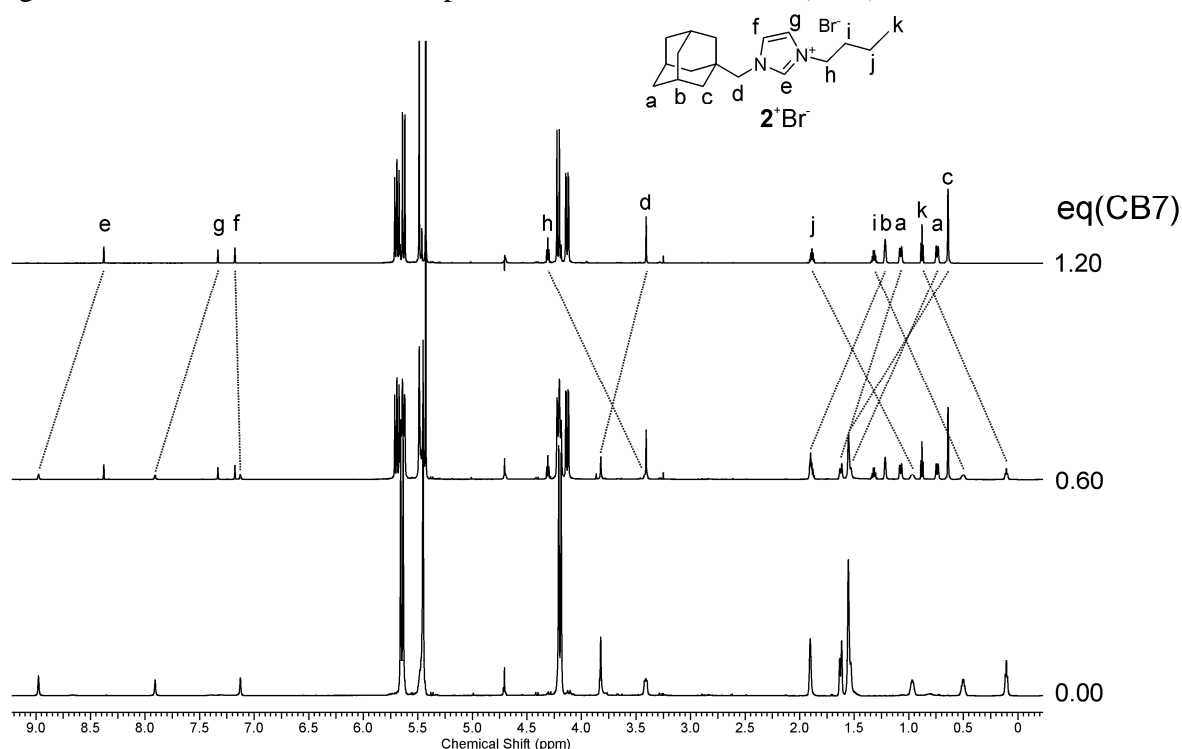
Figure S42: Stacking plot of ^{1}H NMR spectra (700 MHz) of mixtures of **2**$^+$Br$^-$@CB6 with CB7 in 50mM NaCl in D$_2$O at 30°C, number of CB7 equivalents (eq) is given next to corresponding line. Signals assignment is based on 2D ROESY spectrum of mixture where eq(CB7)=0.6.
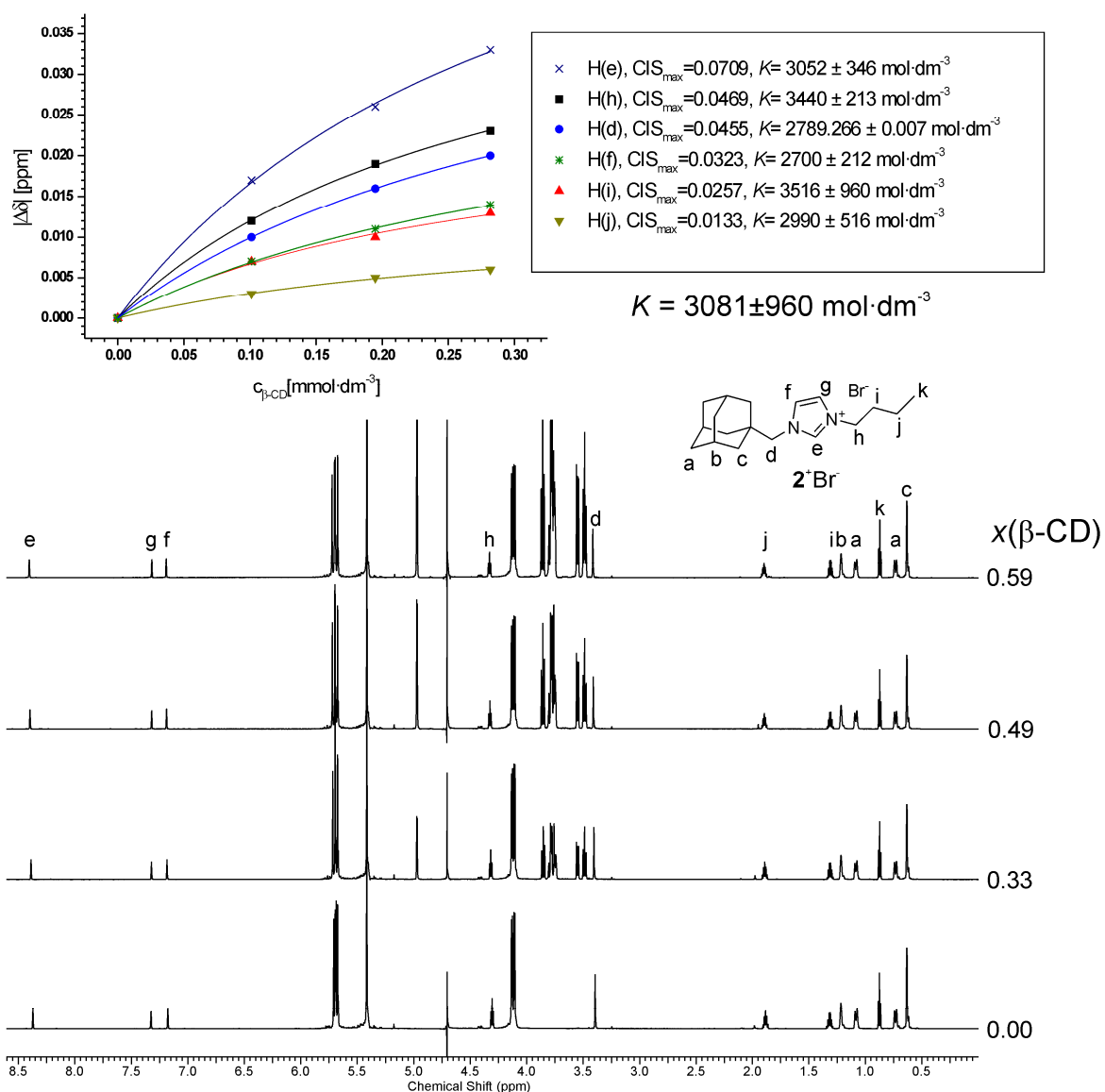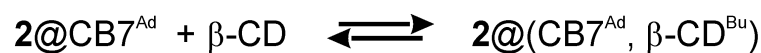
Figure S43: Stacking plot of ^{1}H NMR spectra (700 MHz) of mixtures of $\mathbf{2^+Br^-}$@CB7 with β-CD in D$_2$O at 30°C, molar ratio x(β−CD is given next to corresponding line.
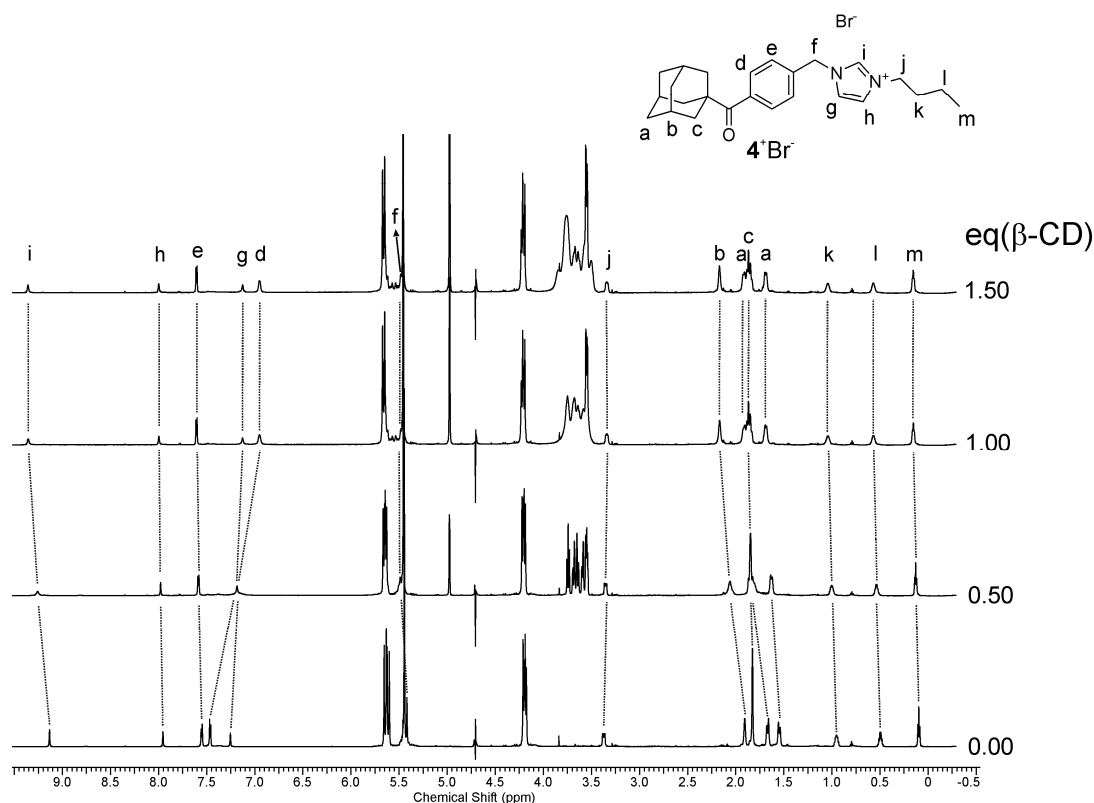
Figure S44: Stacking plot of ^{1}H NMR spectra (700 MHz) of mixtures of $\mathbf{4^+Br^-}$@CB6 with β-CD in 50 mM NaCl in D$_2$O at 30°C, the number of β-CD equivalents is given next to corresponding line. Signals assignment is based on 2D ROESY spectrum of mixture where eq(β-CD)=1.5.
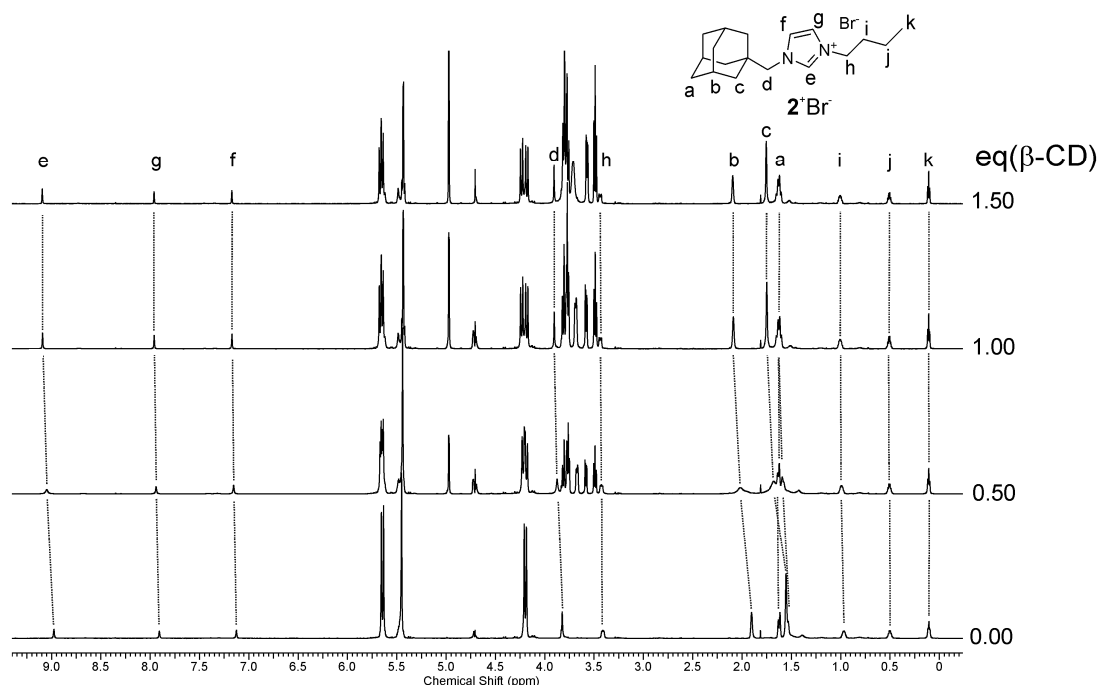
Figure S45: Stacking plot of ^{1}H NMR spectra (700 MHz) of mixtures of $\mathbf{2^+Br^-}$@CB6 with β-CD in 50 mM NaCl in D$_2$O at 30°C, the number of β-CD equivalents is given next to corresponding line. Signals assignment is based on 2D ROESY spectrum of mixture where eq(β-CD)=1.5.
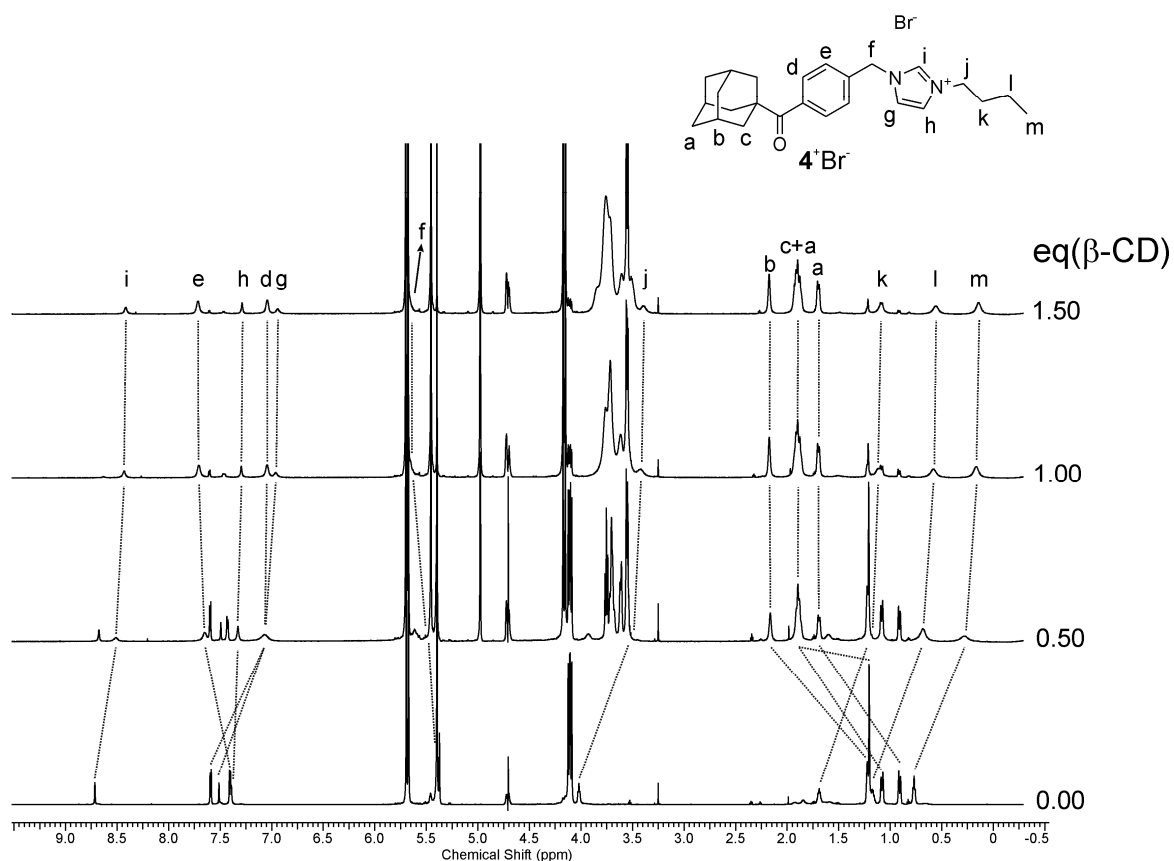
Figure S46: Stacking plot of ^{1}H NMR spectra (700 MHz) of mixtures of **4^{+}Br^{-}@CB7** with β-CD in 50 mM NaCl in D$_2$O at 30°C, the number of β-CD equivalents is given next to corresponding line. Signals assignment is based on 2D ROESY spectrum of mixture where eq(β-CD)=1.5.
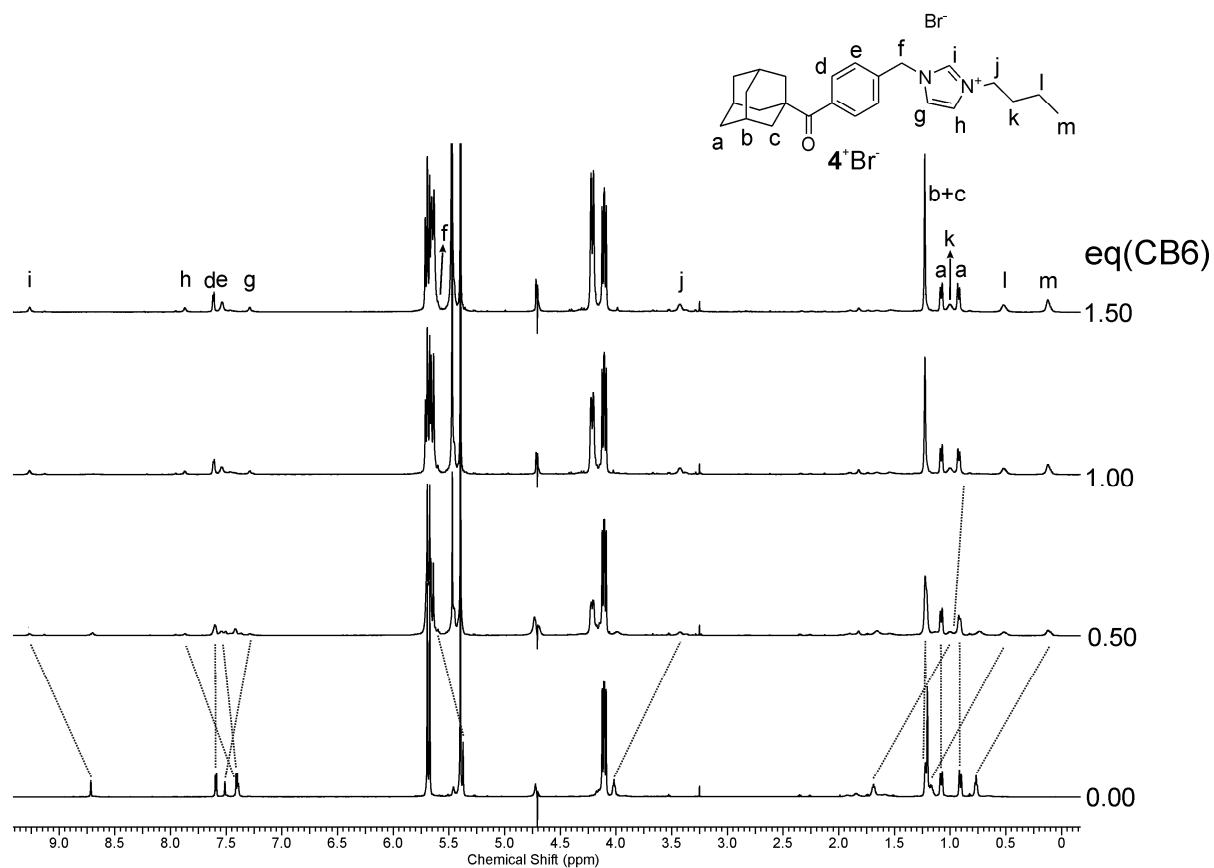
Figure S47: Stacking plot of ^{1}H NMR spectra (700 MHz) of mixtures of $\mathbf{4^+Br^-}$@CB7 with CB6 in 50mM NaCl in D$_2$O at 30°C, the number of β-CD equivalents is given next to corresponding line. Signals assignment is based on 2D ROESY spectrum of mixture where eq(CB6)=0.5.

Isothermal titration calorimetry data
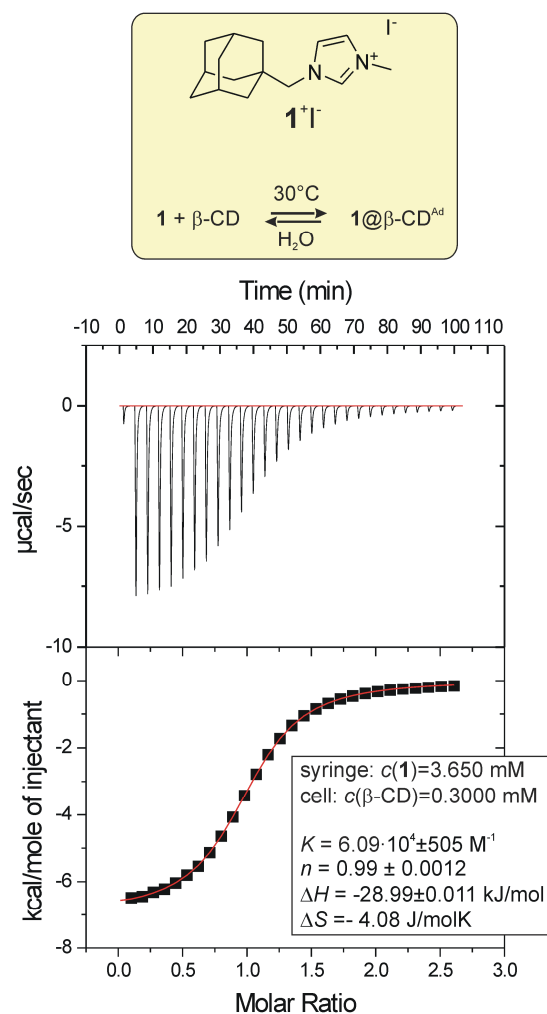

Figure S48: ITC experiment on complexation of $\mathbf{1^+I^-}$ with β-CD in water at 30°C.
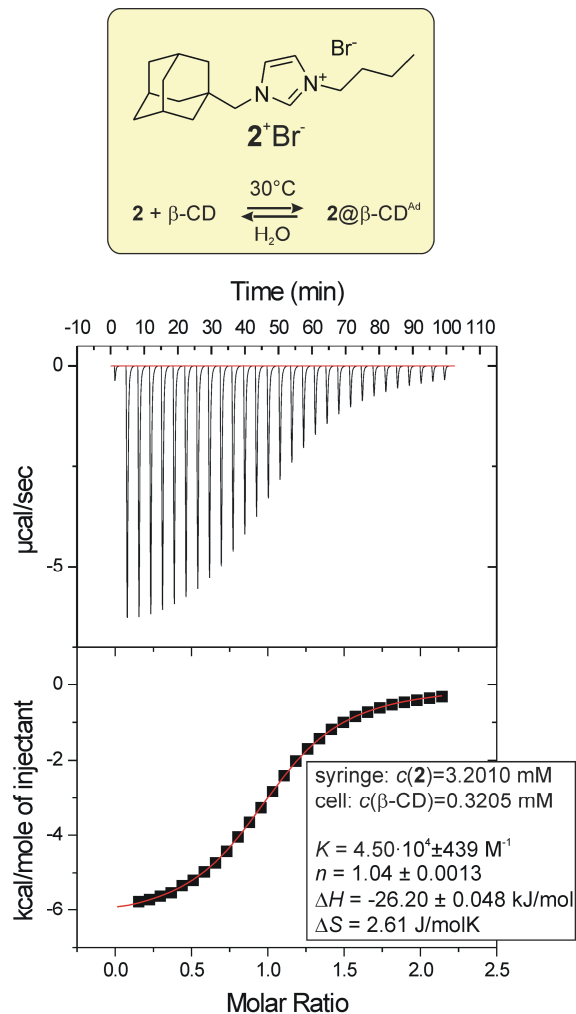
Figure S49: ITC experiment on complexation of $\mathbf{2^+Br^-}$ with β-CD in water at 30°C.
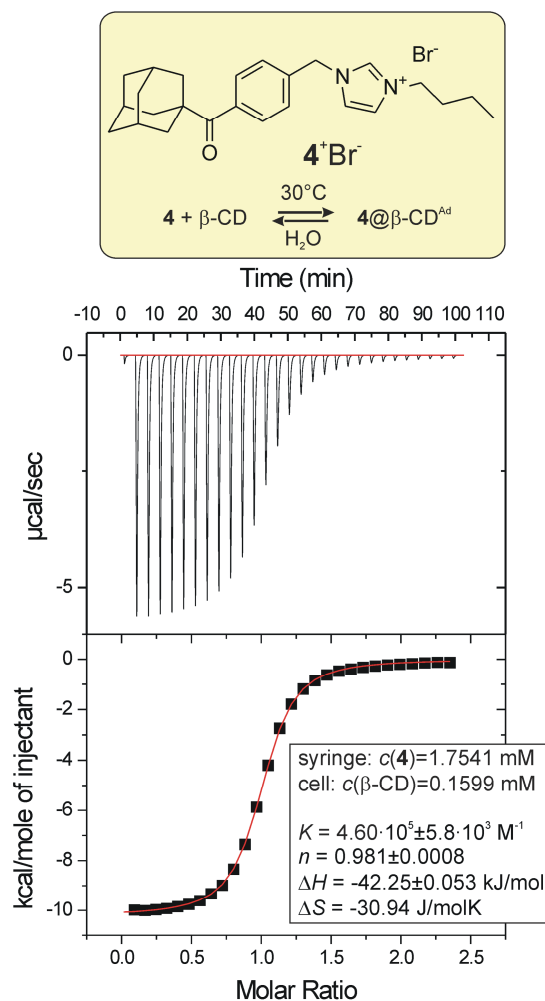
Figure S50: ITC experiment on complexation of **4⁺**Br⁻ with β-CD in water at 30°C.
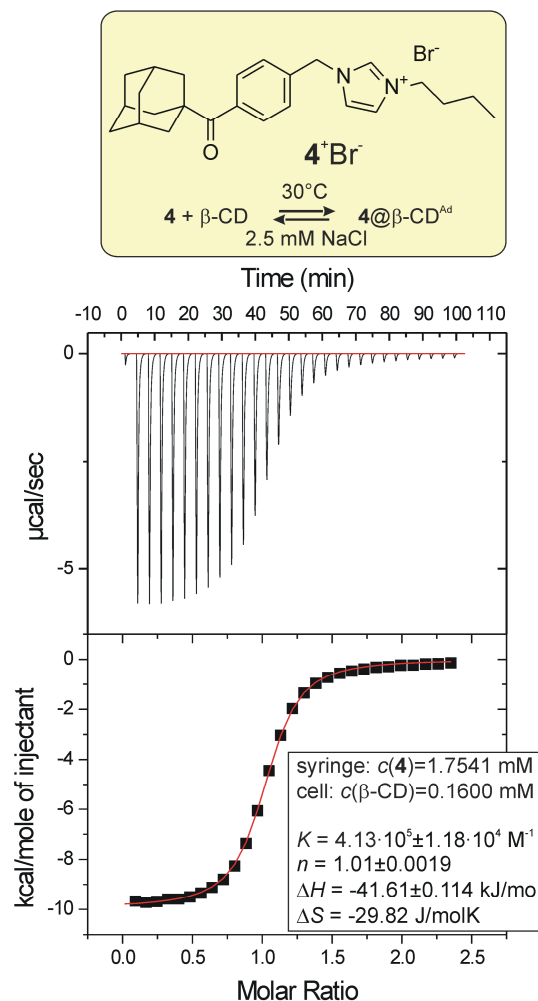
Figure S51: ITC experiment on complexation of **4⁺**Br⁻ with β-CD in 2.5 mᴍ NaCl at 30°C.
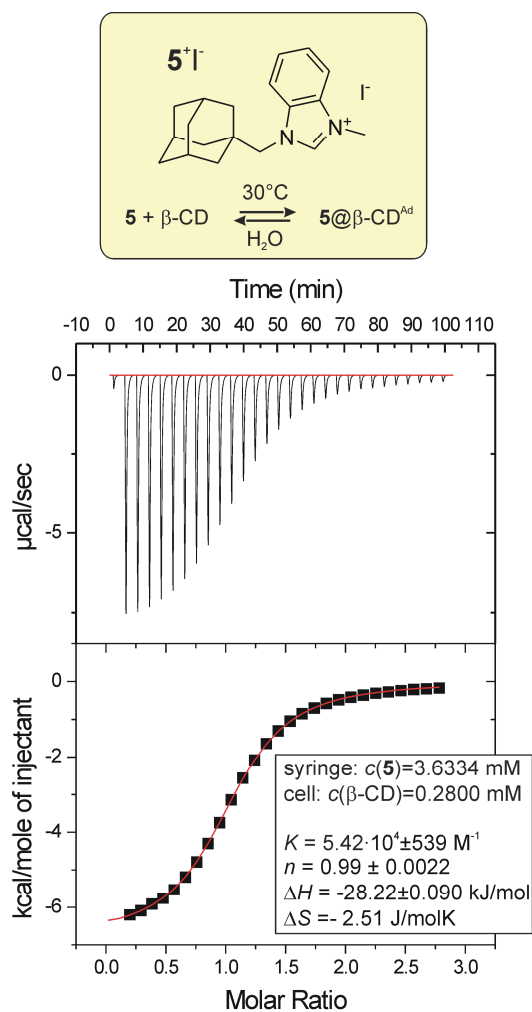
Figure S52: ITC experiment on complexation of **5**⁺I⁻ with β-CD in water at 30°C.
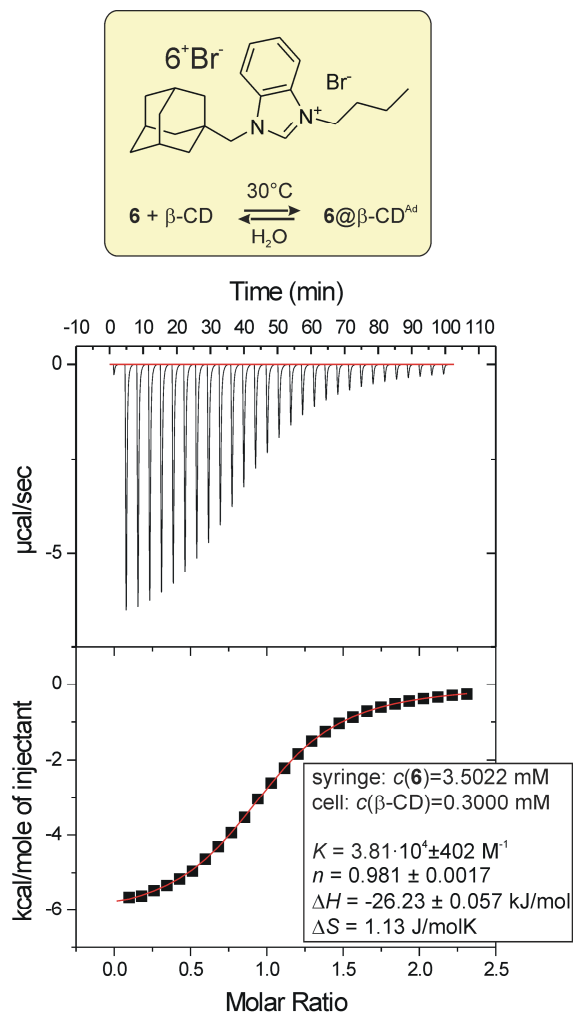
Figure S53: ITC experiment on complexation of **6**⁺Br⁻ with β-CD in water at 30°C.

Branná, Černochová, Rouchal, Kulhánek, Babinský, Marek, Nečas, Kuřitka and Vícha   S.I.

Page S37
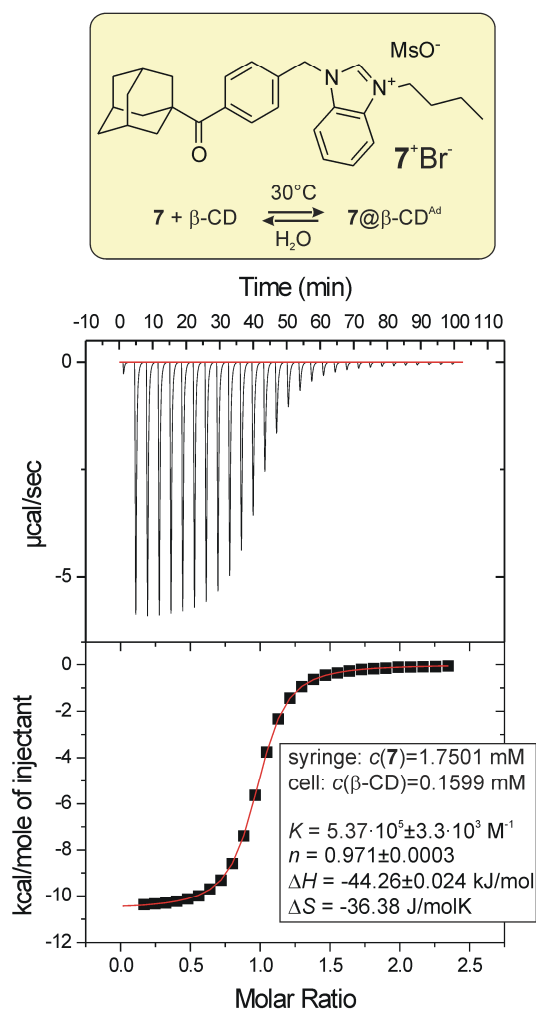
Figure S54: ITC experiment on complexation of **7**$^+$MsO$^-$ with β-CD in water at 30°C.
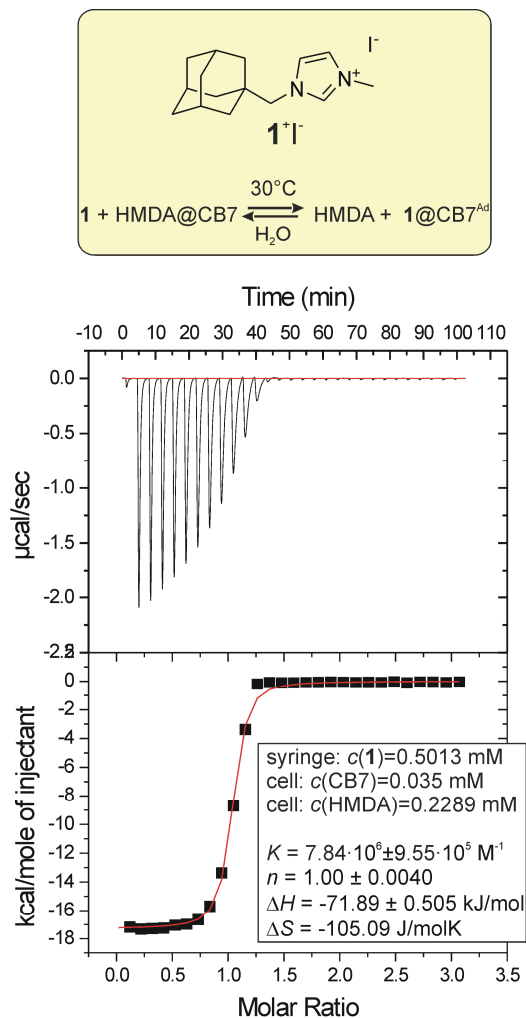
Figure S55: Competitive ITC experiment on complexation of **1**$^+$I$^-$ with CB7 in water at 30°C. The hexamethylene diamine 2HCl (HMDA) was used as a competitor.
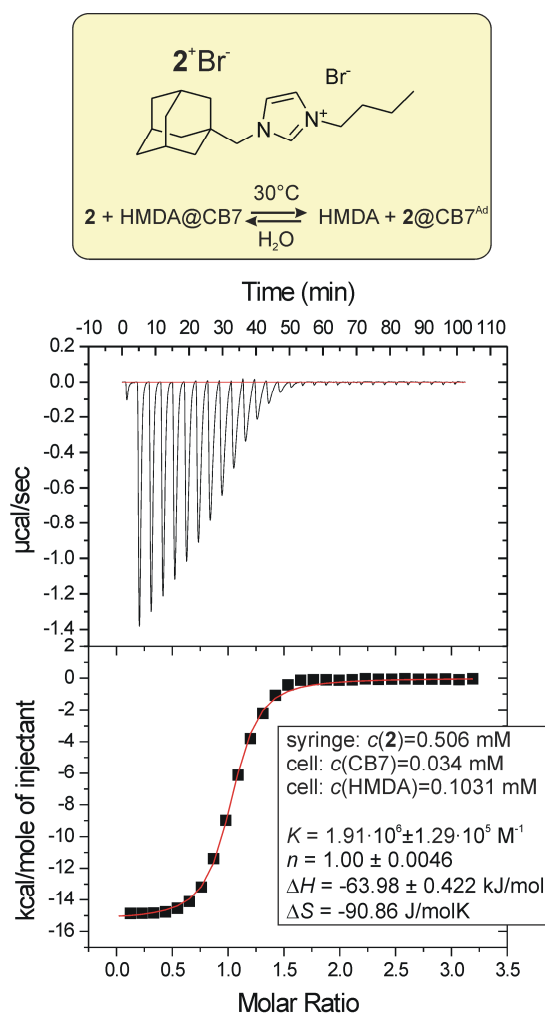
Figure S56: Competitive ITC experiment on complexation of **2**+Br⁻ with CB7 in water at 30°C. The hexamethylene diamine 2HCl (HMDA) was used as a competitor.
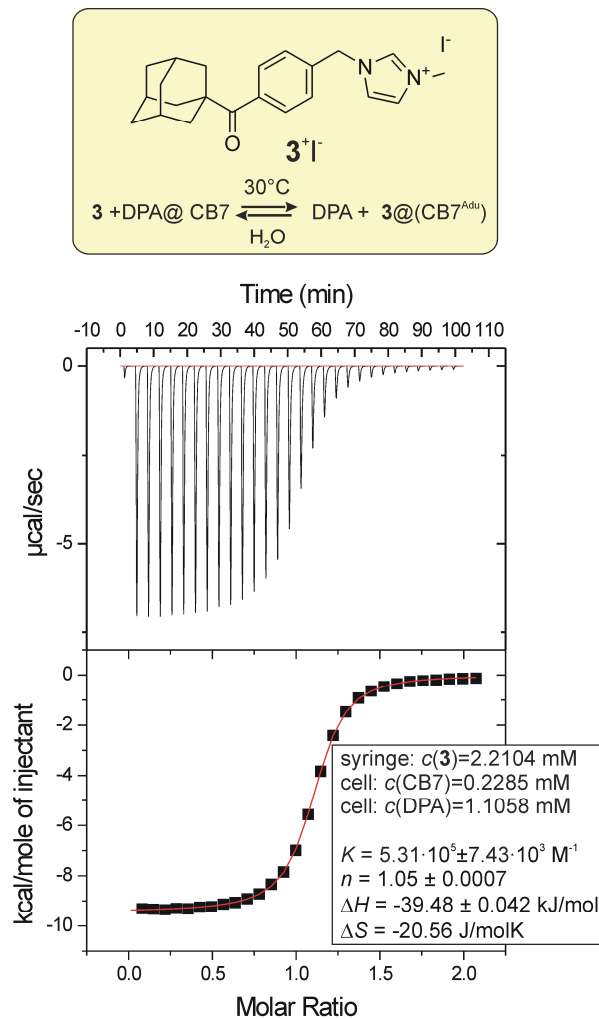
Figure S57: Competitive ITC experiment on complexation of **3**+I⁻ with CB7 in water at 30°C. The dopamine HCl (DPA) was used as a competitor.
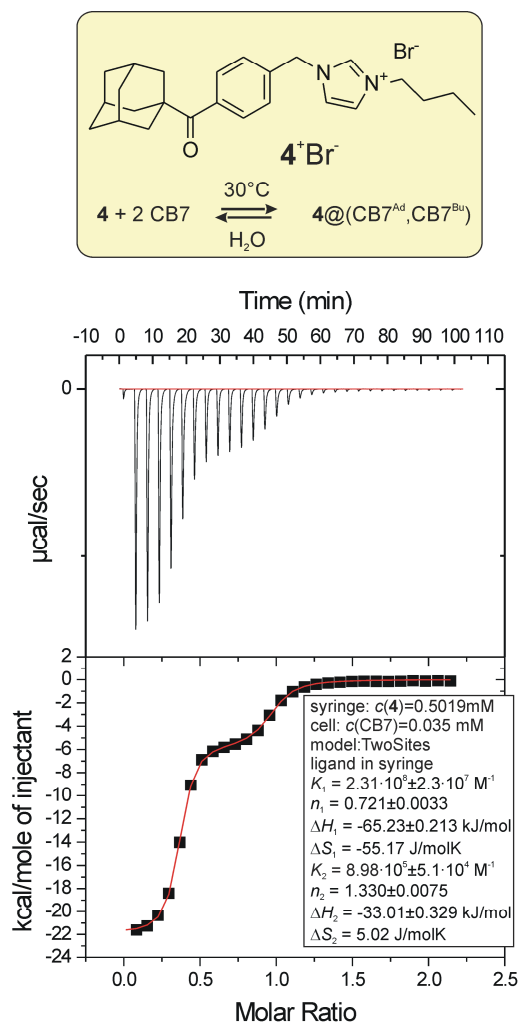
Figure S58: ITC experiment on complexation of **4**⁺Br⁻ with CB7 in water at 30°C.
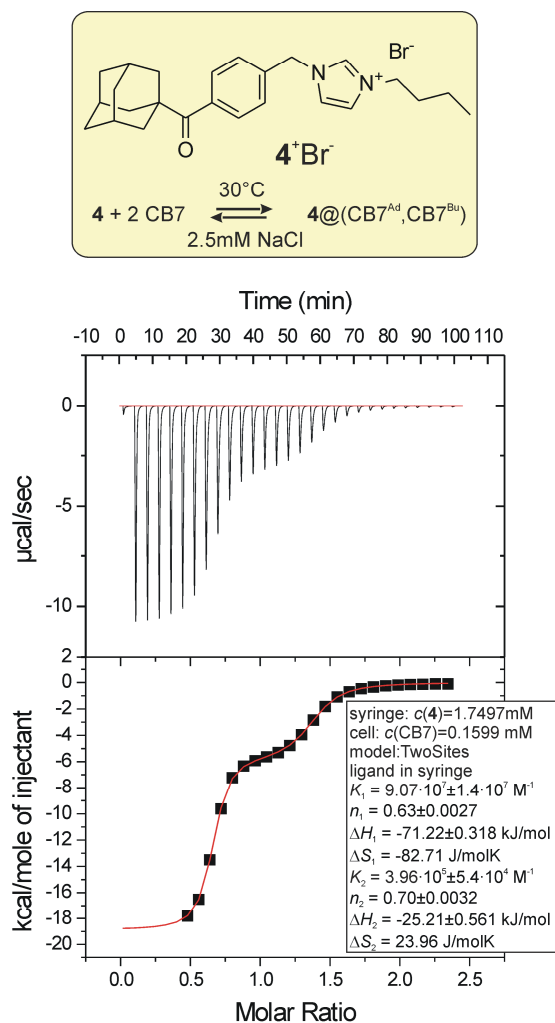
Figure S59: ITC experiment on complexation of **4**⁺Br⁻ with CB7 in 2.5mM NaCl at 30°C.
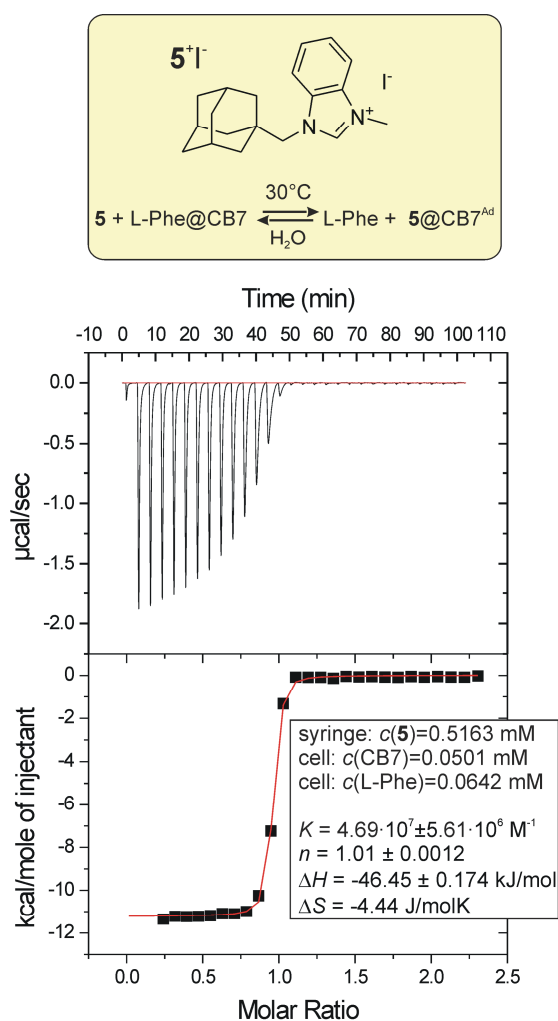
Figure S60: Competitive ITC experiment on complexation of **5**⁺I⁻ with CB7 in water at 30°C. The L-phenylalanine (L-Phe) was used as a competitor.

syringe: $c(\mathbf{5})$=0.5163 mM
cell: c(CB7)=0.0501 mM
cell: c(L-Phe)=0.0642 mM

$K = 4.69 \cdot 10^7 \pm 5.61 \cdot 10^6$ M⁻¹
$n = 1.01 \pm 0.0012$
$\Delta H = -46.45 \pm 0.174$ kJ/mol
$\Delta S = -4.44$ J/molK
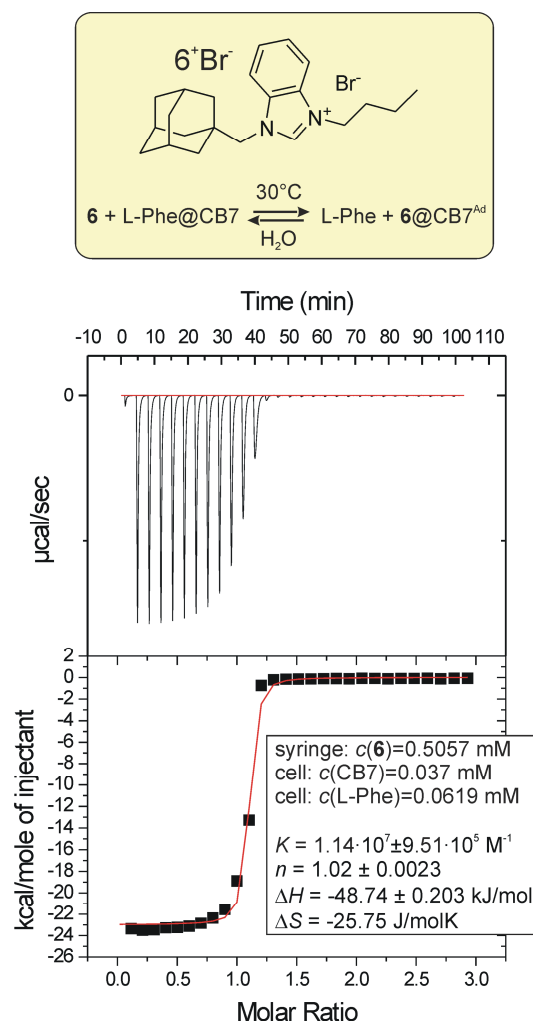
Figure S61: Competitive ITC experiment on complexation of **6**⁺Br⁻ with CB7 in water at 30°C. The L-phenylalanine (L-Phe) was used as a competitor.

syringe: $c(\mathbf{6})$=0.5057 mM
cell: c(CB7)=0.037 mM
cell: c(L-Phe)=0.0619 mM

$K = 1.14 \cdot 10^7 \pm 9.51 \cdot 10^5$ M⁻¹
$n = 1.02 \pm 0.0023$
$\Delta H = -48.74 \pm 0.203$ kJ/mol
$\Delta S = -25.75$ J/molK
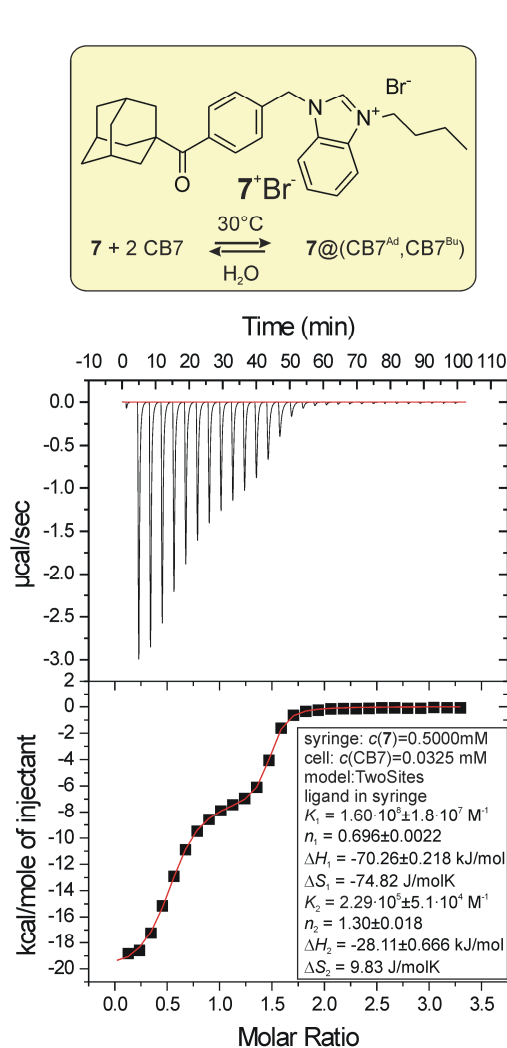
Figure S62: ITC experiment on complexation of **7**$^+$Br$^-$ with CB7 in water at 30°C.
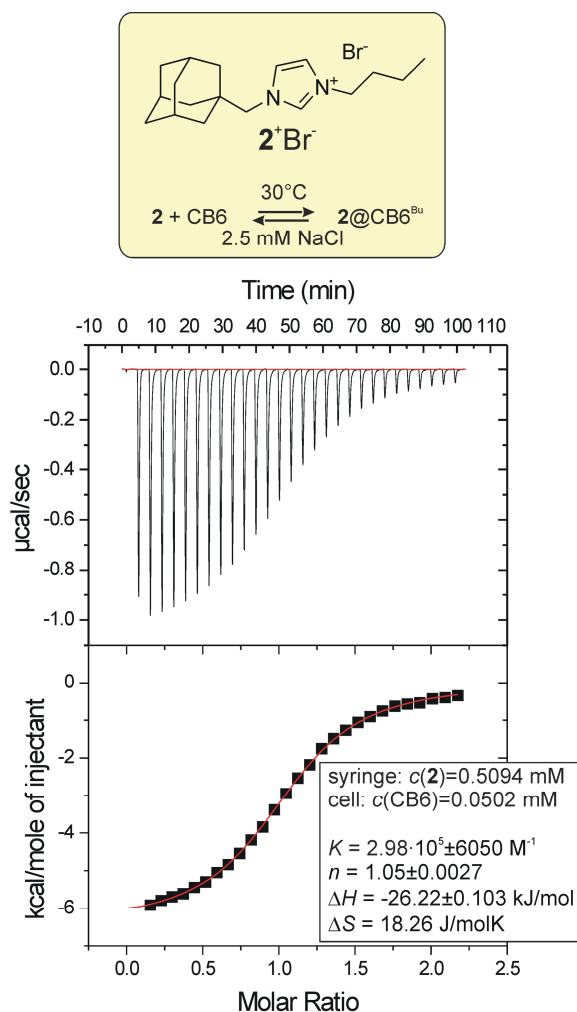
Figure S63: ITC experiment on complexation of **2**$^+$Br$^-$ with CB6 in 2.5 mM NaCl at 30°C.
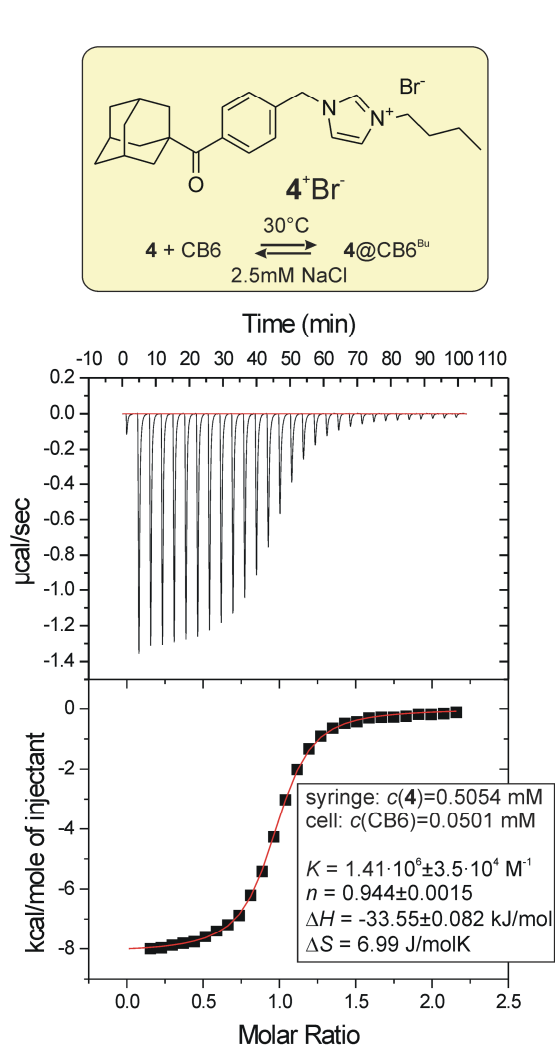
Figure S64: ITC experiment on complexation of **4**⁺Br⁻ with CB6 in 2.5 mᴍ NaCl at 30°C.
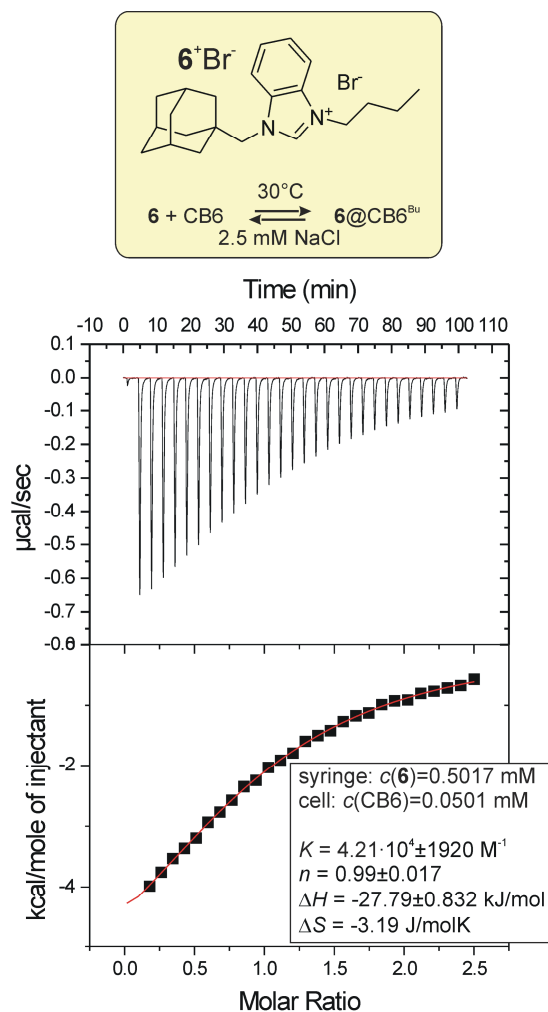
Figure S65: ITC experiment on complexation of **6**⁺Br⁻ with CB6 in 2.5 mᴍ NaCl at 30°C.
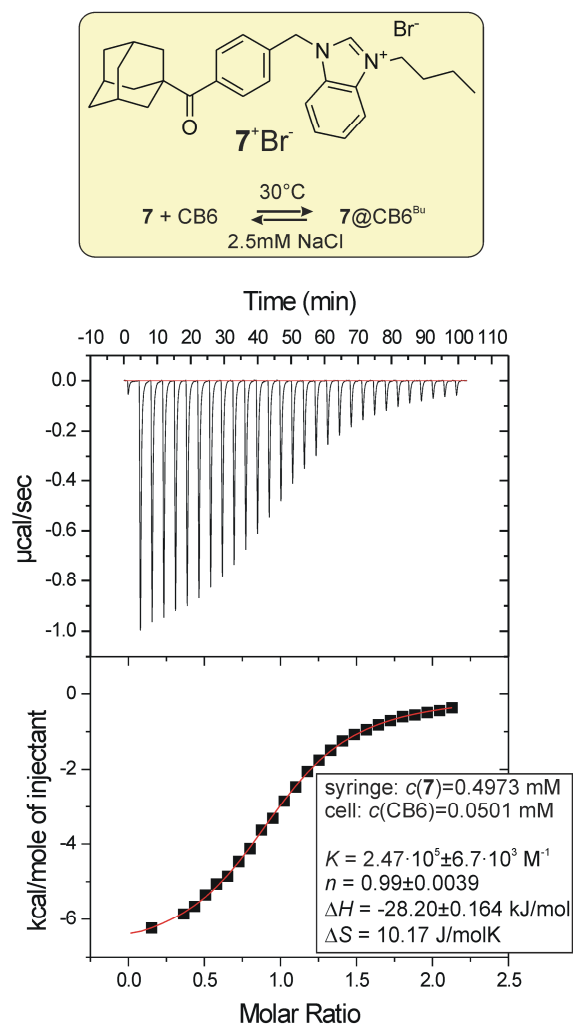
Figure S66: ITC experiment on complexation of **7**⁺Br⁻ with CB6 in 2.5 mM NaCl at 30°C.
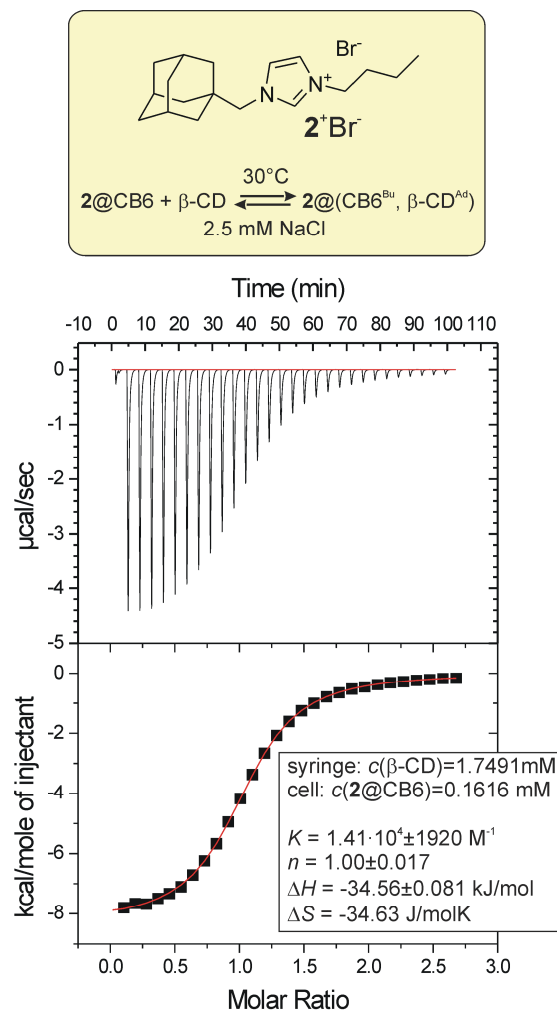
Figure S67: Subsequent ITC experiment on complexation of **2**@CB6 with β-CD in 2.5 mM NaCl at 30°C.
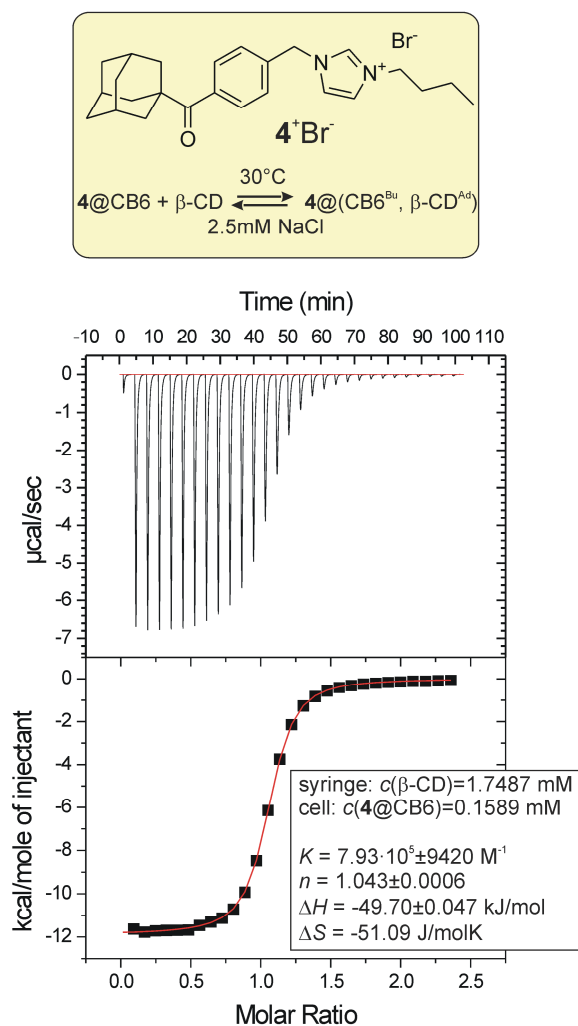
Figure S68: Subsequent ITC experiment on complexation of **4**@CB6 with β-CD in 2.5 mм NaCl at 30°C.
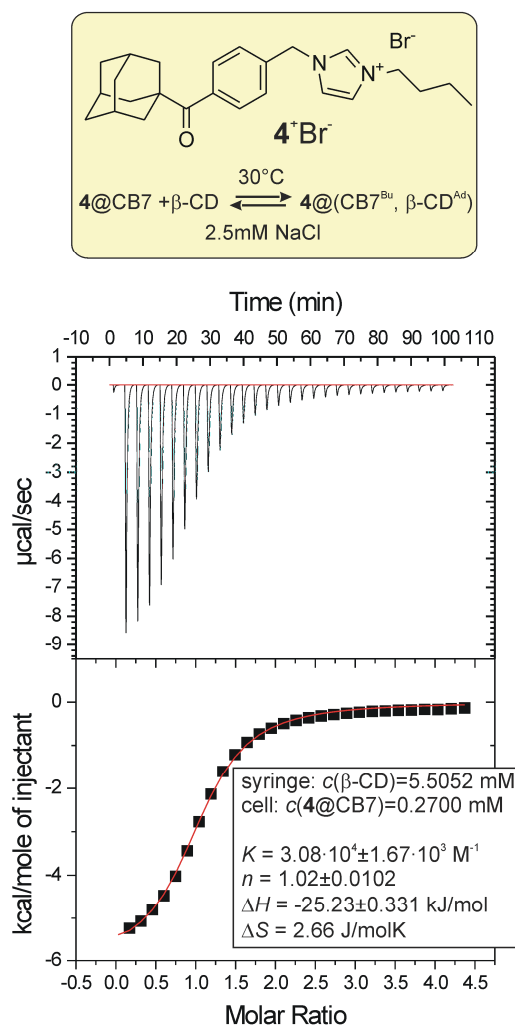
Figure S69: Subsequent ITC experiment on complexation of **4**@CB7 with β-CD in 2.5 mм NaCl in D₂O at 30°C.

Branná, Černochová, Rouchal, Kulhánek, Babinský, Marek, Nečas, Kuřitka and Vícha   S.I.

Page S45
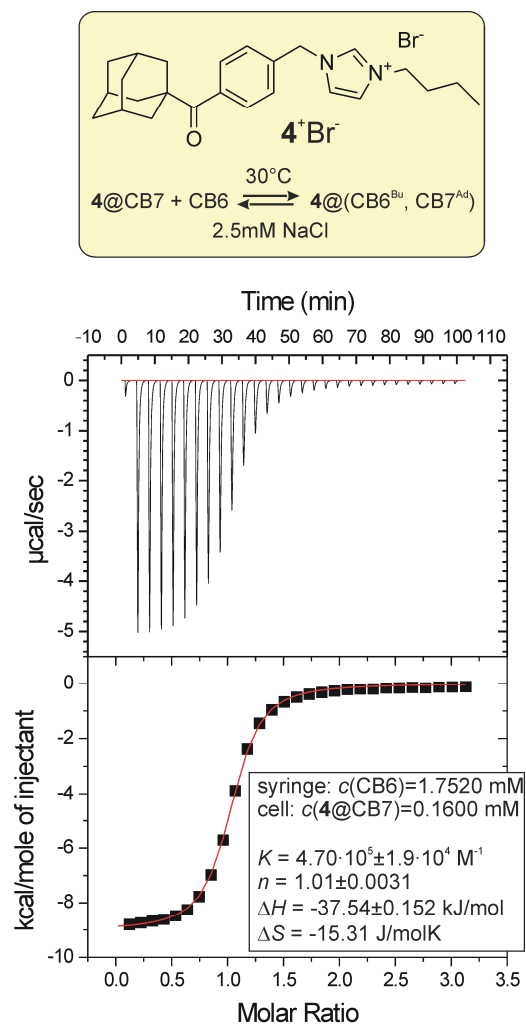
Figure S70: Subsequent ITC experiment on complexation of **4**@CB7 with CB6 in 2.5 mM NaCl at 30°C
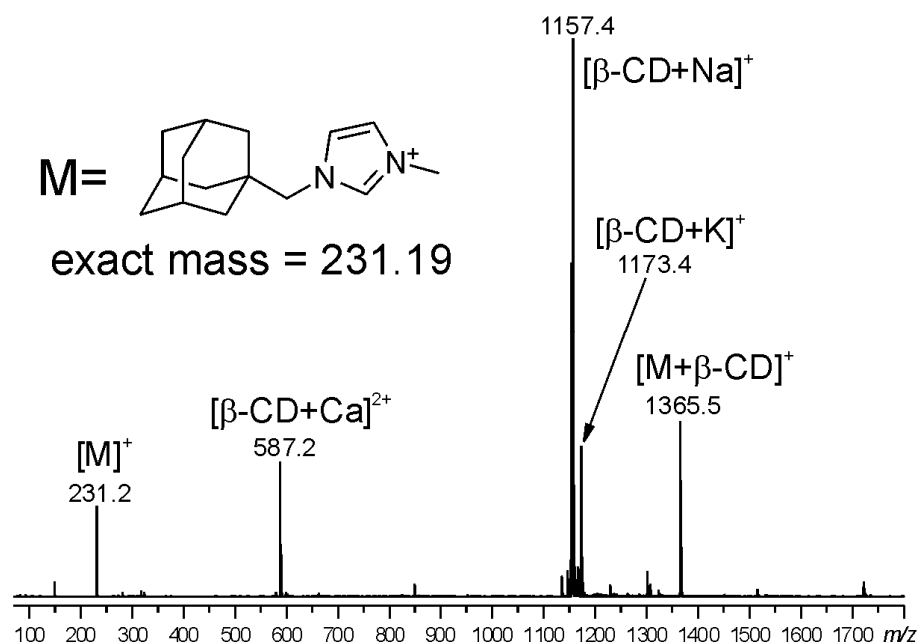
Figure S71: Positive-ion mode ESI mass spectra (full scan) of aqueous solutions of **1**·β-CD.
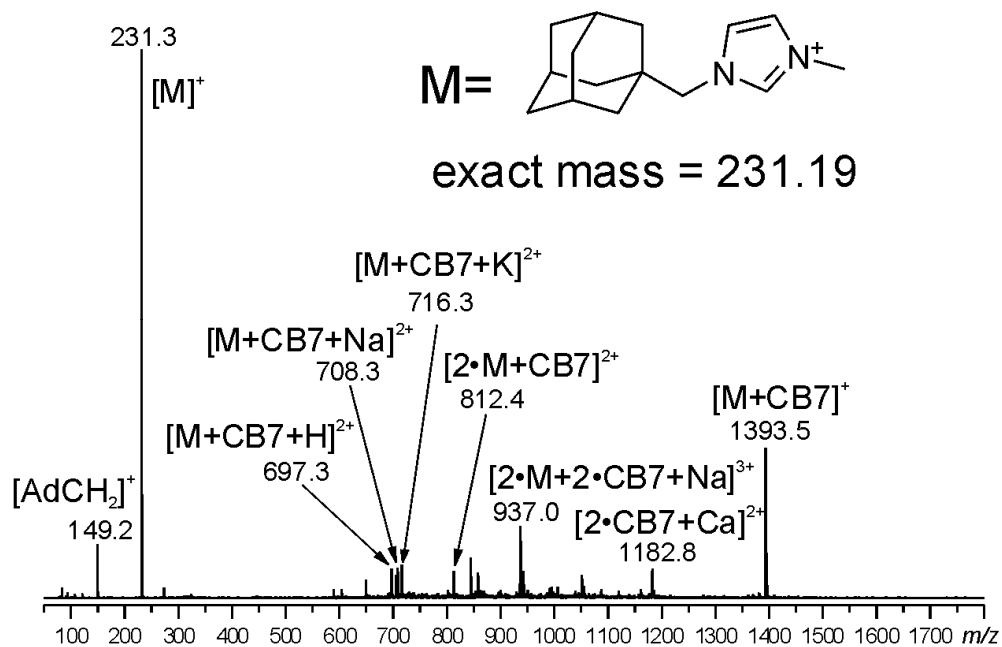
Figure S72: Positive-ion mode ESI mass spectra (full scan) of aqueous solutions of **1**·CB7.
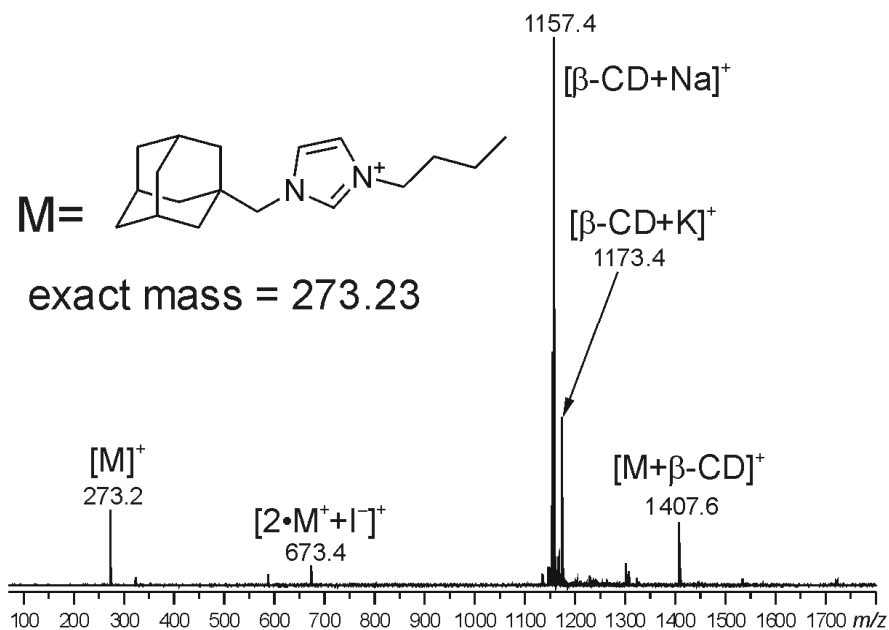
Figure S73: Positive-ion mode ESI mass spectra (full scan) of aqueous solutions of **2·β-CD**.
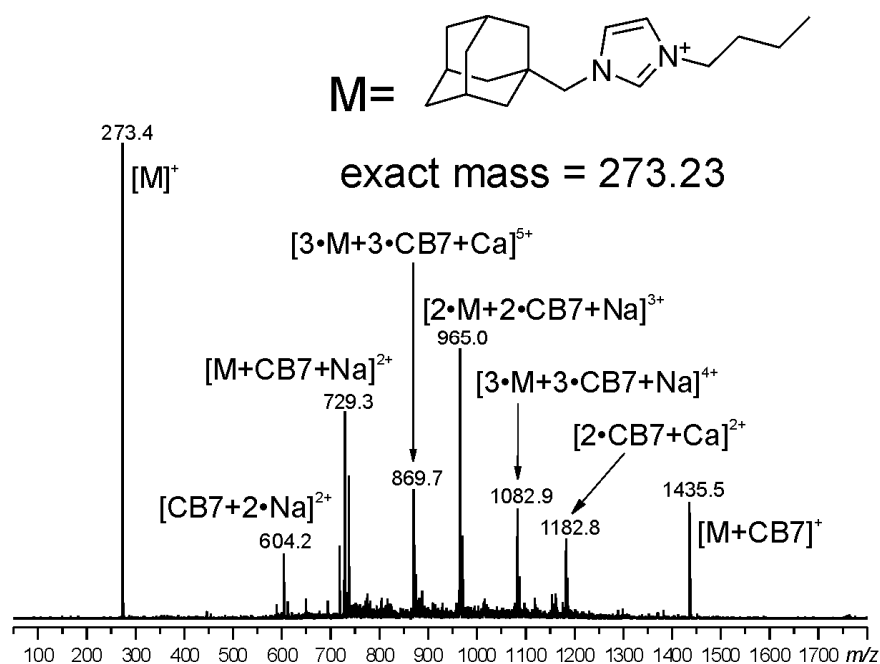
Figure S74: Positive-ion mode ESI mass spectra (full scan) of aqueous solutions of **2·CB7**.
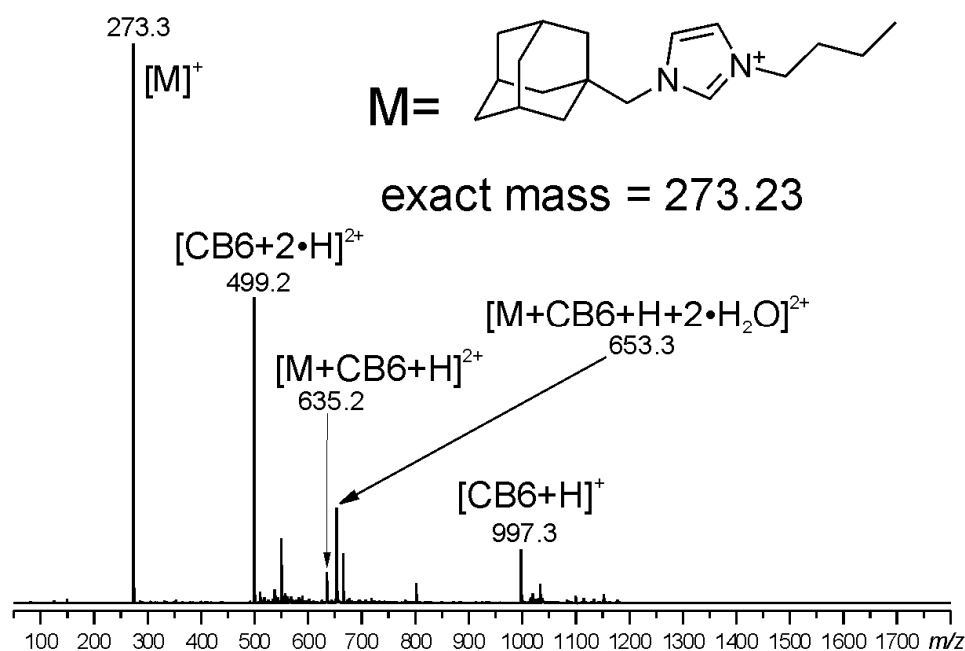
Figure S75: Positive-ion mode ESI mass spectra (full scan) of aqueous solutions of **2·CB6**.
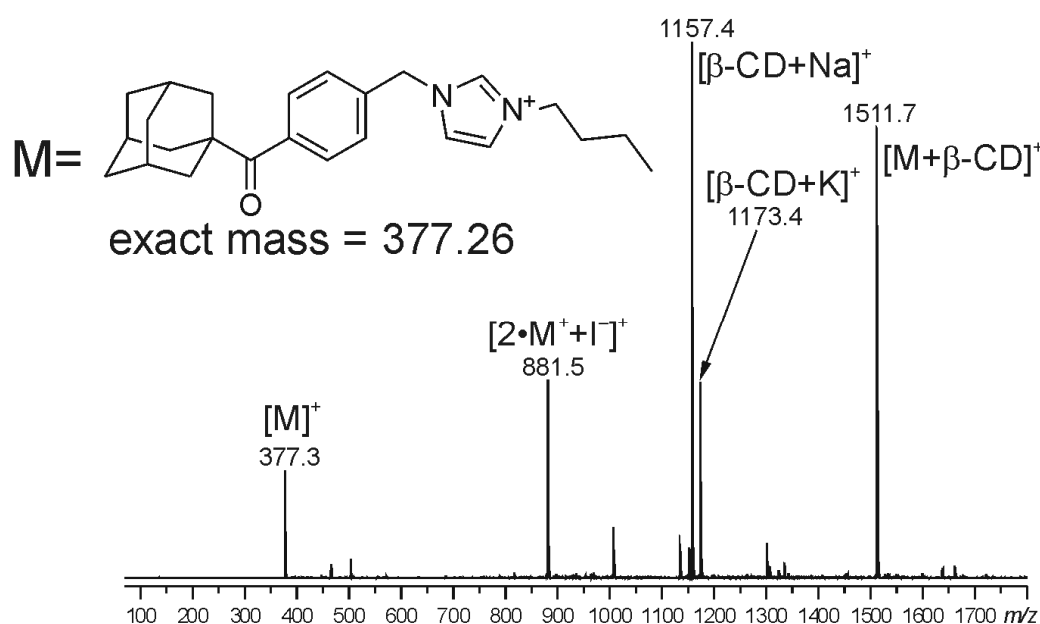
Figure S76: Positive-ion mode ESI mass spectra (full scan) of aqueous solutions of **4·β-CD**.

377.4

[M]⁺

M= exact mass = 377.26

[M+CB7+Na]²⁺
781.3

[M+CB7]⁺
1539.6

100 200 300 400 500 600 700 800 900 1000 1100 1200 1300 1400 1500 1600 1700 *m/z*
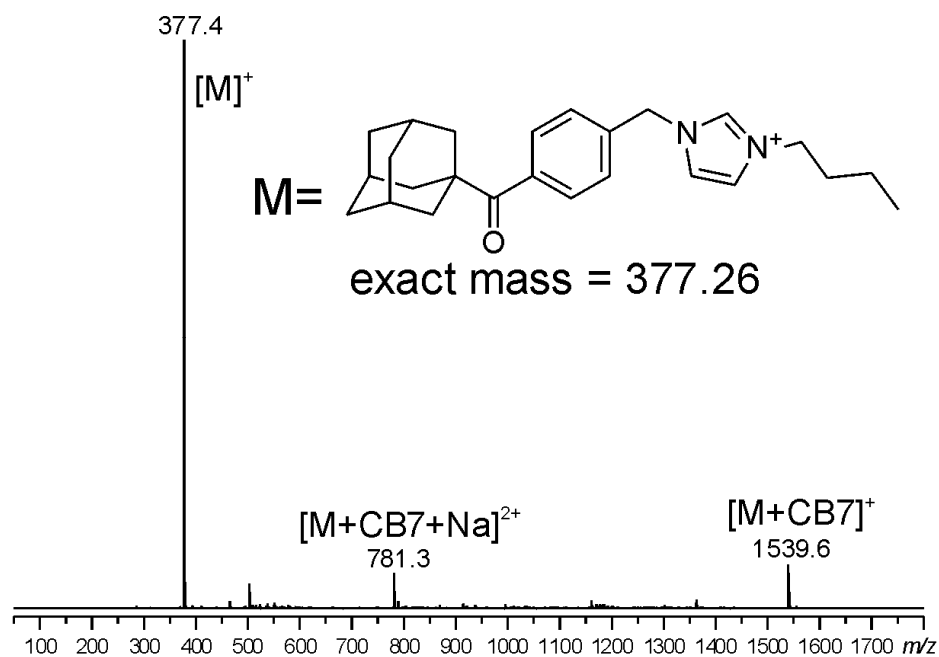
Figure S77: Positive-ion mode ESI mass spectra (full scan) of aqueous solutions of **4·CB7**.

377.4

[M]⁺

M=

exact mass = 377.26

[M+CB6+H+2·H₂O]²⁺
705.3

[M+CB6+H]²⁺
687.3

[2·M+2·CB6+H]³⁺

[CB6+2·H]²⁺

499.2

997.3

916.3

[CB6+H]⁺

100 200 300 400 500 600 700 800 900 1000 1100 1200 1300 1400 1500 1600 1700 *m/z*
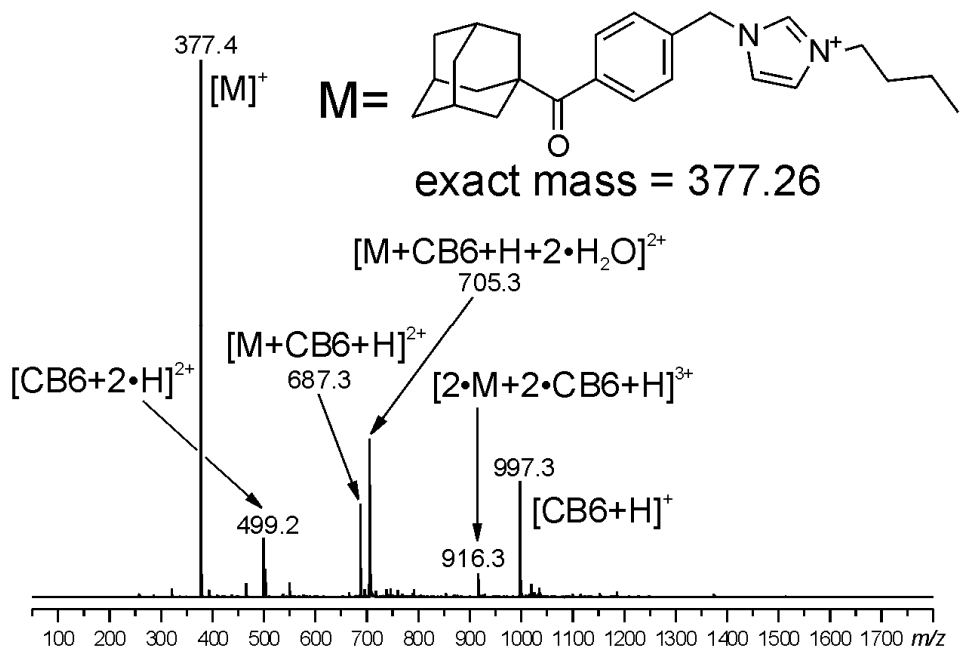
Figure S78: Positive-ion mode ESI mass spectra (full scan) of aqueous solutions of **4·CB6**.
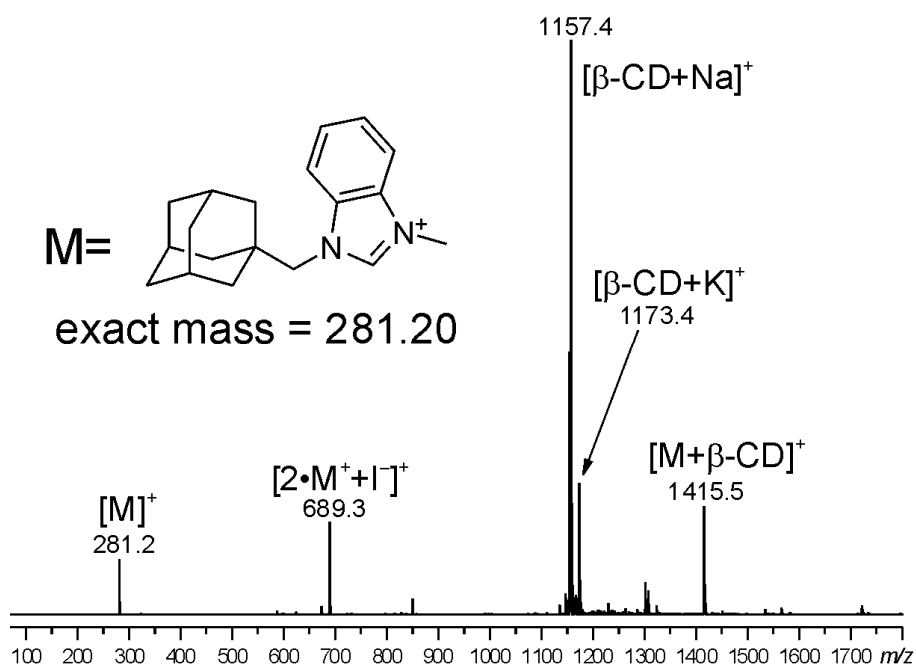
Figure S79: Positive-ion mode ESI mass spectra (full scan) of aqueous solutions of **5·β-CD**.
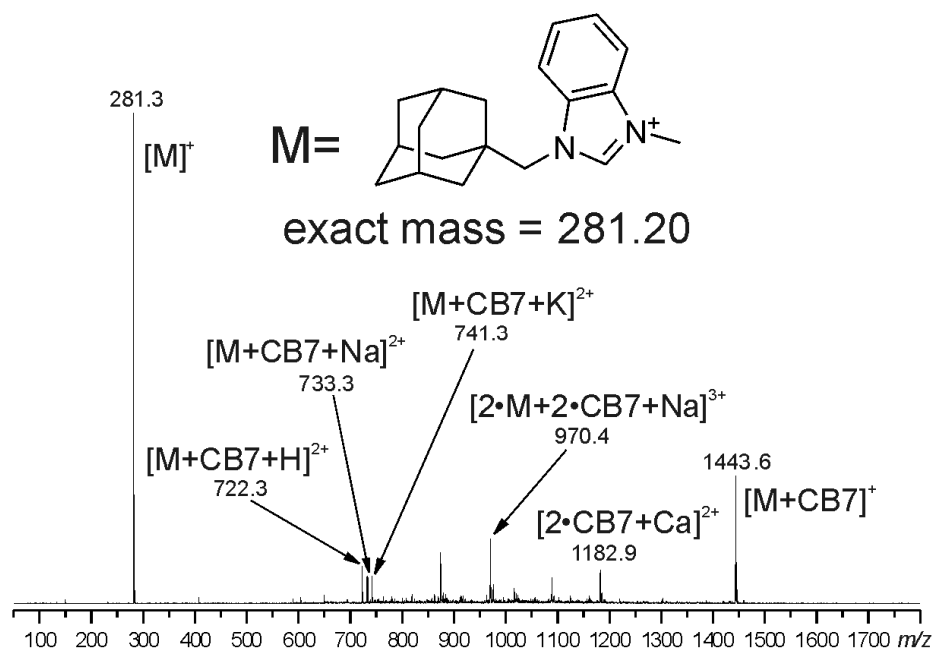
Figure S80: Positive-ion mode ESI mass spectra (full scan) of aqueous solutions of **5·CB7**.
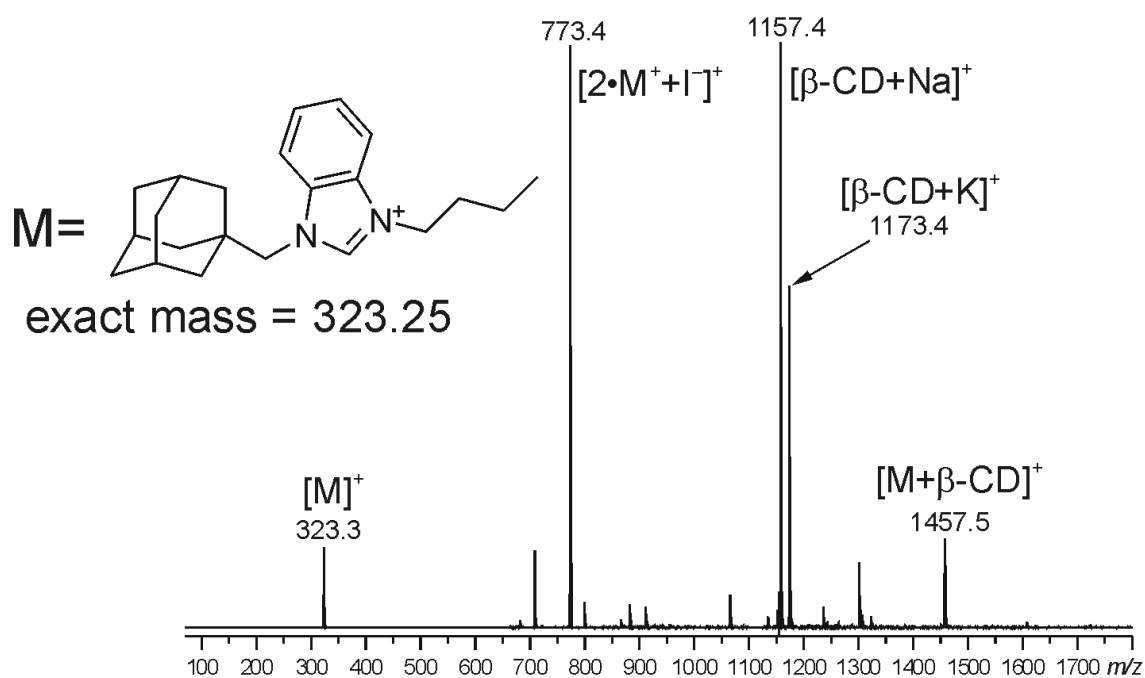
Figure S81: Positive-ion mode ESI mass spectra (full scan) of aqueous solutions of **6·β-CD**.
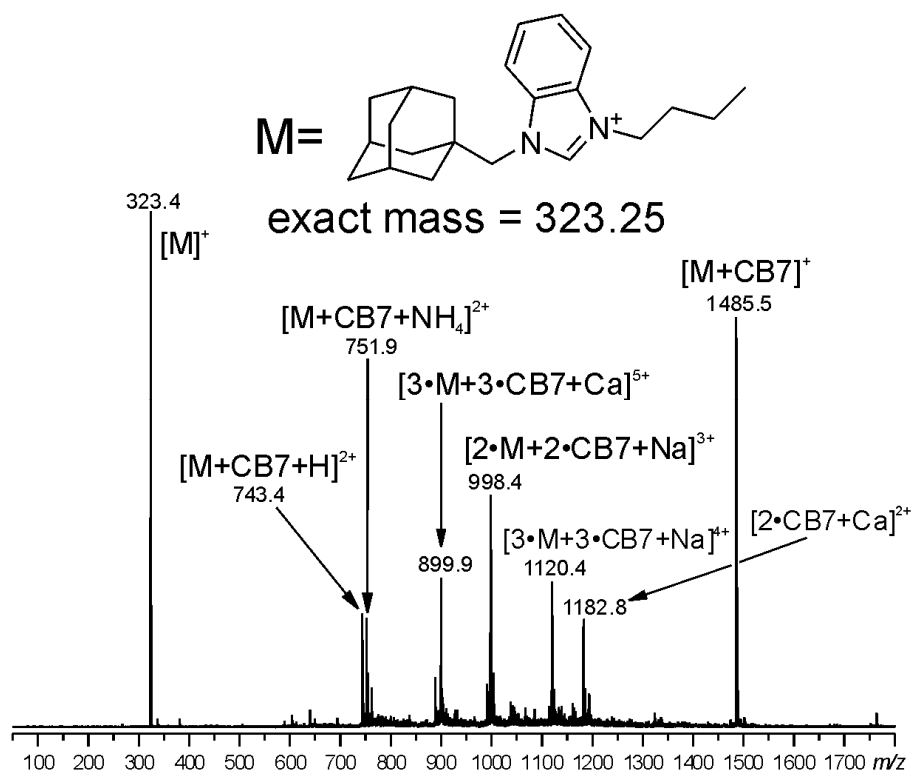
Figure S82: Positive-ion mode ESI mass spectra (full scan) of aqueous solutions of **6·CB7**.
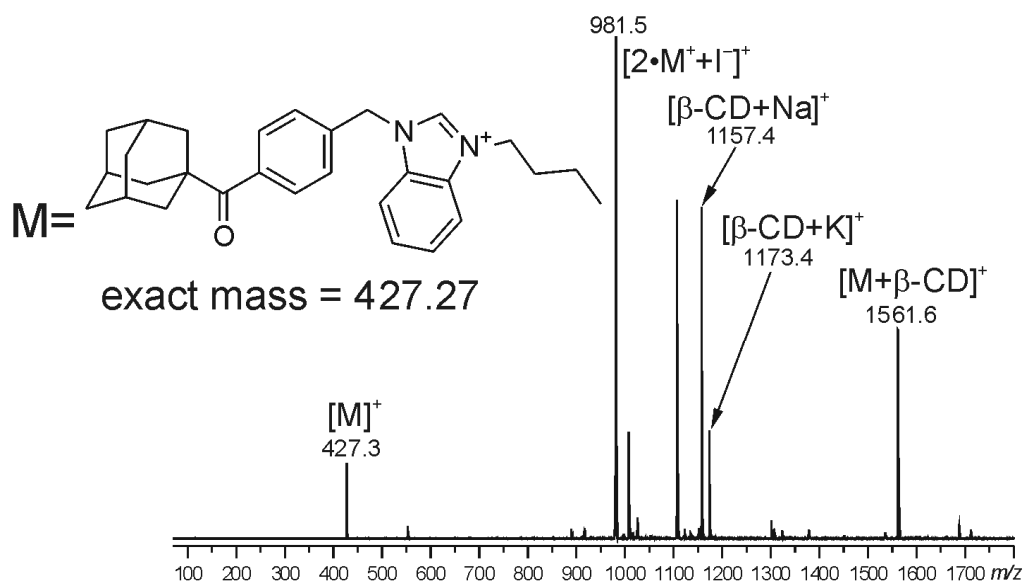
Figure S83: Positive-ion mode ESI mass spectra (full scan) of aqueous solutions of **7·β-CD**.
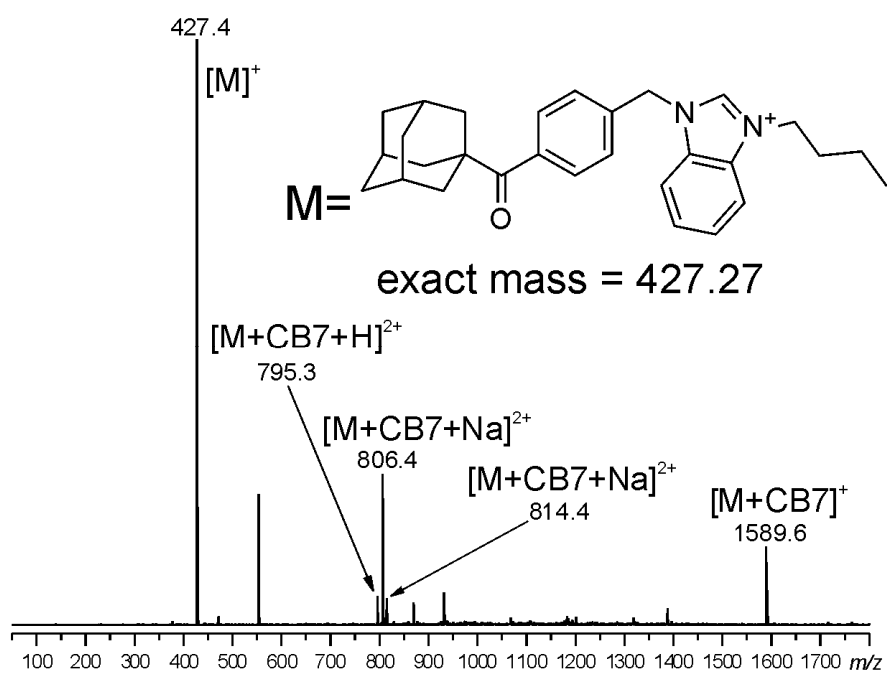
Figure S84: Positive-ion mode ESI mass spectra (full scan) of aqueous solutions of **7·CB7**.

Branná, Černochová, Rouchal,
Kulhánek, Babinský, Marek, Nečas,
Kuřitka and Vícha   S.I.

Page S53
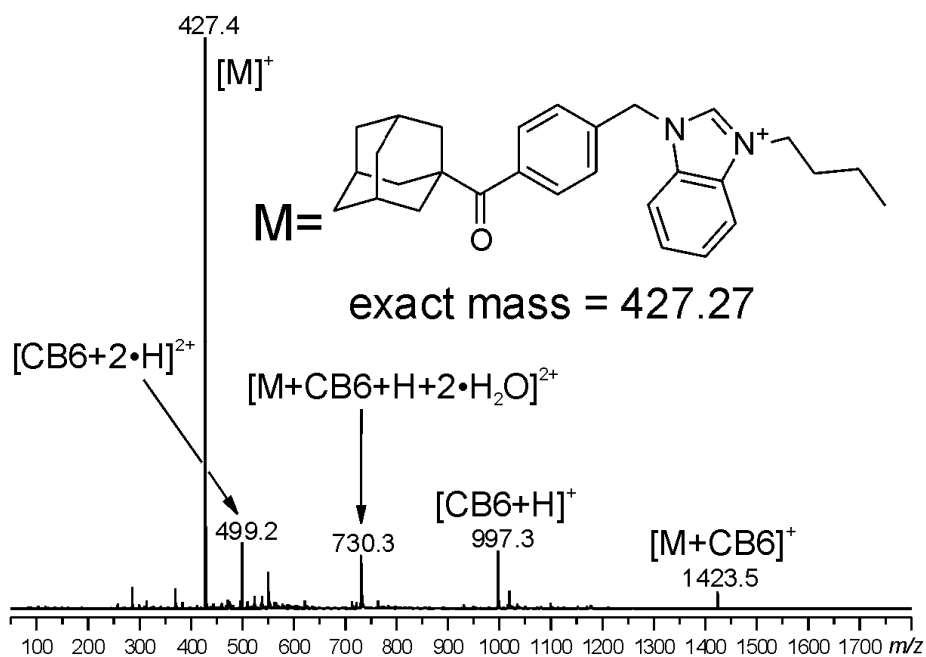
Figure S85: Positive-ion mode ESI mass spectra (full scan) of aqueous solutions of **7·CB6**.

Computation Results

Preparation of Hosts and Guests. β-CD, CB6, and CB7 were used as hosts and the compounds **2** and **4** were used as the guests in the computational studies. Their initial structures were generated *in silico*. The initial geometries of all structures were pre-optimized using the UFF[3] and GAFF[4] force fields as implemented in OpenBabel.[5] The structures of β-CD, CB6, and CB7 were further symmetrized using the Symmol program[6] to obtain the C_7, D_{6h}, and D_{7h} point groups, respectively. The symmetrized geometries were once again re-optimized employing the aforementioned force fields. The resulting geometries were refined further in subsequent calculations.

Nucleus Independent Chemical Shift (NICS). The input coordinates of β-CD, CB6, and CB7 were optimized using the PBE0 density functional[7,8,9] and the 6-31G* basis set[10,11] employed the Gaussian 09.A2 software package.[12] The resulting coordinates were used to compute the spatial magnetic shielding using the NICS approach.[13] First, a three-dimensional grid of pseudoatoms spaced 0.25 Å apart was generated around the macrocycle. Then, the magnetic shielding was evaluated at the position of each pseudoatom using the PBE0/6-311G** level of theory[14] using the Gaussian 03.E1 software package.[15] The PyMOL program[1614] was used to visualize the computed data (Figure S86).

[3] Rappe, A. K.; Casewit, C. J.; Colwell, K. S.; Goddard, W. A.; Skiff, W. M. *J. Am. Chem. Soc.* **1992**, *114*, 10024.

[4] Wang, J. M.; Wolf, R. M.; Caldwell, J. W.; Kollman, P. A.; Case, D. A. *J. Comput. Chem.* **2004**, *25*, 1157.

[5] O'Boyle, N. M.; Banck, M.; James, C. A.; Morley, C.; Vandermeersch, T.; Hutchison, G. R. *J. Cheminformatics* **2011**, *3*, 33.

[6] Pilati, T.; Forni, A. *J. Appl. Crystallogr.* **1998**, *31*, 503.

[7] Perdew, J. P.; Burke, K.; Ernzerhof, M. *Phys. Rev. Lett.* **1996**, *77*, 3865.

[8] Perdew, J. P.; Burke, K.; Ernzerhof, M. (vol 77, Pg 3865, 1996). *Phys. Rev. Lett.* **1997**, *78*, 1396.

[9] Adamo, C.; Barone, V. *J. Chem. Phys.* **1999**, *110*, 6158.

[10] Hehre, W.J.; Ditchfie, R.; Pople, J.A. *J. Chem. Phys.* **1972**, *56*, 2257.

[11] Harihara, P.C.; Pople, J.A. *Theor. Chim. Acta* **1973**, *28*, 213.

[12] Frisch, M. J.; Trucks, G. W.; Schlegel, H. B.; Scuseria, G. E.; Robb, M. A.; Cheeseman, J. R.; Scalmani, G.; Barone, V.; Mennucci, B.; Petersson, G. A.; et al. *Gaussian 09, Revision A.2*; Gaussian, Inc.: Wallingford CT, 2009.

[13] Schleyer, P. von R.; Maerker, C.; Dransfeld, A.; Jiao, H.; Hommes, N. J. R. van E. *J. Am. Chem. Soc.* **1996**, *118*, 6317.

[14] Krishnan, R.; Binkley, J.S.; Seeger, R.; Pople, J.A. *J. Chem. Phys.* **1980**, *72*, 650.

[15] Frisch, M. J.; Trucks, G. W.; Schlegel, H. B.; Scuseria, G. E.; Robb, M. A.; Cheeseman, J. R.; Montgomery, J. A.; Vreven, T.; Kudin, K. N.; Burant, J. C.; et al. *Gaussian 03, Revision E.1*; Gaussian, Inc.: Wallingford, CT, 2003.

[16] *The PyMOL Molecular Graphics System, Version 1.6.1*; Schrödinger, LLC.
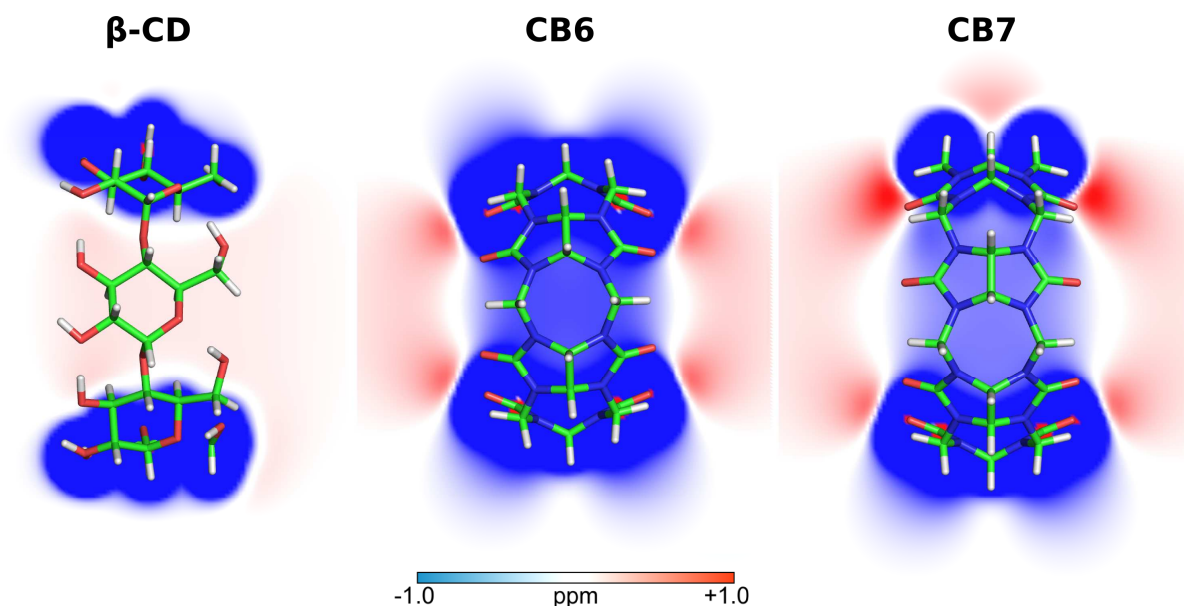
Figure S86: Nucleus independent chemical shifts for β-CD, CB6, and CB7 shown as a slice passing through the center of mass of the macrocycle.

Molecular Dynamics Simulations. CB6, CB7, and compounds **2** and **4** were described by the GAFF force field employing atomic point charges calculated by the RESP procedure[17] using the electrostatic potential calculated at the HF/6-31G*//B3LYP/6-31+G** level of theory. [18,19,20] β-CD was described by the GLYCAM06 force field[21] employing atomic point charges included in the force field. Various complexes were assembled *in silico* employing the tleap program from the AMBER 12 software package[22] (Figure S87). The complexes were solvated with the SPC/E water model[23] using the solvate package[24] with a 15 Å thick water shell, which was later transformed to a truncated octahedral box. Sodium and chloride ions[25] were added to neutralize the net charge of the complex and increase the ionic strength of solution (c_{NaCl}~0.05 M) to improve the sampling of ions around the solute. Each system was first equilibrated using the following procedure: a) a system geometry optimization to remove any steric conflicts; b) slow heating of the system from 5 to 300 K at constant volume for 100 ps; and c) a volume equilibration at a temperature and pressure 300 K and 1 bar, respectively, for 500 ps. A time step of 1 fs was used during all molecular dynamics simulations. Bond lengths involving hydrogen atoms were kept fixed using the SHAKE algorithm.[26] The temperature was maintained using the Langevin stochastic thermostat with a friction frequency of 1 ps^{-1} during equilibration to avoid uneven kinetic energy distribution in the system, and a weak-coupling Berendsen thermostat was used during the production dynamics with a time constant of 1 ps. The pressure was maintained by a weak-coupling barostat with a

[17] Cieplak, P.; Cornell, W.; Bayly, C.; Kollman, P. *J. Comput. Chem.* **1995**, *16*, 1357.

[18] Becke, A. *Phys. Rev. A* **1988**, *38*, 3098.

[19] Lee, C.; Yang, W.; Parr, R. *Phys. Rev. B* **1988**, *37*, 785.

[20] Becke, A. *J. Chem. Phys.* **1993**, *98*, 5648.

[21] Kirschner, K. N.; Yongye, A. B.; Tschampel, S. M.; González-Outeiriño, J.; Daniels, C. R.; Foley, B. L.; Woods, R. J. *J. Comput. Chem.* **2008**, *29*, 622.

[22] Case, D.; Darden, T.; Cheatham, T.; Simmerling, C.; Wang, J.; Duke, R.; Luo, R.; Walker, R.; Zhang, W.; Merz, K.; et al. AMBER 12. **2012**.

[23] Berendsen, H. J. C.; Grigera, J. R.; Straatsma, T. P. *J. Phys. Chem.* **1987**, *91*, 6269.

[24] Grubmuller, H. *Solvate 1.0*; Ludwig-Maximilians-Universität München, 1996.

[25] Joung, I. S.; Cheatham, T. E. *J. Phys. Chem. B* **2008**, *112*, 9020.

[26] Ryckaert, J. P.; Ciccotti, G.; Berendsen, H. J. C. *J. Comput. Phys.* **1977**, *23*, 327.

time constant of 1.2 ps. Long-range electrostatic interactions under periodic boundary conditions were described by the particle-mesh Ewald method[27] using an 8 Å cutoff for the direct summation. Van der Waals interactions were truncated using an 8 Å cutoff. Production dynamics were calculated by a GPU accelerated version[28] of the pmemd package in AMBER and each simulation was performed for 1 μs.
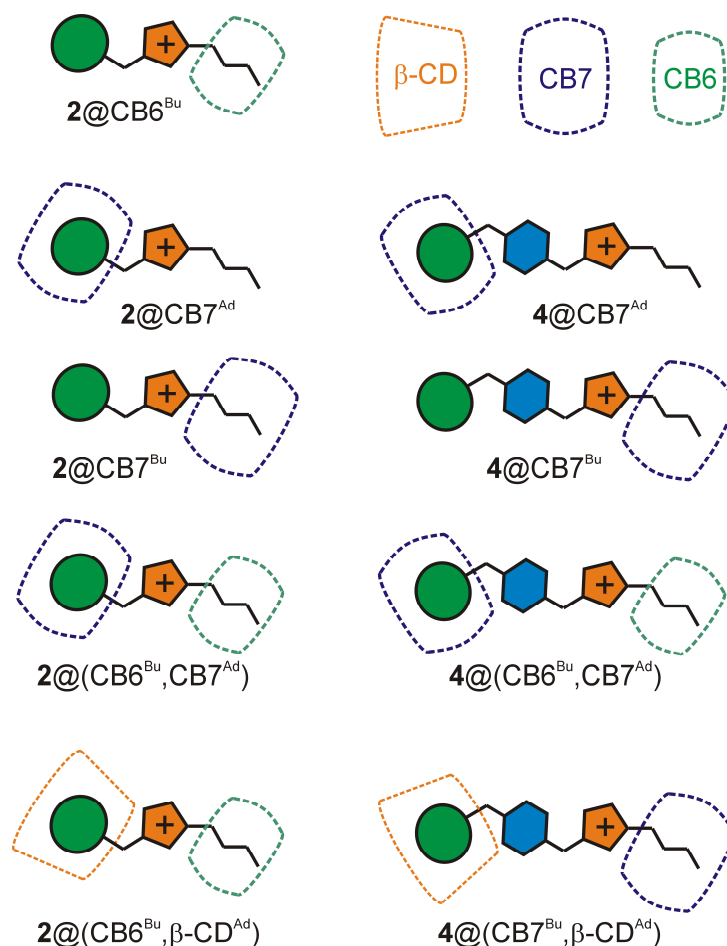
Figure S87: Schematic composition of the simulated binary and ternary complexes.

Stability of the Complexes. Stability was evaluated by measuring the distance between the hosts and the Ad and Bu section of the guests. The Ad position of the guest was defined as the center of mass of all carbon atoms of the adamantyl group. The Bu position of the guest was defined as the center of mass of the butyl carbon atoms. The positions of the hosts were defined as the center of mass of the methine carbon atoms in CB6 and CB7 and the center of mass of the O4 oxygen atoms (glycosidic bridges) in β-CD. The results are shown in Figures S88, S89, S90, S91, S92, and S93. The analysis revealed that all of the simulated complexes are stable on the timescale of the simulations as the measured distances only slightly fluctuated (because of thermal effects) around constant values. However, two exceptions were noted. First, slight movement of CB7 along the tail was observed at the beginning of the

[27] Darden, T.; York, D.; Pedersen, L. *J. Chem. Phys.* **1993**, *98*, 10089.
[28] Salomon-Ferrer, R.; Götz, A. W.; Poole, D.; Le Grand, S.; Walker, R. C. *J. Chem. Theory Comput.* **2013**, *9*, 3878.

simulation of **4**@(CB7^{Bu},β-CD^{Ad}) (Figure S93). The slight movement was toward the central part of guest **4** during the equilibration procedure, which was later reversed during the initial stages of the production stage. No such movement was observed for the remainder of the simulation; thus, the complex was considered to be stable in the configuration depicted in Figure S87. The second exception was a movement of CB7 along guest **4** in the similation of **4**@CB7^{Bu}. The host quickly moved to the central part of the guest at approximately 450 ns and remained there for approximately 50 ns. Then, the host quickly shifted to the Ad part of the guest and stayed there for the remainder of the simulation (bottom of Figure S89). An independent simulation of the same binary system starting from a different **4**@CB7^{Ad} configuration (top of Figure 107) confirms that CB7 preferentially binds to the Ad site of the guest as no movement was observed in this other simulation. This supports our hypothesis that CB7 preferentially binds to the Ad site of guest **4** in the binary complex but shifts along the guest to the Bu site when β-CD is added to form a stable ternary complex **4**@(CB7^{Bu},β-CD^{Ad}) (Figure S93).
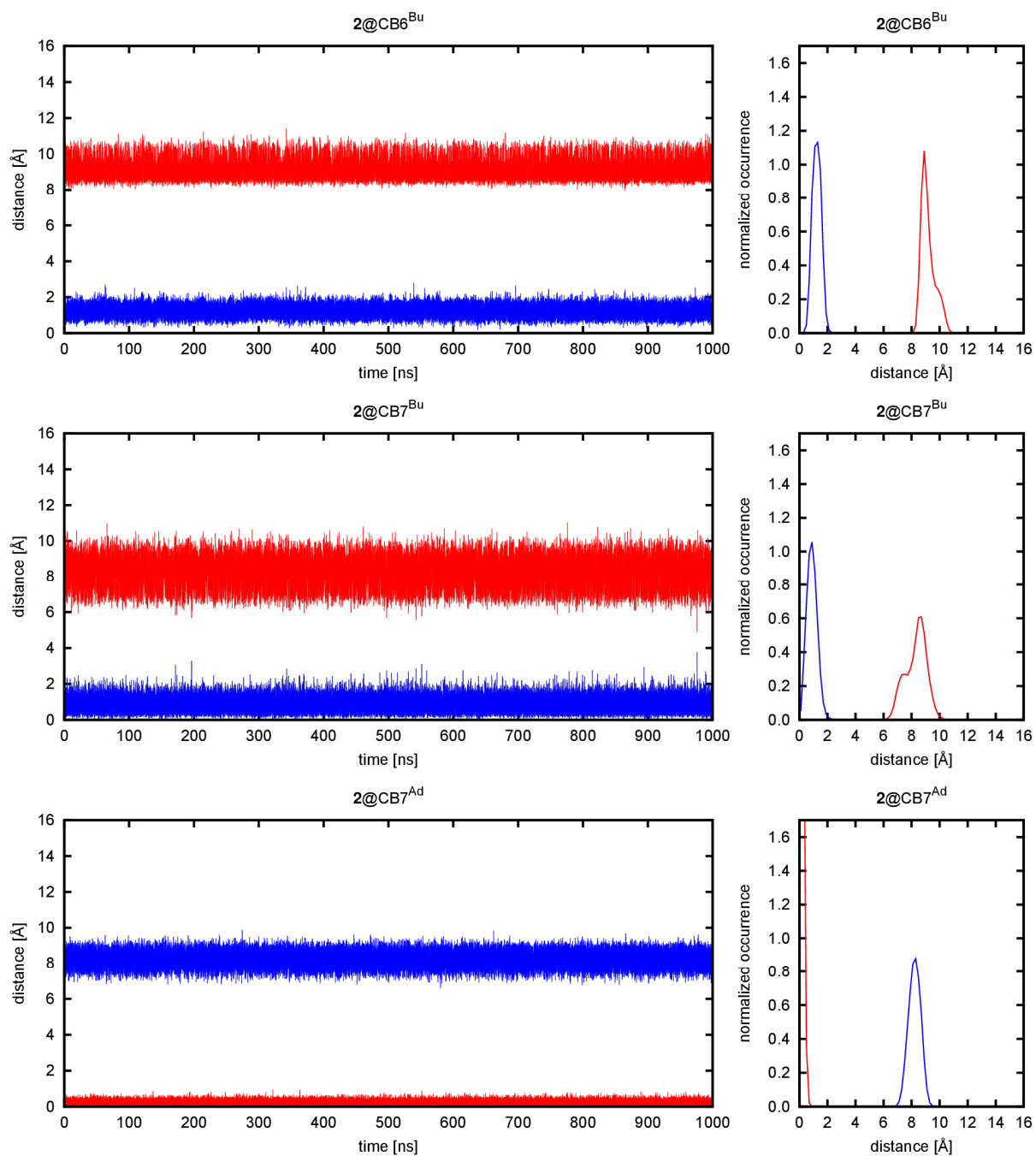
Figure S88: left) distance of guest **2** Ad (red) and Bu (blue) from a host in course of MD simulation. right) histogram analysis of distance
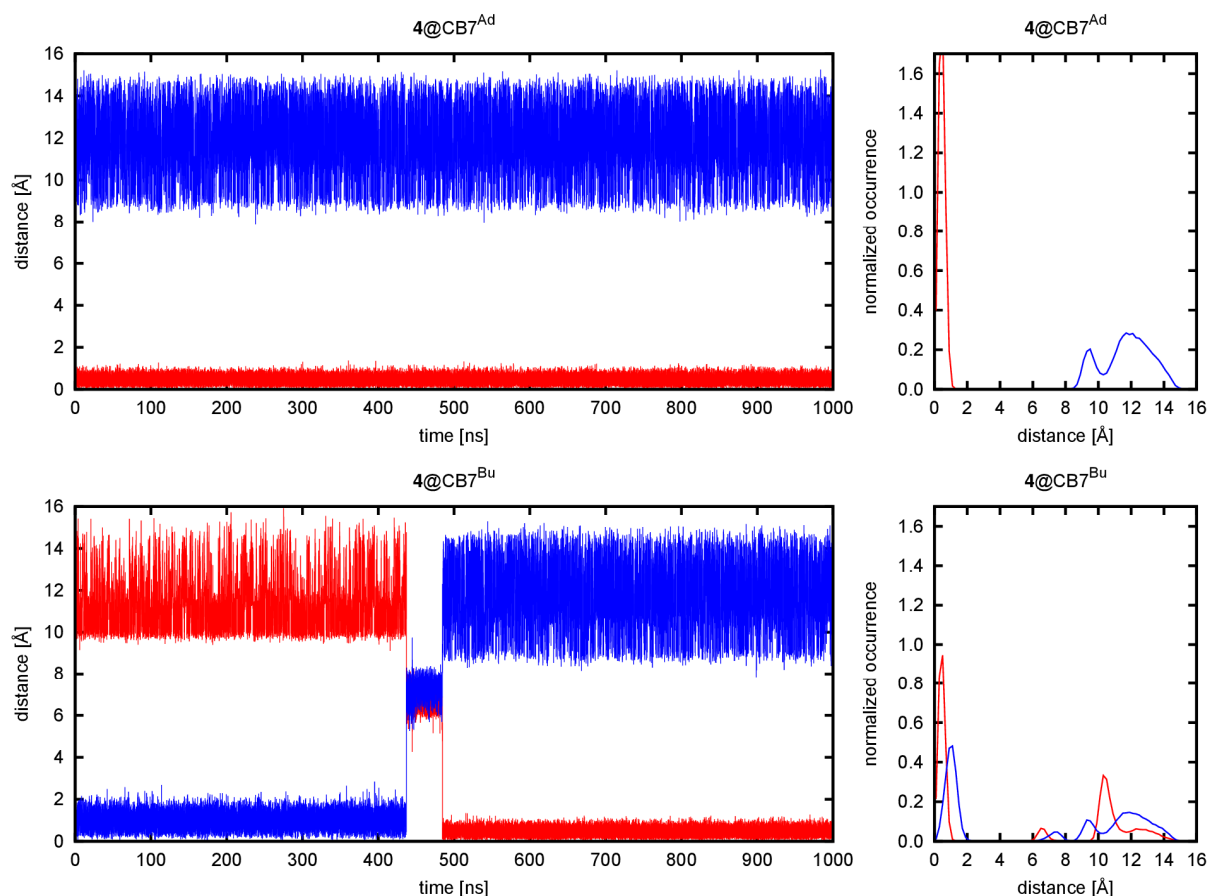
Figure S89: left) distance of guest **4** Ad (red) and Bu (blue) from a host in course of MD simulation. right) histogram analysis of distance
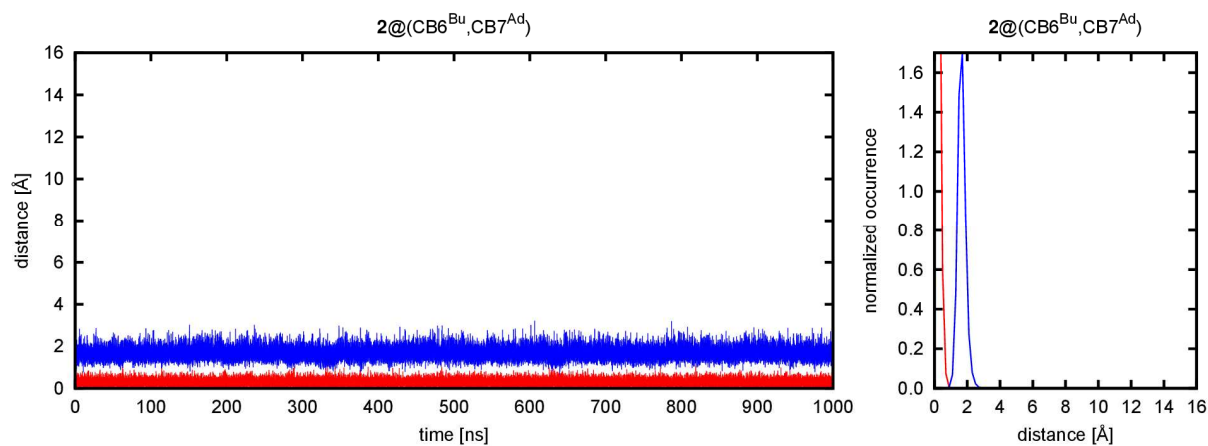
Figure S90: left) distance of guest **2** Ad (red) to CB7 and Bu (blue) to CB6 in course of MD simulation. right) histogram analysis of distance
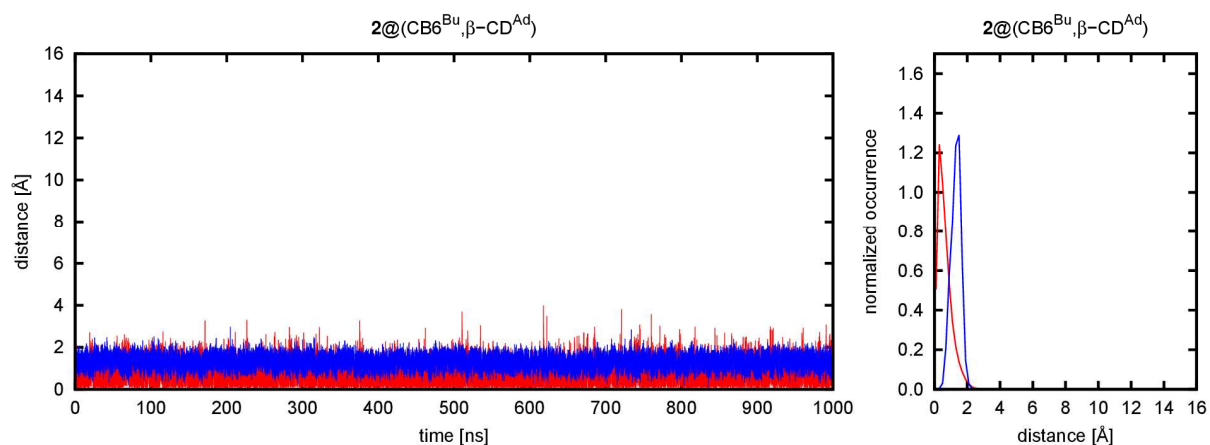
Figure S91: left) distance of guest **2** Ad (red) to β−CD and Bu (blue) to CB6 in course of MD simulation. right) histogram analysis of distance
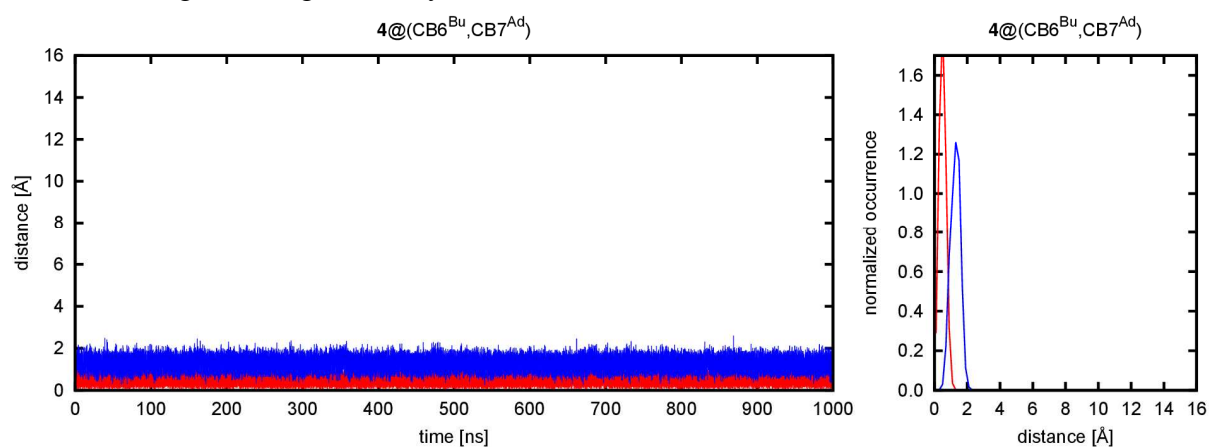
Figure S92: left) distance of guest **4** Ad (red) to CB7 and Bu (blue) to CB6 in course of MD simulation. right) histogram analysis of distance
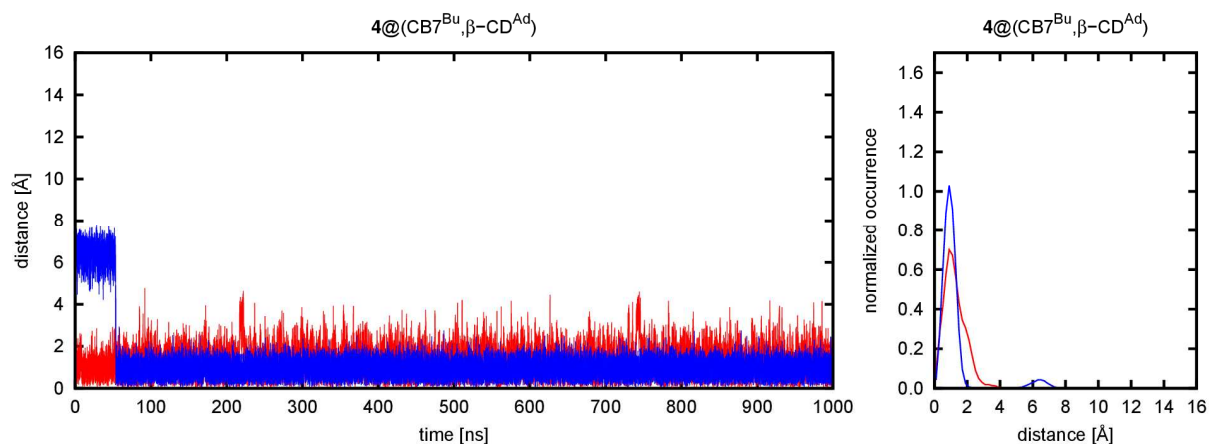
Figure S93: left) distance of guest **4** Ad (red) to β−CD and Bu (blue) to CB7 in course of MD simulation. right) histogram analysis of distance

Calculations of Complexation Induced Shifts (CIS) from MD simulations. To strengthen our conclusions regarding the complex configurations drawn from our experimental observations we calculated CIS values for the hydrogen atoms of the guests in various complex compositions and compared the obtained values with those obtained experimentally. The MD simulations provided no representative structures that could be used directly in the CIS calculations. This results from the substantial flexibility of the guests, even though the complexes are quite stable when the hosts were positioned toward the Ad and Bu sites of the guests (see Figure 4). Thus, we decided to use snapshots from the MD simulations, where the final CIS values are obtained by averaging the CIS values calculated for each individual snapshot. As this would not be normally possible because the required QM calculations are computationally expensive, we employed the following approximation: instead of direct CIS calculations in the binary and ternary complexes, NICS data were employed. Each snapshot was re-oriented such that the host macrocycle was best fitted to the macrocycle structure used in the NICS calculation described above. Then, the NICS value was retrieved for each hydrogen atom of the guest from the volumetric map (Figure S94). These values were grouped according to topicity and averaged along the trajectory (only the last 900 ns were used). This approximation assumes that the macrocycle is a rigid moiety, which is satisfied for the CB6 and CB7 hosts but not for β-CD, which was thus omitted from the calculations. Thus, the contribution from β-CD, which would be rather small (Figure S86), is not considered in the calculated data. Another assumption introduced by the employed approximation is that the guest does not influence the NICS values of the host upon complexation. Similar errors arise from the exclusion of solvent effects, which were not directly accounted for in the NICS calculation. For these reasons, the calculated values are valuable in a qualitative sense only (Table S2).
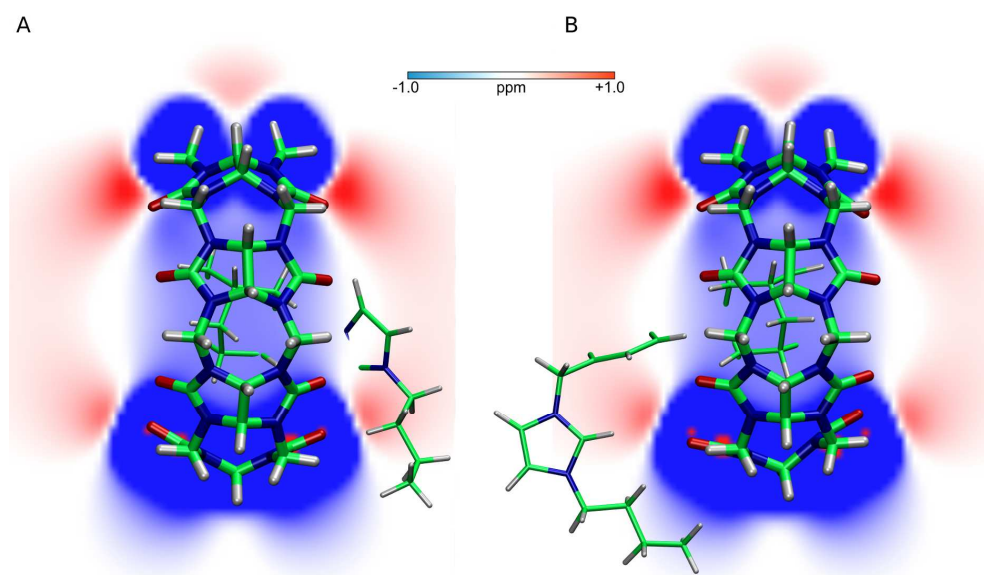
Figure S94. Representative snapshots of **2**@CB7[ad] (A) and **4**@CB7[ad] (B) complexes superimposed into NICS volumetric data calculated for CB7. A representative plane with mapped NICS slices the system through the center of mass of the macrocycle in the same way as it is shown in Figure S86.
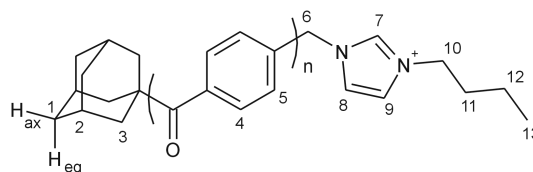
Figure S95: Hydrogen atom assignments

Table S2. Experimental and computed complexation induced chemical shifts $\Delta\delta$ [ppm] – binary systems.

	2@CB6			4@CB6			2@CB7					4@CB7[b]				
	exp	calc		exp	calc		exp	calc(2@CB7[Ad])		calc(2@CB7[Bu])		exp	calc(4@CB7[Ad])		calc(4@CB7[Bu])[c]	
assg[a]	$\Delta\delta$	$\Delta\delta$	$\sigma(\Delta\delta)$[d]	$\Delta\delta$	$\Delta\delta$	$\sigma(\Delta\delta)$	$\Delta\delta$	$\Delta\delta$	$\sigma(\Delta\delta)$	$\Delta\delta$	$\sigma(\Delta\delta)$	$\Delta\delta$	$\Delta\delta$	$\sigma(\Delta\delta)$	$\Delta\delta$	$\sigma(\Delta\delta)$
1ax	0.003	−0.001	0.022	0.010			−0.543	−0.555	0.054	0.011	0.040	−0.576	−0.569	0.035	−0.023	0.024
1eq	0.052	−0.009	0.100	−0.045			−0.749	−0.583	0.028	0.071	0.121	−0.680	−0.575	0.019	−0.036	0.055
2	0.016	0.010	0.039	−0.033			−0.670	−0.573	0.033	0.068	0.093	−0.715	−0.571	0.025	−0.043	0.076
3	0.167	0.129	0.155	−0.026			−0.744	−0.594	0.024	0.201	0.128	−0.644	−0.614	0.030	−0.093	0.177
4	–			0.023			–	–	–	–	–	0.079	−0.014	0.075	0.068	0.097
5	–			0.201			–	–	–	–	–	0.115	0.291	0.072	0.239	0.141
6	0.044	0.163	0.093	0.066	not performed		−0.370	−0.434	0.107	0.249	0.121	0.108	0.070	0.082	0.221	0.089
7	0.315	0.424	0.145	0.369			−0.284	0.108	0.116	−0.236	0.290	0.031	0.097	0.103	−0.005	0.232
8	−0.181	0.232	0.024	−0.152			−0.132	0.071	0.100	0.091	0.254	0.096	0.043	0.073	0.210	0.088
9	0.517	0.390	0.148	0.521			−0.058	0.252	0.037	−0.368	0.277	−0.081	0.005	0.015	−0.106	0.273
10	−0.701	−0.635	0.256	−0.733			0.198	0.294	0.101	−0.574	0.063	−0.138	0.007	0.030	−0.546	0.084
11	−0.792	−0.862	0.055	−0.792			0.127	0.209	0.165	−0.585	0.027	−0.111	0.003	0.057	−0.579	0.033
12	−0.700	−0.767	0.019	−0.696			0.118	0.083	0.113	−0.577	0.031	−0.079	−0.009	0.059	−0.580	0.016
13	−0.713	−0.770	0.022	−0.703			0.062	0.029	0.062	−0.557	0.080	−0.087	−0.029	0.095	−0.575	0.040

[a] See Figure S95 for the H-atoms assignment. [b] Data are given for equimolar mixture.Further shifts were observed with increasing portion of CB7. [c] Calculated only in interval from 100 to 400 ns. [d] $\sigma(\Delta\delta)$ – variance (fluctuations) of $\Delta\delta$.

Table S2 – continued. Experimental and computed complexation induced chemical shifts Δδ [ppm] – ternary systems.

	2@(CB6^{Bu},CB7^{Ad})							4@(CB6^{Bu},CB7^{Ad})						
	exp	calc(all)		calc(CB6)		calc(CB7)		exp	calc(all)		calc(CB6)		calc(CB7)	
assg[a]	Δδ	Δδ	σ(Δδ)[b]	Δδ	σ(Δδ)	Δδ	σ(Δδ)	Δδ	Δδ	σ(Δδ)	Δδ	σ(Δδ)	Δδ	σ(Δδ)
1$_{ax}$	−0.547	−0.561	0.046	0.000	0.000	−0.561	0.046	−0.578	−0.571	0.029	0.000	0.000	−0.571	0.029
1$_{eq}$	−0.749	−0.580	0.024	0.000	0.000	−0.580	0.024	−0.404	−0.574	0.016	0.000	0.002	−0.574	0.016
2	−0.670	−0.572	0.032	0.000	0.001	−0.572	0.032	−0.711	−0.571	0.021	0.000	0.001	−0.571	0.021
3	−0.746	−0.585	0.047	0.011	0.040	−0.596	0.028	−0.624	−0.619	0.036	−0.005	0.019	−0.615	0.032
4	–	–	–	–	–	–	–	0.057	−0.009	0.096	−0.010	0.059	0.001	0.074
5	–	–	–	–	–	–	–	0.272	0.390	0.140	0.113	0.120	0.278	0.073
6	−0.372	−0.224	0.134	0.163	0.061	−0.386	0.111	0.105	0.234	0.102	0.161	0.077	0.073	0.081
7	−0.285	0.679	0.126	0.450	0.081	0.229	0.083	0.502	0.561	0.180	0.451	0.138	0.110	0.087
8	−0.130	0.271	0.106	0.231	0.033	0.040	0.101	−0.113	0.248	0.061	0.227	0.024	0.021	0.054
9	−0.058	0.695	0.094	0.443	0.085	0.252	0.037	0.440	0.406	0.110	0.405	0.110	0.001	0.008
10	0.197	−0.033	0.209	−0.282	0.184	0.249	0.059	−0.674	−0.583	0.252	−0.588	0.250	0.005	0.022
11	0.127	−0.828	0.096	−0.863	0.071	0.034	0.069	−0.742	−0.863	0.053	−0.863	0.053	0.001	0.006
12	0.118	−0.791	0.034	−0.795	0.030	0.004	0.019	−0.672	−0.770	0.021	−0.769	0.020	−0.001	0.007
13	0.060	−0.767	0.014	−0.767	0.014	0.000	0.001	−0.676	−0.771	0.021	−0.770	0.020	−0.001	0.004

[a] See Figure S95 for the H-atoms assignment. [b] σ(Δδ) – variance (fluctuations) of Δδ.

Table S2 – continued. Experimental and computed complexation induced chemical shifts $\Delta\delta$ [ppm] – ternary systems.

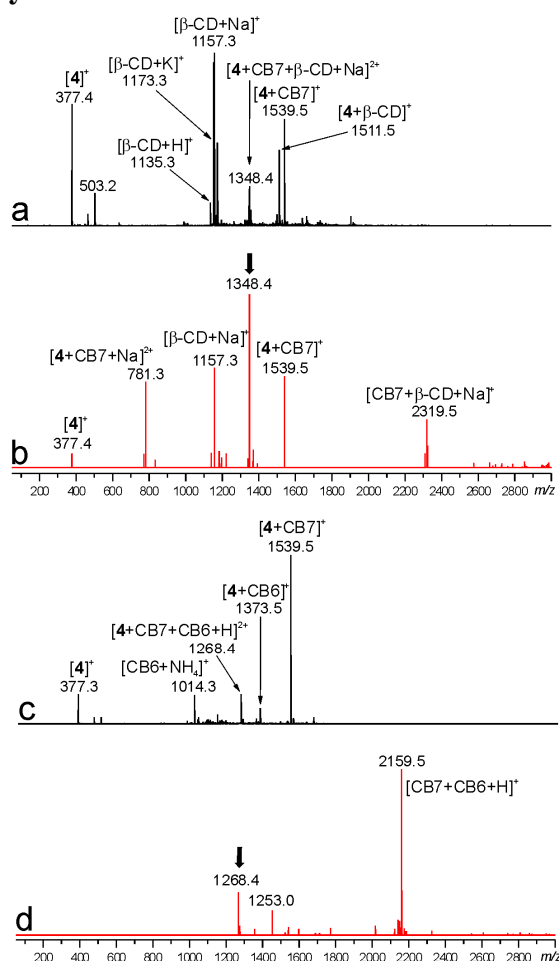| assg[a]	2@(CB6,β-CD) exp $\Delta\delta$	calc(CB6) $\Delta\delta$	$\sigma(\Delta\delta)$[b]	4@(CB6,β-CD) exp $\Delta\delta$	calc(CB6) $\Delta\delta$	$\sigma(\Delta\delta)$	2@(CB7,β-CD) exp $\Delta\delta$	calc(CB7) $\Delta\delta$	$\sigma(\Delta\delta)$	4@(CB7,β-CD) exp $\Delta\delta$	calc(CB7) $\Delta\delta$	$\sigma(\Delta\delta)$
1$_{ax}$	0.024	0.001	0.006	0.259			−0.540			0.240	0.000	0.001
1$_{eq}$	0.123	0.005	0.029	0.359			−0.757			0.368	0.000	0.003
2	0.207	0.006	0.021	0.230			−0.671			0.235	0.000	0.004
3	0.368	0.071	0.104	0.006			−0.754			0.046	0.002	0.016
4	–	–	–	−0.393			–			−0.298	0.045	0.075
5	–	–	–	0.124			–			0.233	0.209	0.150
6	0.127	0.196	0.062	0.204	not performed		−0.339	not performed		-	0.293	0.106
7	0.431	0.449	0.122	0.595			−0.221			−0.347	−0.114	0.263
8	−0.134	0.237	0.024	−0.276			−0.098			−0.460	0.216	0.109
9	0.571	0.398	0.143	0.569			–			−0.488	−0.219	0.285
10	−0.673	−0.569	0.252	−0.761			0.242			−0.706	−0.562	0.080
11	−0.755	−0.862	0.054	−0.699			0.149			−0.650	−0.582	0.023
12	−0.694	−0.770	0.020	−0.624			0.100			−0.635	−0.581	0.019
13	−0.710	−0.770	0.020	−0.644			0.053			−0.654	−0.574	0.045

Branná, Černochová, Rouchal,
Kulhánek, Babinský, Marek, Nečas,
Kuřitka and Vícha

S.I.

Mass spectra of ternary systems

Spectrum a:
$[\beta\text{-CD+Na}]^+$ 1157.3
$[\mathbf{4}]^+$ 377.4
$[\beta\text{-CD+K}]^+$ 1173.3
$[\mathbf{4}\text{+CB7+}\beta\text{-CD+Na}]^{2+}$
$[\mathbf{4}\text{+CB7}]^+$ 1539.5
$[\mathbf{4}\text{+}\beta\text{-CD}]^+$ 1511.5
$[\beta\text{-CD+H}]^+$ 1135.3
503.2
1348.4
a

Spectrum b:
1348.4
$[\mathbf{4}\text{+CB7+Na}]^{2+}$ 781.3
$[\beta\text{-CD+Na}]^+$ 1157.3
$[\mathbf{4}\text{+CB7}]^+$ 1539.5
$[\text{CB7+}\beta\text{-CD+Na}]^+$ 2319.5
$[\mathbf{4}]^+$ 377.4
b
200 400 600 800 1000 1200 1400 1600 1800 2000 2200 2400 2600 2800 *m/z*

Spectrum c:
$[\mathbf{4}\text{+CB7}]^+$ 1539.5
$[\mathbf{4}\text{+CB6}]^+$ 1373.5
$[\mathbf{4}\text{+CB7+CB6+H}]^{2+}$ 1268.4
$[\text{CB6+NH}_4]^+$ 1014.3
$[\mathbf{4}]^+$ 377.3
c

Spectrum d:
2159.5
$[\text{CB7+CB6+H}]^+$
1268.4
1253.0
d
200 400 600 800 1000 1200 1400 1600 1800 2000 2200 2400 2600 2800 *m/z*

Figure S95. Positive-ion mode ESI mass spectra (full scan) of $\mathbf{4}\cdot\text{CB7}\cdot\beta\text{-CD}$ and $\mathbf{4}\cdot\text{CB7}\cdot\text{CB6}$ in aqueous solution. a) First-order mass spectrum of $\mathbf{4}\cdot\text{CB7}\cdot\beta\text{-CD}$, b) MS^2 of *m/z* 1348, c) first-order mass spectrum of $\mathbf{4}\cdot\text{CB7}\cdot\text{CB6}$, d) MS^2 of *m/z* 1268. The assignments for the observed signals are shown in the brackets. The fragmented ions in the tandem mass spectra are marked with bold downward-facing arrows.

In the case of ternary systems containing β-CD, the corresponding complexes were detected as adducts with sodium cation (i.e., $[\text{guest}\cdot\text{CB7}\cdot\beta\text{-CD}\cdot\text{Na}]^{2+}$). Signals of the protonated aggregates (e.g., $[\text{guest}\cdot\text{CB7}\cdot\beta\text{-CD}\cdot\text{H}]^{2+}$) were observed in the spectra of systems containing only CBs as the host molecules. The tentative assignment of these signals was further supported by an analysis of tandem mass spectra. As is evident from Figure S95(b), the collision-induced dissociation of $[\mathbf{4}\cdot\text{CB7}\cdot\beta\text{-CD}\cdot\text{Na}]^{2+}$ resulted in two pairs of singly-charged fragments: $[\beta\text{-CD}\cdot\text{Na}]^+/[\mathbf{4}\cdot\text{CB7}]^+$ and $[\mathbf{4}]^+/[\text{CB7}\cdot\beta\text{-CD}\cdot\text{Na}]^+$. Such electrostatic-repulsion-driven cleavage is not surprising for doubly-charged starting aggregates. However, the formation of the latter pair was unexpected considering their respective association constants. In addition, the loss of the neutral β-CD unit was observed, resulting in the doubly-charged aggregate $[\mathbf{4}\cdot\text{CB7}\cdot\text{Na}]^{2+}$. In contrast, the sole fragment $[\text{CB7}\cdot\text{CB6}\cdot\text{H}]^+$ was observed for the protonated aggregate $[\mathbf{4}\cdot\text{CB7}\cdot\text{CB6}\cdot\text{H}]^{2+}$, as depicted in Figure S95(d).